2001

Linear vibration welding of different melting temperature amides.

Liying. Qi
University of Windsor

INFORMATION TO USERS

This manuscript has been reproduced from the microfilm master. UMI films the text directly from the original or copy submitted. Thus, some thesis and dissertation copies are in typewriter face, while others may be from any type of computer printer.

The quality of this reproduction is dependent upon the quality of the copy submitted. Broken or indistinct print, colored or poor quality illustrations and photographs, print bleedthrough, substandard margins, and improper alignment can adversely affect reproduction.

In the unlikely event that the author did not send UMI a complete manuscript and there are missing pages, these will be noted. Also, if unauthorized copyright material had to be removed, a note will indicate the deletion.

Oversize materials (e.g., maps, drawings, charts) are reproduced by sectioning the original, beginning at the upper left-hand corner and continuing from left to right in equal sections with small overlaps.

Photographs included in the original manuscript have been reproduced xerographically in this copy. Higher quality 6" x 9" black and white photographic prints are available for any photographs or illustrations appearing in this copy for an additional charge. Contact UMI directly to order.

ProQuest Information and Learning
300 North Zeeb Road, Ann Arbor, MI 48106-1346 USA
800-521-0600

LINEAR VIBRATION WELDING OF DIFFERENT MELTING TEMPERATURE AMIDES

By

Liying Qi

A Thesis
Submitted to the Faculty of Graduate Studies and Research
Through the Department of Mechanical, Automotive and Materials Engineering
In Partial Fulfillment of the Requirements for
The Degree of Master of Applied Science
In Engineering Materials at the
University of Windsor

Windsor, Ontario, Canada

October, 2001

To my family

ABSTRACT

This thesis is concerned with the linear vibration welding of nylons reinforced with chopped glass fibers. This process and these materials are already used to make automotive air induction modules. To further integrate more parts into these modules, it is sometimes necessary to use higher temperature more expensive amides.

An earlier senior undergraduate project found that it was possible to make sound welds between different melting temperature amides under some welding conditions. The present thesis extends this work.

The weld geometries used included mainly T-joint samples, and also butt welds were done, and some further analyses were done on CWF and shear samples made previously.

Three different Design of Experiments (DOE) matrices were used to create three sets of T-joint samples which were analyzed to understand the interactions among the process parameters. The usual analysis of variance was extended by multivariate analysis to better define the individual roles of each of the process parameters. This attempt met with some success, and showed that the vibration amplitude was by far the most important factor affecting the strength. Holding time after vibration was insignificant in the range of values studied.

An unexpected benefit of the DOE tests was that a new general understanding of the residual stresses developed in T-joint samples evolved. This led further experimental measurements on the amount that the T-joint flanges (arms) were bent by these residual stresses. This in turn led to a qualitative explanation of why linear vibration welds which involve embedding one member of the weld in the interior of the other member produces

poor strength results. Because of this the results of the work of the previous student are now much better understood.

Cross-sections of the various types of welds were examined. In some cases the fibers were aligned along the welding direction. At times the weld interface was very difficult to locate. Both optical microscopy and the scanning electron microscope were used. Some fracture surfaces were also examined, and here the fiber alignment was highly evident. For short fiber reinforcements the fibers tended to align in the welding vibration direction. For long fibers (1 mm) used on some cup welded to flange (CWF) samples, the fibers maintained the alignment created during injection.

DOE matrices were also performed on butt welds where the samples were either 3mm thick welded to 3 mm thick samples, or 6 mm thick to 6mm thick welds. The unexpected result was that when high strength amides (HTN) were welded to lower strength nylons, the fracture surface was sometimes completely in the parent high strength material. This may have been due to the glass alignment in the HTN material.

A set of resistance welds was also done, as this method had produced very strong welds in induction heated samples. In the present experiments the strength values were rather low due to difficulties in maintaining the 3 dimensional geometry of the resistor implant.

ACKNOWLEDGEMENT

Let me begin by thanking my supervisor, Dr. Daniel F Watt. Without his ambition and perseverance, this project would never have gotten off the ground. It is his passion for academic knowledge and the pursuit of engineered solutions that propelled this project through to completion. I am very grateful to have worked with such a keen and selfless individual.

I would like to recognize Siemens Automotive Powertrain Group (Tilbury) and the Materials and Manufacturing Ontario (MMO) for their financial support of the project. I would, also, like to acknowledge the personal contributions of Dr. Bobbye Baylis of Siemens Automotive Powertrain Group. She was instrumental in establishing this collaborative research project with the University of Windsor, and offered practical insights during the course of the project.

I would also like to express my thanks to John Robinson, and the people who work in the Central Research Workshop.

TABLE OF CONTENTS

ABSTRACT v

ACKNOWLEDGEMENTS vii

LIST OF FIGURES x

LIST OF TABLES xiii

CHAPTER 1 INTRODUCTION 1
- 1.1 Purposes, requirements and manufacturing of air intake manifolds 1
- 1.2 Motivation 6
- 1.3 Factors affecting the welded strength in amides 8
- 1.4 Geometries of welds used in this research. 8

CHAPTER 2 REVIEW OF POLYMER JOINING PROCESSES 10
- 2.1 Mechanical fastening 11
- 2.2 Adhesive bonding 11
- 2.3 Polymer welding processes 12
- 2.4 Linear vibration welding(LVW) 15
  - 2.4.1 A detailed introduction to LVW technology 16
  - 2.4.2 Vibration welding process analysis 18
- 2.5 Material requirements related to welding joint performance 26

CHAPTER 3 TESTS FOR THE EVALUATION OF WELD STRENGTH 29
- 3.1 Welding machines and weld geometries 29
- 3.2 Tensile tests and fixtures 31

CHAPTER 4 PREVIOUS WORK ON THE WELDING OF DISSIMILAR MELTING TEMPERATURE MATERIALS 34
- 4.1 A Description of amide materials 34
- 4.2 Review of previous work 36
- 4.3 Shear-lap welds 39

CHAPTER 5 DESIGN OF EXPERIMENT TEST RESULTS AND ANALYSES 44
- 5.1 Design of experiments (DOE) and materials used 47
  - 5.1.1 DOE matrix and results for the TA group 47
  - 5.1.2.Interactions between weld strength, meltdown and flash weight 51
  - 5.1.3 Predictive mathematical models for weld strength 52
  - 5.1.4 Regression analyses 62
  - 5.1.5 On the Co-dependence of UTS and meltdown 74

5.2 Experimental Design Set TB 75
5.2.1 Experimental results for the TB group 75
5.3 Experimental design Set TC 80
5.4 Correlation of flash parameters with the strength of the welds 80

CHAPTER 6 THE EFFECT OF TESTING FIXTURE DESIGN ON THE TENSILE STRENGTH OF T-JOINTS 81
6.1 Measurement of curvature in T-joint flanges 81
6.2 Effects of curvature on tensile strength measurement 87

CHAPTER 7 RESULTS FOR BUTT WELD JOINTS 97
7.1 Tensile strengths 97
7.2 Tensile strengths in 6mm thick samples 100
7.3 Tensile strength in 3mm thick samples 104

CHAPTER 8 MICROSTRUCTURE ANALYSIS 111
8.1 Weld microstructures Observed in T-joint samples 111
8.2 Observations on weld-cap-flange joints 113

CHAPTER 9 RESISTANCE WELDING RESEARCH 118
9.1 Overview 118
9.2 Experimental procedure 121
9.3 Resistance welding results and analysis 125

CHAPTER 10 RESISTANCE WELDING RESEARCH 129

REFERENCES 133

APPENDIX I PROCESS PARAMETERS AND RESULTS FOR TC GROUP T-JOINT DOE 135

APPENDIX II WELD STRENGTHS AND FLASH GEOMETRY 136

APPENDIX III UPPER ARM CURVATURES ON TA SAMPLES 141

APPENDIX IV BUTT WELD RESULTS 150

VITA AUCTORIS 155

LIST OF FIGURES

Figure 1.1	Manifold for Honda	3
Figure 1.2a	Before welding, part 1	5
Figure 1.2b	Before welding, part2	5
Figure 1.2c	Final assembly, including a steel insert, made by vibration welding	5
Figure 1.3	Geometry of four joints	9
Figure 2.1	Classification of joining methods	10
Figure 2.2	Classification of welding of thermoplastics	13
Figure 2.3	Schematic representation of the DRI process	14
Figure 2.4	Schematic representations of part geometry and motion in vibration welding	17
Figure 2.5	Schematic penetration-time curve showing four phases of the vibration welding process (after Stokes)	19
Figure 2.6	Relative motion of the linear vibration showing the relationship between position and velocity	20
Figure 2.7	Definition of friction	21
Figure 2.8	One cycle of welding vibration amplitude	23
Figure 2.9	Schematic diagram to illustrate the geometry assumed for shear. The upper block (with lower surface area bd) floats on a layer of viscous liquid	24
Figure 3.1	Four different geometries	29
Figure 3.2	Mini-Vibration Welder Model MINI II	30
Figure 3.3	Instron machine	33
Figure 3.4	Two different T-joint testing fixtures showing sample set up for Test type a, b and c respectively	33
Figure 4.1	The material 73G30 in nylon6	40
Figure 4.2	The polished cross-sectional areas of the shear lap welds provides information on the interface microstructure. The sample number is indicated in the boxes on the far left and far right hand side	39
Figure 4.3	Porosity at weld interface of 51G15 weld (Sample 25) x250	41
Figure 4.4	Weld interface of 51G15 material (Sample 25) x75	41
Figure 4.5	Weld interface of 70G33 material (Sample 36) x75	42
Figure 4.6	Weld interface of 70G33/51G15 weld (Sample 46) x75	43
Figure 4.7	Weld interface of 51G15/73G30 weld (Sample 32) x75	43
Figure 5.1	Weld parameters of DOE	50
Figure 5.2	UTS vs. Meltdown	51
Figure 5.3	Tensile strength as a function of Flash weight	52
Figure 5.4	UTS vs. weld pressure	53
Figure 5.5	UTS vs. weld amplitude	53
Figure 5.6	UTS vs. weld time	55
Figure 5.7	UTS vs. weld hold time	55
Figure 5.8	Individual data for UTS vs. weld pressure	57

Figure 5.9	Individual data for UTS vs amplitude	57
Figure 5.10	Individual data for UTS vs. weld time	58
Figure 5.11	Individual data for UTS vs weld hold time	58
Figure 5.12	UTS vs. weld time * amplitude(total sliding dispance)	60
Figure 5.13	UTS vs. pressure * weld time * amplitude	61
Figure 5.14a	Experimental UTS vs. formula UTS1	63
Figure 5.14b	Experimental UTS and formula UTS1 vs. A*Wt	63
Figure 5.15a	Experimental UTS vs. formula UTS2	64
Figure 5.15b	Experimental UTS and formula UTS2 vs. A*Wt	65
Figure 5.16	Experimental UTS and formula UTS3 vs. A*Wt	66
Figure5.17a	Experimental UTS vs. formula UTS4	67
Figure 5.17b	Experimental UTS and formula UTS4 vs. A*Wt	68
Figure 5.18a	Experimental UTS vs. formula UTS5	69
Figure 5.18b	Experimental UTS and formula UTS5 vs. A*Wt	70
Figure 5.19	Standard error of estimate vs. t1	71
Figure 5.20a	Experimental UTS vs. formula UTS6	72
Figure 5. 20b	Experimental UTS vs. formula UTS6	72
Figure 5.21	Experimental meltdown vs. formula meltdown	74
Figure 5.22	TB group, UTS vs. weld amplitude	77
Figure 5.23	TB group, UTS vs. hold time	77
Figure 5.24	UTS vs. vibration amplitude times welding time	78
Figure 5.25	UTS vs. weld pressure	78
Figure 6.1	Bridgeport milling machine temporarily converted to measure the curvature in the flanges of T-joint welds	83
Figure 6.2a	Curvature measurements for welds 56 and 49. These samples are for a high temperature amide A-1133 welded to nylon 6	85
Figure 6.2b	Curvature measurements for tests 29 and 34. These samples are for nylon 6 welded to nylon 66 86	
Figure 6.3.	The consequences of pulling a sample with bent flanges against a holder with flat horizontal surfaces	88
Figure 6.4	Test fixtures of types a, b and c. Tester type c was also used for Valerie's samples	90
Figure 6.5	Histographic summary of Tables 6.1 and 6.2	93
Figure 6.6	Correlation between the tensile strength ratio (between fixtures a and V as a-V/V) versus the depth of curvature	95
Figure 6.7	The relationship between curvature and the melting temperature of the flange	96
Figure 7.1	The black sample (70G33) and the "natural" sample (A1133)have been butt welded together	99
Figure 7.2	Tensile strength of 6mm thickness butt joints	100
Figure 7.3	Individual test sample weld strength variation of samples of HTN/70G33.The ID numbers are in the same order that they were in the welded sample	101
Figure 7.4	Unsuccessful butt joint for BA14, HTN to HTN	102
Figure 7.5	Tensile sample BA10B broken in the HTN base material	103

Figure 7.6	Tensile strength of 3mm thick material combinations	104
Figure 7.7	Meltdown distance for different combinations of materials in 3 mm thick butt welds	105
Figure 7.8	Meltdown distance vs strength for 3 mm samples excluding 70G33/70G33	106
Figure 7.9	Strength comparison for 6mm thick samples and 3mm samples of 70G33/70G33 butt welds	107
Figure 7.10	Meltdown distances for 6mm thick samples and 3mm samples of 70G33/70G33 butt welds	108
Figure 7.11	Geometry of the BA40E 3 mm cross-section	109
Figure 7.12	Another 3 mm weld cross-section.	109
Figure 8.1	The cross-sectional areas of the three weld interface shape	
Figure 8.2	High temperature part penetrate into low temperature material (SEM x 80)	112
Figure 8.3	Geometry of weld-cap-flange samples	113
Figure 8.4	Photographic of the fracture surface showing the locations chosen for the micrographs in Figure 8.5	114
Figure 8.5a	Long glass fibers at the area around point 1. The outer wall of the cap is on the left hand side of the picture	115
Figure 8.5b	Fibers in the fracture surface around point 5;which is adjacent to Figure 8.5a	115
Figure 8.5c	The area around point 4, adjacent to Figure 8.5b. The inner wall surface is on the right hand side of the figure	116
Figure 8.5d	Fracture surface around point 2 near inner wall	116
Figure 9.1	The resistance welding process	119
Figure 9.2	Sample being welded on the Instron machine	122
Figure 9.3	Before welding, grooves have been added to keep the resistor in place	124
Figure 9.4	Sectioned resistance welded T sample	125

LIST OF TABLES

Table 1-1	Some properties of A-1133 and PA66	7
Table 5.1	L18 (4^3) Taguchi matrix +1 extra test with regression results	49
Table 5.2	L18 (4^3) Taguchi matrix +1 extra test with regression results.	50
Table 5.3	Summary of TA result	73
Table 5.4	The experimental matrix for welding parameters with meltdown and strength results for Test Set TB	76
Table 5.5	Experiments with A*W = or > 11.2 arranged in ranked order of UTS	81
Table 6.1	Curvature measurements for the upper flanges of T-joint samples	84
Table 6.2	Strength results using different test fixtures on nominally identical samples	94
Table 7.1	Butt joint combinations for which welds have been made	98
Table 9.1	Resistance welding test results	126

CHAPTER 1
INTRODUCTION

1.1 Purpose, requirements and manufacturing of air intake manifolds

This project involved experimental research, including statistical analysis, on aspects of the feasibility of manufacturing intake manifolds using the linear vibration welding method when the manifold is to be made of amides of different melting temperatures.

Recently, the use of lightweight air induction manifolds (AIMs) on spark ignition automotive engines has increased [1,2]. The performance of these engines is increased if the correct amount of air enters the cylinder chamber during the down stroke of the piston. The result can be an increase in horsepower. Another benefit is that the exhaust fumes are easier for the catalytic converter to react to a more acceptable gas mixture. Ideally the inlet mixture of air and fuel should be close to the stoichiometric ratio. The design of these manifolds is complicated, as it involves delivering the correct amount of air to each cylinder at different throttle settings as the engine speed changes.

The use of glass-reinforced plastics for manifolds has several advantages. They are relatively light in weight. They can be made into very complicated hollow shapes with smooth interior surfaces.

Alternatively, these and other hollow parts such as resonators and fluid reservoirs can also be produced by the lost core injection molding process. The internal (hollow segment) of the manifold shape is first die cast using a low melting point metal. This is then used as an insert in an injection molding process in which glass reinforced plastic encases the metal core. After the plastic has frozen, the low melting point metal is heated and poured out, leaving the final hollow plastic shell.

An alternative and increasingly popular method, is to make the manifold from a few injection-molded parts that can be assembled and welded together to create the final product.

Designing to make use of a one-piece hollow plastic part is ideal because it eliminates the need for a lot of assembly [3,4]. However, design, processing technology, product performance, reliability, and other considerations often make it necessary to join thermoplastic parts and components. In fact, a typical passenger car uses 18 kilograms of nylon-based plastics, primarily in under-the-hood components. The trend of developments in the automobile is toward making it more safe, comfortable, and inexpensive to manufacture.

The advantages of plastic intake manifolds are:

- Weight reduction;
- Cost reduction by elimination of machining process;

- Achievement of high performance in the engine due to high interior surface smoothness and an increase in heat isolation.

The lost-core process is more capital intensive compared with the linear vibration plastic welding process, because the former involves additional forming, melting, and metallic core removal. Of late, welded manifolds are becoming more popular than the lost core manifolds due to ease of manufacturing, lower costs, and design flexibility and parts consolidation.

In the linear vibration welding process, the intake manifold is produced by joining several injection molded plastic pieces together into one final manifold assembly. Figure 1.1 is a manifold for Honda produced by Siemens Automotive (Tilbury, Ontario). It is produced by welding together three injection molded parts as indicated.

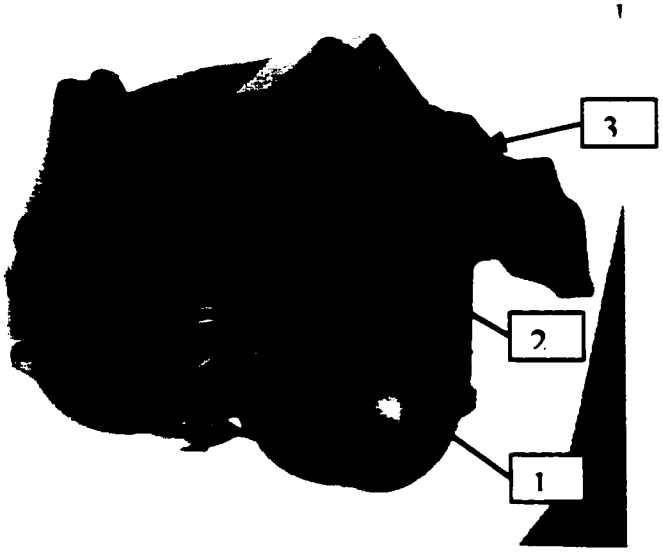

Figure 1.1 Manifold for Honda

Polyamides (PA), commonly called nylons, are high-performance, semi-crystalline thermoplastics with a number of attractive chemical, physical, and mechanical properties. Molded nylon parts are more resistant to creep, fatigue, repeated impact, and challenging chemical environments than parts made of many less-durable thermoplastics. There are more than a dozen classes of nylon resins [5], including nylon 6, nylon 12, nylon 46 and nylon 66. Short glass fiber reinforced nylons are the materials of choice for several automotive components found under the hood. Reinforced-nylon plastics (containing 30-35% glass fiber by weight) are typically used in the high production volume plastic parts.

Designing and assembling these critically stressed components requires advanced analysis of structure, noise, vibration and harshness. Short and long term strength and life criteria for the joint should be established before any parts are welded. There are geometrical limitations to the molding process that create the need to include a joining method. One such method is linear vibration welding, which is fast, easy and ideal for large components. Part consolidation becomes an inviting option when the two adjacent parts can both be manufactured using thermoplastics and a joining method such as vibration welding is available. Figure 1.2 shows parts before welding and after welding.

Linear vibration welding consists of holding two thermoplastic parts together, and then vibrating them against each other in a direction along which they share a common interface. At first solid-solid friction causes heating and then melting of the interface.

Further vibration causes viscoelastic hysteresis heating of the molten interface. At the end of vibration, the two parts are held together until the polymer solidifies.

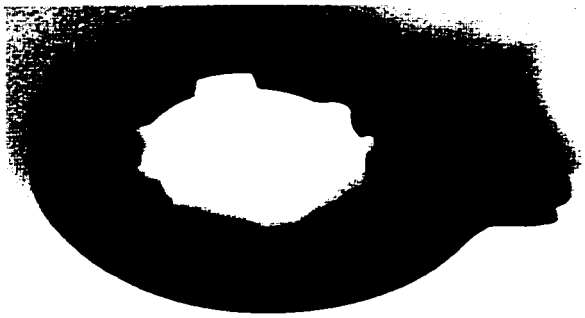

Figure 1.2a Before welding, part 1

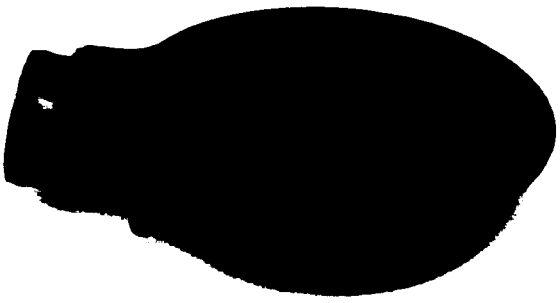

Figure 1.2b Before welding, part2

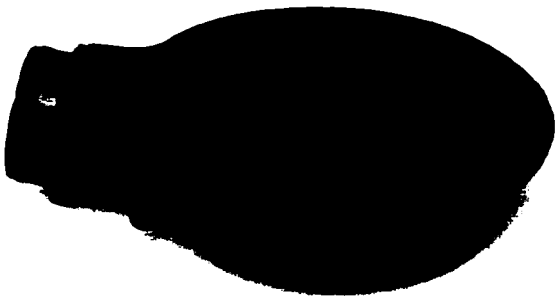

Figure 1.2c Final assembly, including a steel insert, made by vibration welding

The goal of this project is to attempt to resolve the question of whether linear vibration welding is still a good option when one of the parts to be consolidated requires greater thermal stability and moisture resistance than the other. Will the polymer with the higher melting temperature participate in forming a sound weld?

Siemens Automotive Powertrain Group (Tilbury) and the Materials and Manufacturing Ontario (MMO) funded the project. One undergraduate and one graduate student (the present author) have been involved in this project.

The research was directed into three distinct areas:

(1) Materials Scanning; with the welding process parameters kept at the same settings, similar and dissimilar material combinations were welded;

(2) Process research; the Design of Experiments statistics tool was used to analyze the process to find the influence of individual process parameters on the tensile strength of the weld joint;

(3) Resistance welds were made to compare with the vibration welding process.

1.2 Motivation

Recently the linear vibration welding (LVW) of the under hood components has become the most cost effective manufacturing process. As the function of the engine has been improved, the material's operating temperature has been increased. High temperature nylon could be a good choice for these components. In the case where this involves the welding together of different melting temperature materials, then only PA6/PA66 has been reported in the general literature[6] in detail. The potential use of high temperature aromatic amide materials, such as HTN (Dupont) or AS1133 (Amoco), welded to PA6 or PA66 has not been reported in the general literature. An important

consideration is that high temperature materials are more expensive than the low temperature nylons PA6 and PA66 (Table 1.1). Table 1.1 lists some properties of the high temperature material A1133 and low temperature PA66. From this table, it can be seen that the high melting temperature material has lower shrinkage, and lower moisture absorption; while the ordinary nylon has a lower melting temperature, higher shrinkage and higher moisture absorption. The high temperature nylons also have lower distortion at engine operating temperatures (150 C). Information on the weldability of the high temperature amides with lower temperature, lower cost nylons is needed in order to deduce the cost and guarantee the quality of these induction systems.

Properties	A-1133	PA 66
Melting temperature (C)	310	263
Tensile Strength (MPa)	131	210
Elongation (1%)	1.2	3
Izod Impact Strength (J/m)	40	13
Specific Gravity	1.85	1.41
Shrinkage (%)	0.3/0.4	0.45/0.75
Moisture absorb (24 h)	0.21%	0.75%

Table 1.1 Some properties of A-1133 and PA66

1.3 Factors Affecting Welded Strength in Amides

From the review of recent developments in this technology [7], it can be concluded that there are several factors that affect the strength of welds:

- Moisture;
- Weld test geometry (T-weld vs. Butt weld);
- Crystallinity;
- Presence of mineral;
- Presence of glass;
- Failure location;
- Optimum welding process pressure;
- Rate of cooling (recrystallization);
- Rate of heating;
- Actual peak temperature.

1.4 Geometries of welds used in this research

Four different weld geometries have been studied (Figure 1.3). Although the actual weld strength values were different, there were similar trends in that the best welds were generally obtained when the melt temperatures were the same or similar, and the worst welds were obtained when the melt temperature difference was greatest.

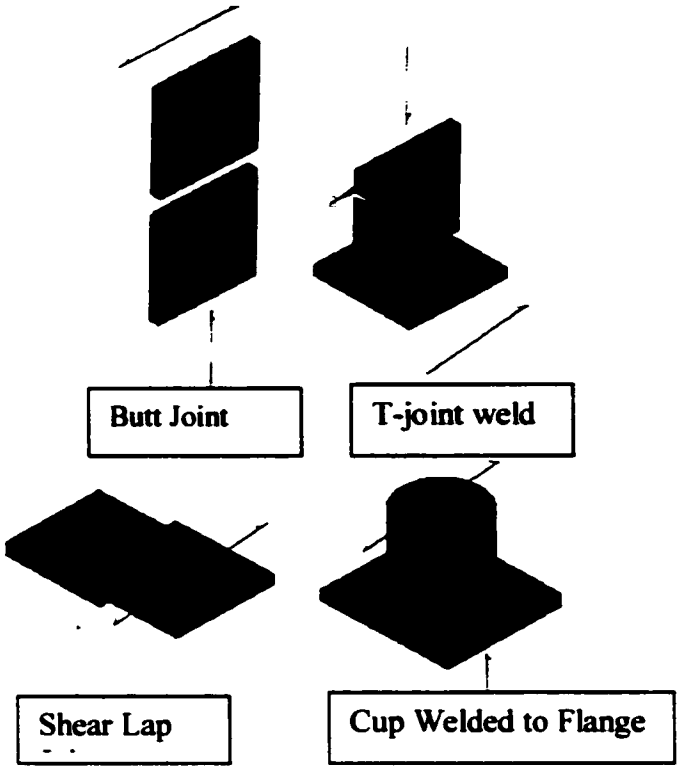

Figure 1.3 Geometry of four joints

CHAPTER 2
REVIEW OF POLYMER JOINING PROCESSES

Joining of plastic materials can broadly be divided into mechanical fastening and bonding [9] (Figure 2.1). Bonding can be further classified into adhesive bonding, solvent bonding, and welding. Mechanical fastening and adhesive bonding can be used for joining all materials. On the other hand, welding, which requires the materials at the joint interface to melt, is only applicable to thermoplastics.

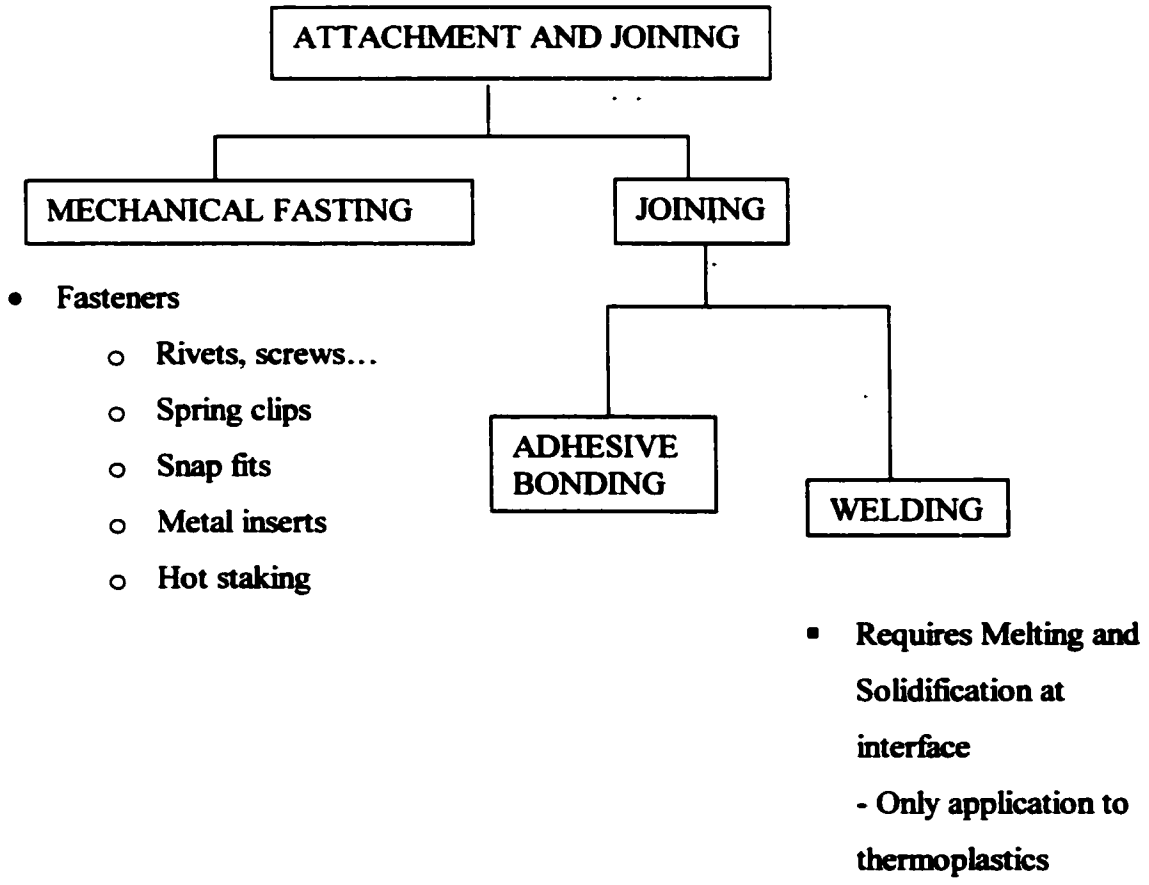

Figure 2.1 Classification of joining methods

2.1 Mechanical Fastening

Mechanical fastening can either be permanent, or consist of joints that can be opened and closed. Snap fits, spring clips, screws, rivet, and metal inserts are used to provide operable joints. Rivets and hot staking are examples of methods used for achieving permanent attachment.

2.2 Adhesive Bonding

Adhesive bonding offers the potential for joining both thermoset plastics and thermoplastics. It has been used in manifolds for many years before welding methods became better developed. Adhesives can be classified into two broad categories:

1) Two-component systems, in which the two components react chemically during the cure cycle, resulting in the desired bond.

2) Single component systems.

The most commonly used structural adhesives are epoxies, urethanes, and acrylics, which are two-component systems, and the single-component class comprising cyanoacrylates, anaerobics, and hot melts. Adhesive bonding is a relatively mature technology, in which chemistry has played an important role.

The advantages of using an adhesive are:

- Low capital costs;
- It is effective for dissimilar materials;
- It can produce hermitic seals;
- It has low residual stresses.

But the disadvantages of adhesives are:

- The curing process is generally slow;
- The consumables are expensive;
- There may be undesirable fumes;
- Preparation of the surface is a critical operation.

2.3 Polymer Welding Processes

A variety of thermal and mechanical joining processes are available for thermoplastics. Choosing the best joining method for thermoplastics requires a thorough understanding of the design, of the purpose of the joint/assembly, and of the characteristics of the joining processes under consideration. In addition, geometry of the component, nature of plastic materials used, the internal and external load, time/temperature requirement, and other environmental conditions, and specific criteria required in the final assembly have to be considered. Because welding requires melting and subsequent freezing of the materials to be joined at the joint surface, it is only applicable to thermoplastic materials.

Depending on how the heat for melting is supplied, welding can broadly be classified as:

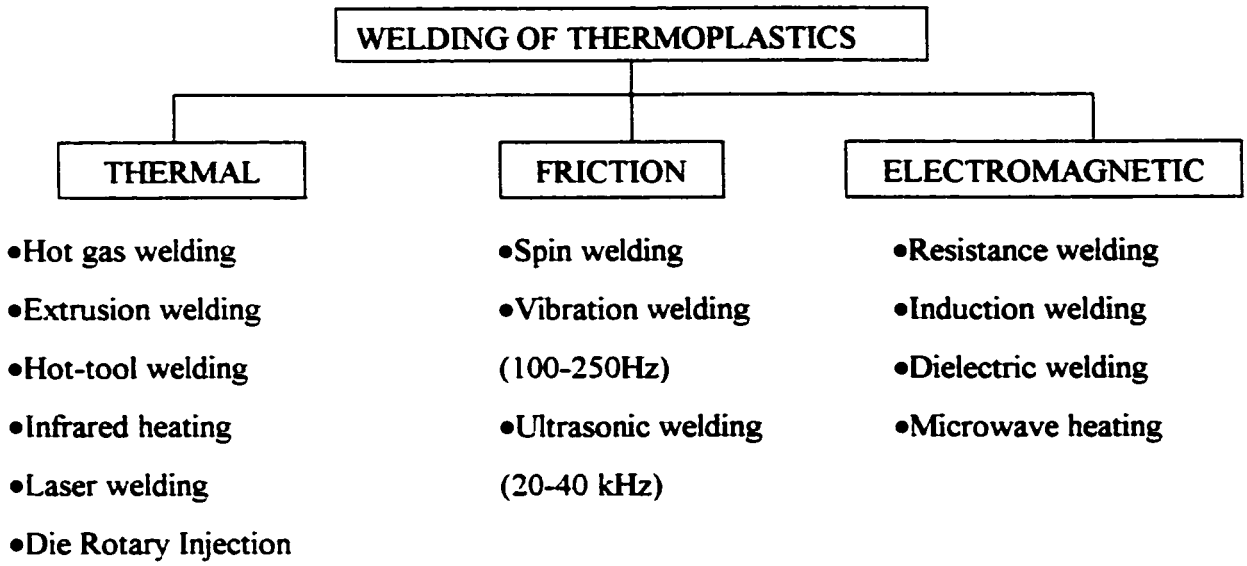

Figure 2.2 Classification of the welding of thermoplastics

Thermal bonding and friction welding are used to assemble various plastic components made from two or more pieces that are molded, extruded and/or thermoformed from similar or dissimilar thermoplastics. These joining technologies all share the following phases:

- Plastic parts are placed or nested in specially designed tools;
- Materials are heated in areas where the joints are to be formed;
- Local melting occurs in joint surface areas;
- Contacting surfaces are pressed together for joining;
- The joint interface and other areas cool;
- Welded parts are removed from the welding machine.

The type of heat generation and heat transfer distinguishes these welding technologies. For hot plate welding, the joined surfaces of thermoplastic parts are plasticized or melted prior to welding. This permits direct control of the preheating and welding temperature during the heating and fusion phases. For linear vibration welding (LVW), the temperature in the interface is a function of processing parameters. It also depends on the physical characteristics of the polymer. Another way to make a plastic intake manifold is by the DRI (Die Rotary Injection) process [10]. This process is shown schematically in Figure 2.3.

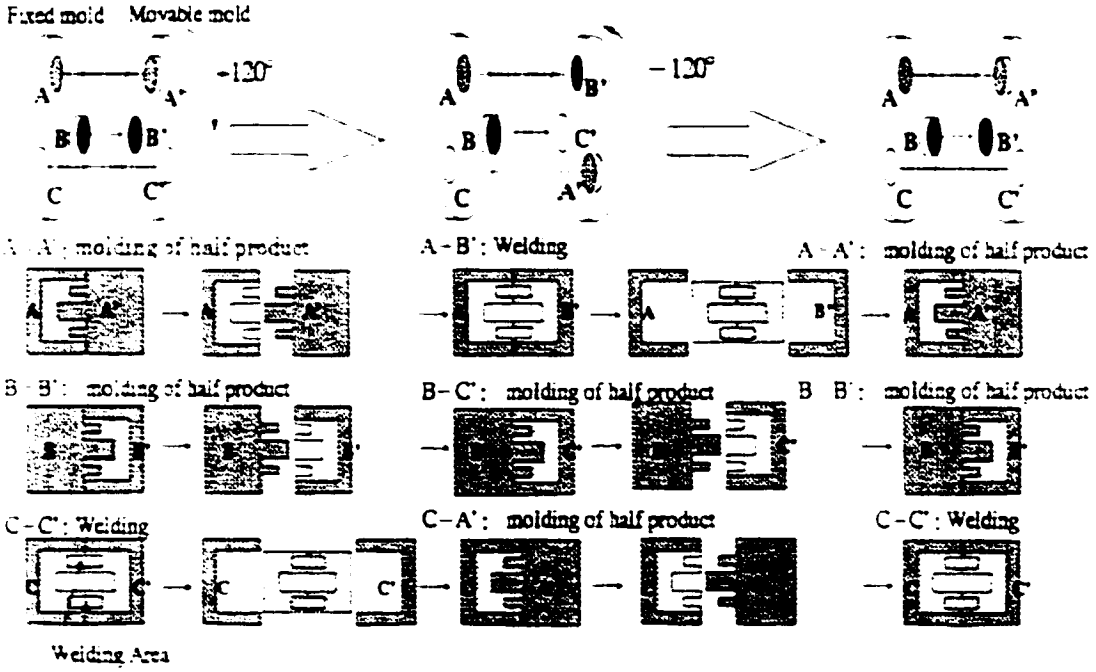

Figure 2.3 Schematic representation of the DRI process

With the molds in the initial position for this process, the upper half (A) and lower half (B') are molded. The mold is opened while retaining the molded part halves in their mold. Next, one die is rotated before the mold is closed. Finally, resin is injected in the

mold to weld the halves (A to B') together. At the same time, two new halves (C and C') are also molded in the other part of the mold. Part C is identical to A, C' is the same as B'. Rotating back to the original position, C is welded to C', and two new A and B' halves are made. In the DRI process, one completed product can be molded after each rotation of the mold. The most important point of this process is to ensure reliability of welding because the welding condition affects the morphology and mechanical properties of welding. The advantage of this process is the lower residual stress. This means the welding strength can be very high. However this process is complex and with high capital investment.

2.4 Linear vibration welding (LVW)

In 1979 [11] France's Peugeot Citroen became the world's first automaker to apply the vibration welding process to air intake manifolds (AIMs). Since this time, Europe has remained the biggest proponent of this technology. A survey [12,13] has shown that by the year 2001, at least 50% of all AIMs will be made of polyamide plastics. Plastics held a 45% share of the Europe AIMs market in 1997, compared with only 25% in North America and 4% in Asia. Welded nylons typically provide weight savings of up to 55%, as well as reductions in production costs.

The growing popularity of LVW in the auto industry can be attributed to its flexibility and low cost. Linear vibration welders are complete plastic assembly systems.

They can be designed to join large or irregularly shaped thermoplastic parts. Additionally, LVW is a fast joining process, with cycle times on the order of 0.5 to 12 seconds. Typical cycle times are 30 seconds, including both welding and cooling time, which is approximately 1/50 the cycle time of other methods, and substantially less energy is required. This makes LVW considerably more cost effective than the hot plate process.

2.4.1 A detailed introduction to LVW technology

LVW is a reliable joining method for injection molded, blow molded and extruded thermoplastics, and is particularly good for hollow components. In the LVW of thermoplastics, frictional work done by vibrating two parts under pressure, along their common interface, is used to generate heat to effect welds. In common applications the vibratory motion is along the weld seam, which is at right angles to the thickness direction for straight and near straight boundaries, as schematically shown in (Figure 2.4). In many applications, such as in the welding of closed seams of box-like or tubular parts, the linear vibratory motion used for generating frictional heat also occurs along the part-thickness direction.

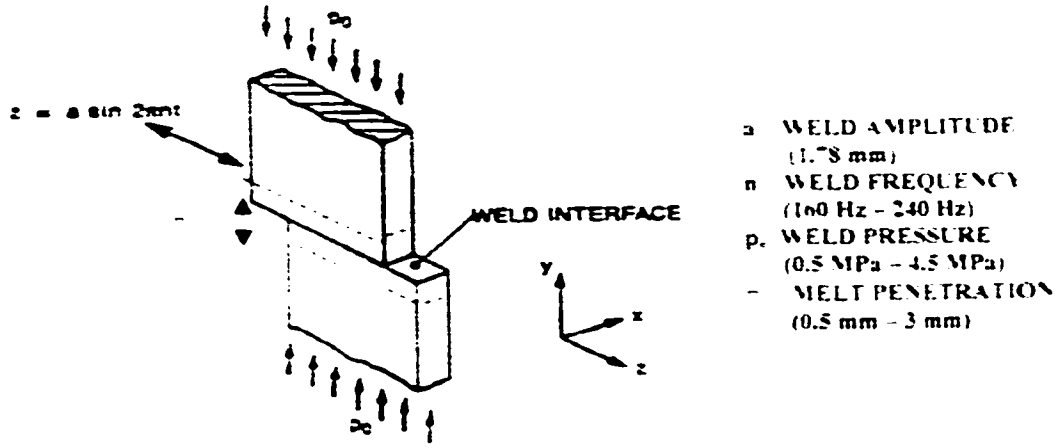

Figure 2.4 Schematic representations of part geometry and motion in vibration welding

LVW equipment, tools and nests are not very expensive, and the welding process itself is not time consuming. It is a PC-controlled process [15], with sensors scanning the positions and automatically reporting the key welding process parameters. Most vibration welding systems are electrically driven and consist of three major components: a vibrator assembly suspended on springs, power supply, and a hydraulic lifting table. The vibrator assembly is a moving element with no bearing surfaces and consists of two electromagnets, which provide alternating energy to both ends of a system of springs. The springs resonate at the frequency of the electromagnetic energy, support the vibrator assembly against vertical welding pressures, and provide precise alignment between parts to be welded by returning the vibrator assembly to its home position at the end of the welding cycle. One of the parts to be welded is attached to the vibrator assembly; the other part (the stationary element) is clamped onto the hydraulic table. Most industrial vibration welding machines operate at weld frequencies of 120 to 240 Hz, although welding machines with higher frequencies are also available. The amplitude of the

vibration is usually less than 5 mm (0.2). Amplitude and frequency are dependent on the geometry of the parts to be joined and are set to attain a maximum frictional force. For the welding cycle, the hydraulic table (the lower tooling) rises up and applies pressure to the vibrating element (the upper tooling). After solidification of the weld, the hydraulic table is lowered, and the welded part is unloaded. A complete cycle normally takes 15-20 seconds.

However, the welding temperature at the interface during the linear vibration process is not a directly controlled parameter in the standard welding equipment available.

2.4.2 Vibration welding process analysis

In linear vibration welding, the surfaces to be joined are rubbed together in an oscillating, linear motion under pressure applied at a 90^0 angle to the vibration. Process parameters are the vibration amplitude and frequency, weld pressure, and weld time, all of which affect the strength of the resulting weld.

Dr. V. J. Stokes identified four separate phases (Figure 2.5) in his description of the linear vibration welding process[14].

In Phase I, (Solid/Solid frictional heating), Coulomb friction generates heat at the interface, raising its temperature to the point at which the polymer can undergo viscous flow. During this phase, the penetration, which is the distance by which the parts

approach each other, h = h(t), is effectively zero. In Phase II, (the transitional phase), the interface begins to melt and the mechanism of heat generation changes from solid Coulomb friction to viscoelastic dissipation in the molten polymer. The molten polymer begins to flow in a lateral direction, resulting in an increase in the weld penetration, as a result of this lateral flow.

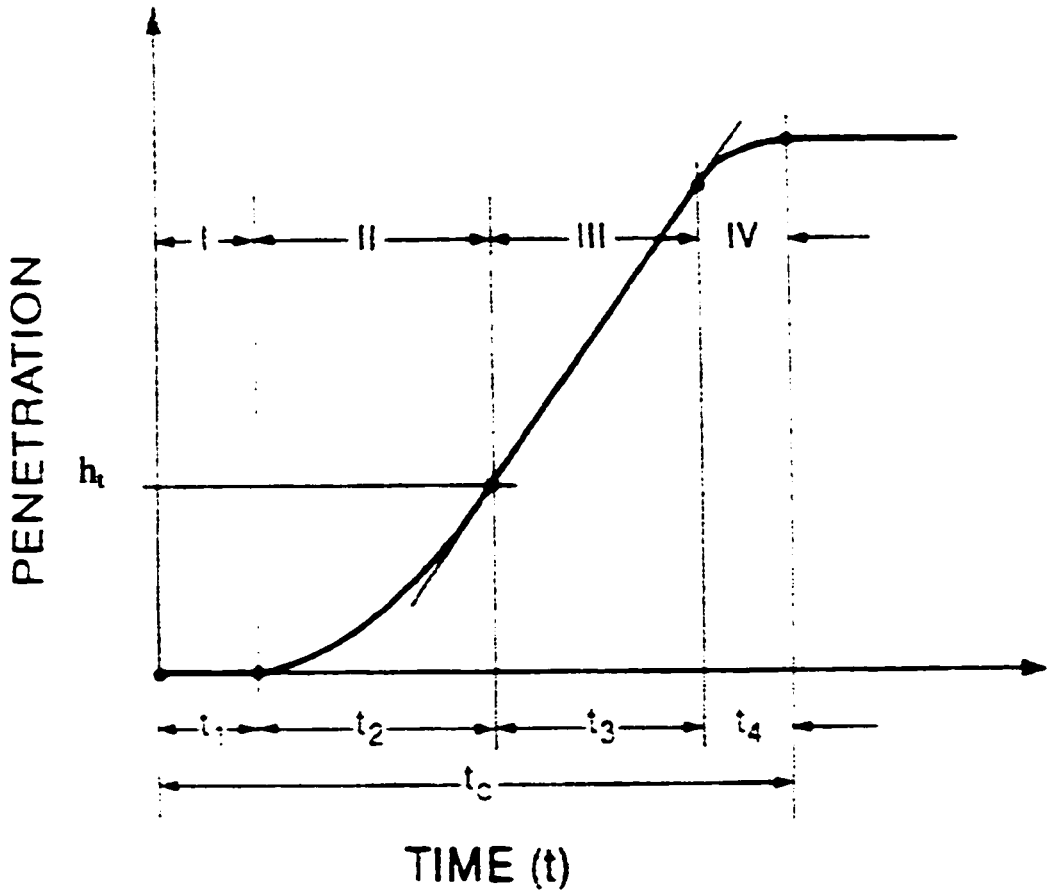

Figure 2.5 Schematic penetration-time curve showing four phases of the vibration welding process (after Stokes)

During this unsteady phase, in which heat is generated by viscous dissipation, lateral outflow of the molten polymer results in the penetration rate increasing from zero

to a value h_t. In Phase III, the steady state shear heating phase, the melting and flow occur at a constant rate, and the weld penetration increases linearly with time. At the beginning of Phase IV, when the machine is shut off, hold-phase solidification occurs, but the weld penetration continues to increase because the weld pressure causes the molten film to flow until it solidifies. The welding of dissimilar materials, chopped glass fiber filled materials, and structural foams also exhibit these four phases.

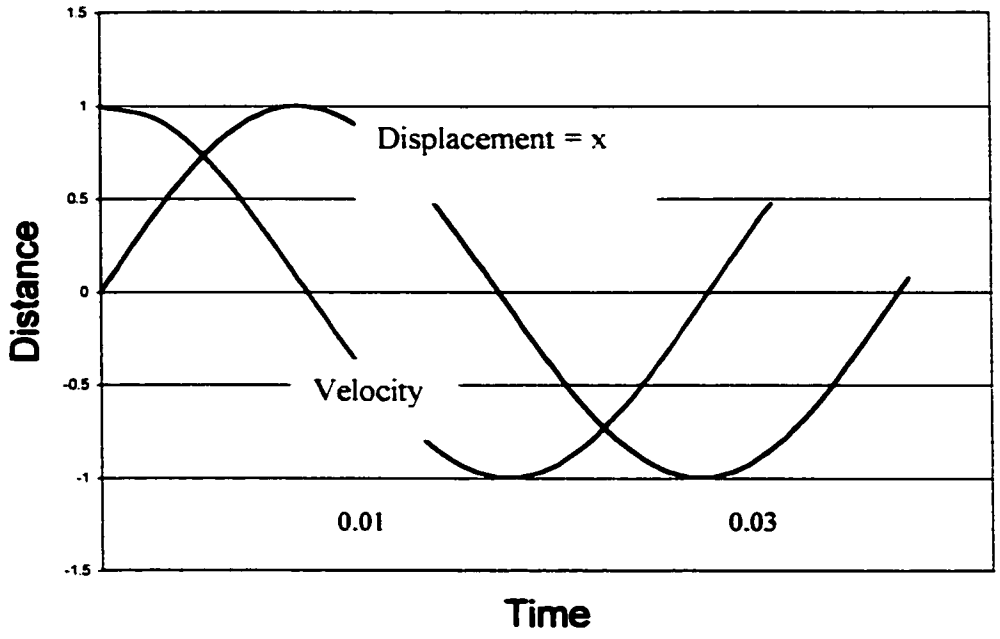

Figure 2.6 Relative motion of the linear vibration showing the relationship between position and velocity

Figure 2.6 shows that the relative motion of the linear vibration is:

$$x = A * \sin(\omega t) \qquad (1)$$

where x is the distance of the moving part from its original position, A is the vibration amplitude, ω is the frequency and t is time. From Equation (1) , we can easily find the relative velocity (v).

$$v = dx/dt = A\omega.\cos(\omega t) \qquad (2)$$

Another important definition is coefficient of friction, illustrated in Figure2.7.

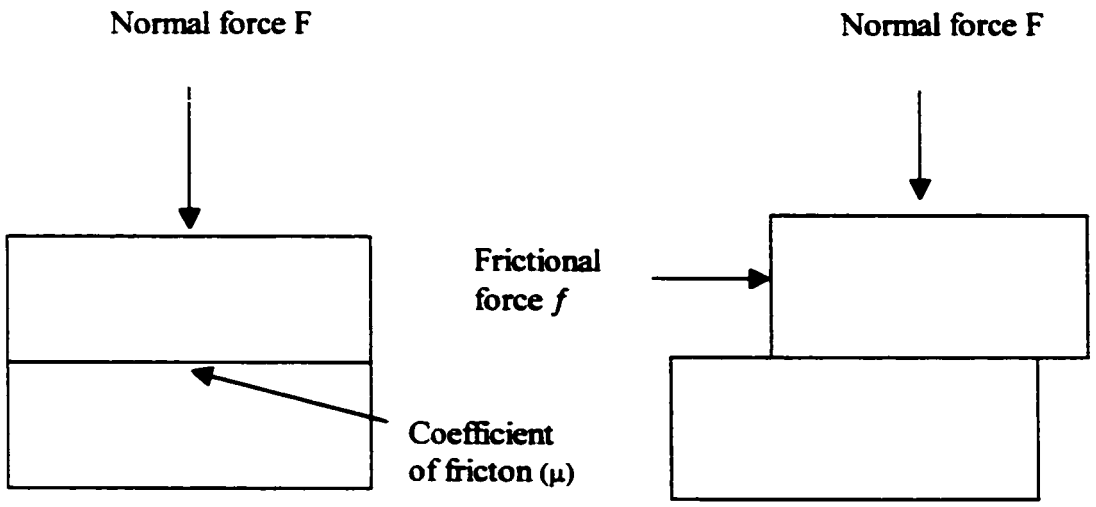

Figure 2.7 Definition of friction

When a normal force is applied to the upper part and then this part is forced to move relative to the lower fixed part, friction is produced at the common interfaces of the two parts. In the welding process, frictional work is related to the coefficient of friction of the material. There are two frictional coefficients involved; static and dynamic. Dynamic friction is responsible for the production of heat, so the frictional force is:

$$f = \mu F \qquad (3)$$

where f is the frictional force applied parallel to the rubbing surfaces (shear force), and μ is the dynamic coefficient of friction.

In Phase I, the energy produced is equal to the frictional force times the relative velocity.

$$P = vf \qquad (4)$$

P is the power required to drive the process, and this is dissipated as heat.

Putting Equation (3) into Equation (4) gives

$$P = \mu F v \qquad (5)$$

And then combining Equations (2) and (5) gives

$$P = \mu FA\,\omega\cos(\omega t) \qquad (6)$$

Equation (6) shows that the power produced in Phase 1 is proportional to the clamping force, the vibration amplitude, the frequency, the coefficient of friction and the time during which the vibration is sustained.

P is the average power, so

P = Average power = Power in one cycle/Radians in one cycle

$$P = \frac{1}{2\pi}\int_0^{2\pi} \mu FA\omega\cos\omega\, td(\omega t) \qquad (7)$$

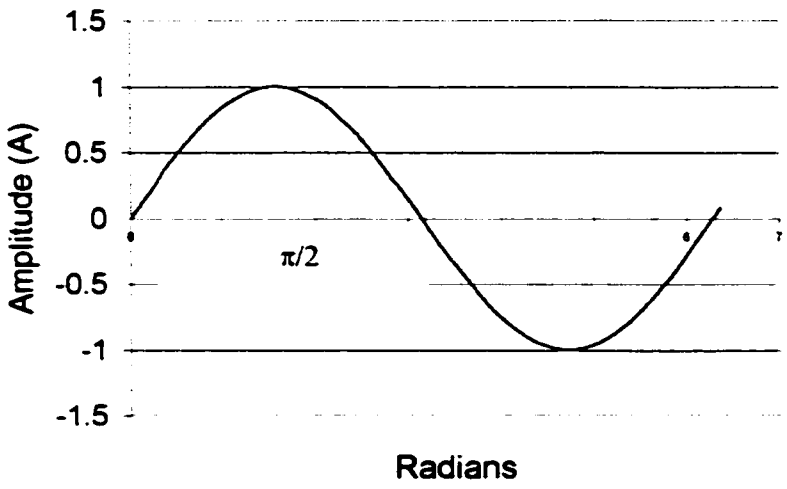

Figure 2.8 One cycle of welding vibration amplitude

$$P = \frac{\mu F \omega}{2\pi} \times 4 \times \int_0^{\pi/2} A\cos\omega t \, d(\omega t) = \frac{4\mu F \omega}{2\pi} {}_0^{2\pi}[A\sin\omega t] \qquad (8)$$

$$P = \frac{4\mu F \omega}{2\pi}[A - 0] = \frac{2\mu F \omega A}{\pi} \qquad (9)$$

Thus, Equation (9) describes the average power.

Phase II is a transitional phase. Material at the interface begins to melt and flow in a lateral direction, and the heat generated is dissipated in the molten polymer. This viscous flow begins to increase the weld penetration, the distance through which the parts approach each other (the meltdown).

In Phase III (see Figure 2.9), melting and flow attain a steady state, and the weld penetration increases linearly with time. Heating is produced by the shear rather than by solid/solid friction. During this phase the liquid material acts as a lubricant to reduce the

forces required to move the surfaces parallel to each other. Heating is caused by viscoelastic heating in this liquid. In this steady condition, the rate at which the liquid is produced is equal to the rate that the liquid is squeezed out by the clamping pressure. At the end of Phase III, the vibratory motion is stopped.

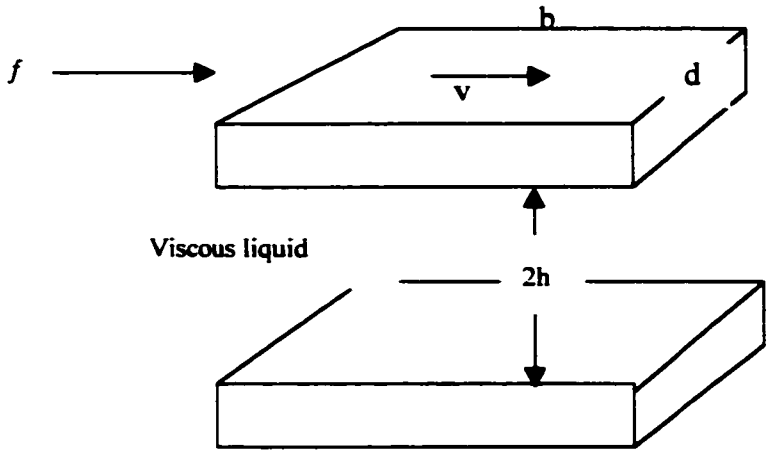

Figure 2.9 Schematic diagram to illustrate the geometry assumed for shear. The upper block (with lower surface area bd) floats on a layer of viscous liquid.

In Figure 2.9, assuming a Newtonian fluid with temperature independent viscosity, the shear force is:

$f = \vartheta \eta$ (Newton's law of viscosity)

Where $\tau = \frac{f}{bd}$ (11)

The shear strain rate $\vartheta = \frac{v}{2h}$ (12)

In above 2h = the melt layer thickness

B = length off the weld interface

D = width of the weld interface

η = viscosity

f = the horizontal force on the upper plate

v = upper plate velocity

ϑ =shear strain rate

τ = shear stress

From Equations (10), (11) and (12), the equation for shear force f , it is clear that the velocity v is a linear function of the horizontal force.

$$f = \frac{\eta v}{2h} bd \qquad (13)$$

Because the power equals the force times velocity

So $$P = f\, v = \frac{\eta v^2}{2h} bd \qquad (14)$$

The power/unit area $$Q = \frac{P}{bd} = \frac{\eta v^2}{2h} \qquad (15)$$

Putting Equation (1) into Equation (15), it can be found that the heating in Phase III is

$$Q = \frac{\eta A^2 \omega^2 \cos^2(\omega\tau)}{2h} = \frac{\eta A^2 \omega^2}{4h} \qquad (16)$$

During Phase IV, no more heat is generated, but the weld penetration increases slightly as the molten film solidifies under pressure.

From Equations (9) and (16), it can be concluded that in Phase I, heating is a function of F, ω, A. In Phase III, heating is a function of ω^2 A^2. These relationships will be made use of in the regression analyses in Chapter 5.

2.5 Material requirements related to welding joint performance

For vibration weld joint technology, the most important requirements for the welded materials are:

1. Types of materials to be joined (similar, dissimilar);
2. Thermoplastic compositions (type of matrix, types of fillers and reinforcement);
3. Optimized content of reinforcement elements, fillers and additives, pigments, etc;
4. Short- and long-term mechanical properties of joined materials and mechanical properties of matrix with the influence of loading, welding, time/temperature, and environment conditions;
5. Dimensional stability of joined materials.

In general, manufacturers of plastic air-intake components and manifolds are looking for tensile strength values of 50-60 MPa at ambient conditions of 23 C to match the mechanical performance of aluminum [15,16]. The performance of the welded joint has a major impact on the ability of manufacturers to meet these requirements. As a base material, 30-35 wt % glass reinforced nylon PA6/PA66 products meet the above mentioned tensile strength requirements.

In order to optimize vibration-welded joint performance for highly stressed structural components, material properties and part-production techniques must be carefully evaluated. The most important parameters for the plastic joints are:

1. Joining and production (molding and welding) flexibility for multi-piece parts;
2. Specific performance requirements (strength, life/durability, chemical resistance, mechanical test conditions, etc) for the vibration welding plastic components and for the assembled parts;
3. Desirable level of welded-joint hermetic seal (burst and backfire pressure);
4. Specific requirements of welded-joint geometry (shape, size, and stiffness);
5. Short-term mechanical properties of joints by tensile, flexural, or combined-load conditions, and impact-strength criteria;
6. Long-term mechanical properties of joints by creep and fatigue strength and life criteria;
7. Noise, vibration and harshness (NVH) performance;
8. Desirable level of quality in weld areas (internal and external surface smoothness;
9. Appearance aspects (no defects, cracks, voids, inclusions, etc.)

Another important design and material requirement for vibration-welded AIMs is dimensional stability. Post-mold warpage will impact the tolerances of joined surfaces. This in turn will affect clamping and welding pressure conditions, and will contribute to the creation of residual stresses. In order to optimize vibration welding process parameters and increase welding joint performance, it is necessary to analyze the part for possible

warpage and its effects on the geometry of joints/surfaces. The contributions of tooling design and molding conditions to warpage should also be examined.

CHAPTER 3
TESTS FOR THE EVALUATION OF WELD STRENGTH

This chapter discusses the machines, fixtures, and standard testing methods used in this project.

3.1 Welding machines and weld geometries

Four different geometries of welds were used in this research: Shear-lap, T-weld, butt joint and CWF. The geometry of these samples are shown in Figure 3.1.

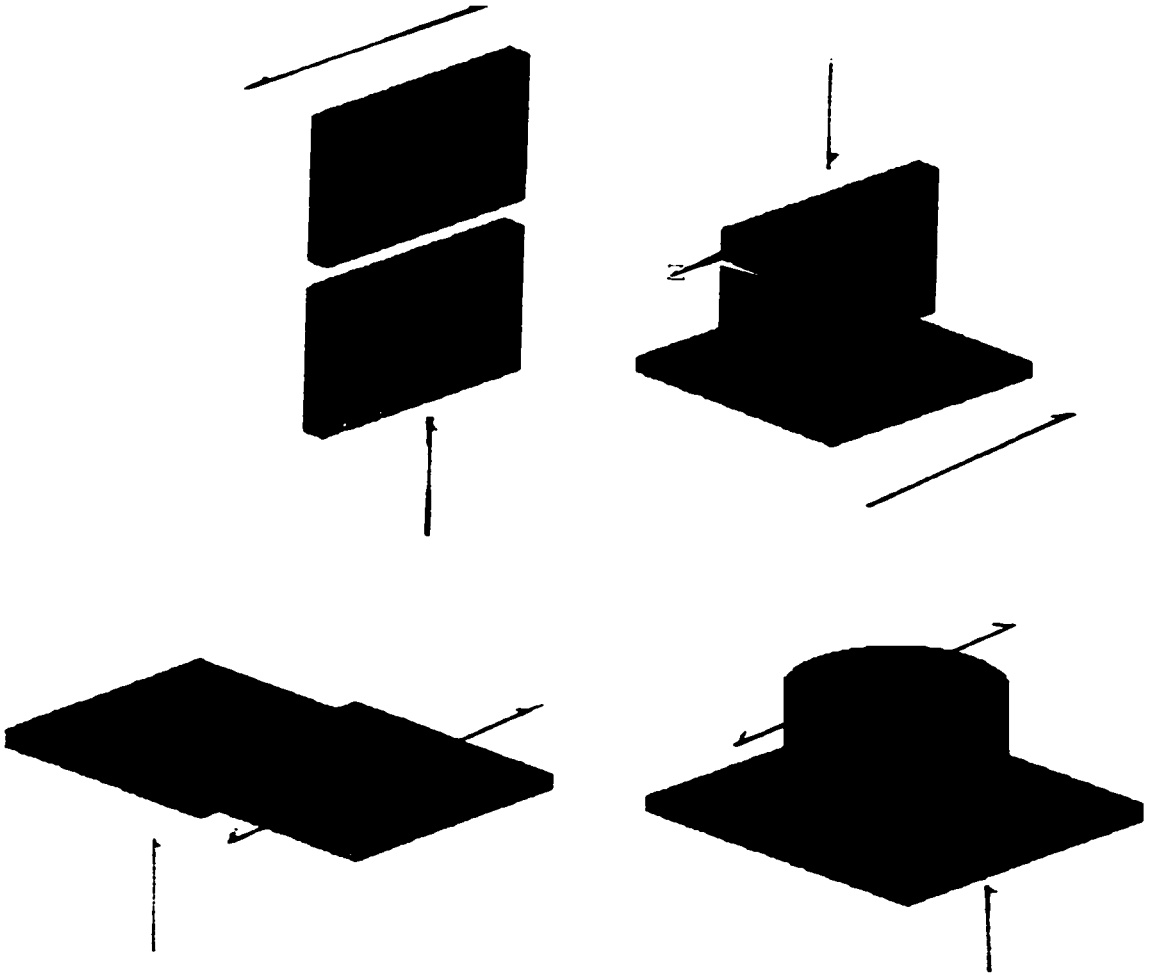

Figure 3.1 The four different weld geometries are, from the upper left in clockwise order: butt weld, T-joint weld, cup welded to flange (CWF), shear lap weld.

Typically, linear vibration welding (LVW) machines combine all the advantages (of vertical, or horizontal) design for joining components made from similar or dissimilar plastics. The size of parts that can be joined vary from very small (such as fuel filter reservoirs) to very large (such as car crossbeams)

In the present research, all the vibration welds were accomplished on a pneumatic Branson linear vibration-welding machine (Model MINI II). (Figure3.2).

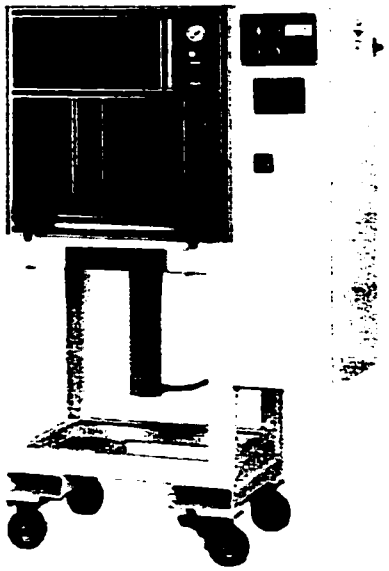

Figure 3.2 Mini-Vibration Welder Model MINI II

The process was time controlled, with an adjustable weld force holding the two parts in contact. The welding force (during Phases 1-3) and the hold force (during Phase IV) were equal and fixed during any given test. For the T-welds, the welding set-up involved the vertical plaque clamped in the lower holder, and the horizontal flange was balanced on the vertical plaque until it was pushed up against the upper plate. When the table was raised, the horizontal plaque was pressed against sandpaper backing to keep it from sliding during the welding process.

For butt-joint welds, the two 127 mm by 76 mm plaques or the two 102mm by 51 mm plaques were clamped independently in the upper and lower fixture. The welds were made along the longer dimension of the two half-samples. Similar and dissimilar material combinations were welded. Just before the end of the hold time, the upper clamp was released so that the air cylinder did not pull on the welded parts as it moved back down to its starting position.

Meltdown distance (the distance which the two parts penetrate into each other) was neither controllable nor measurable during the welding in this set of tests. It has been calculated by subtracting the final height of the welded T sample from the corresponding initial dimensions of the two parts before welding.

3.2 Tensile tests and fixtures

Welded T-samples and butt-joint samples, both 102 mm long, were cut into three 25mm wide strips suitable for tensile testing, leaving two strips 10 mm wide suitable for cross-sectional examination for glass orientation and flash shape and size. As well, a number of photographs of the tensile samples were taken so as to record the flash shape and size created on several of the tensile samples. Before tensile testing, the flash was carefully removed (T-sample) from each individual tensile sample using a utility knife and it was then weighed. The tests were carried out on an Instron screw driven tensile machine (Figure 3.3) using either a 1000 lb load cell or a 20000 lb cell. The cross-head speed was 2.54 mm/min.

The ultimate tensile fracture strength was found by dividing the fracture load by the weld area (sample width times the thickness).

Figure 3.3 Instron machine set up for T joint testing

There are two kind of testing fixtures designed for T-welds. Both test fixtures had a 55 mm by wide slot to accept the horizontal plaque of the T joint sample. The vertical leg was pulled downward by the standard Instron grip. On one of the upper fixtures (a,b) the slot for the leg is 3.6mm wide; on the other (c) it is about 6.5 mm (see Figure 3.4).

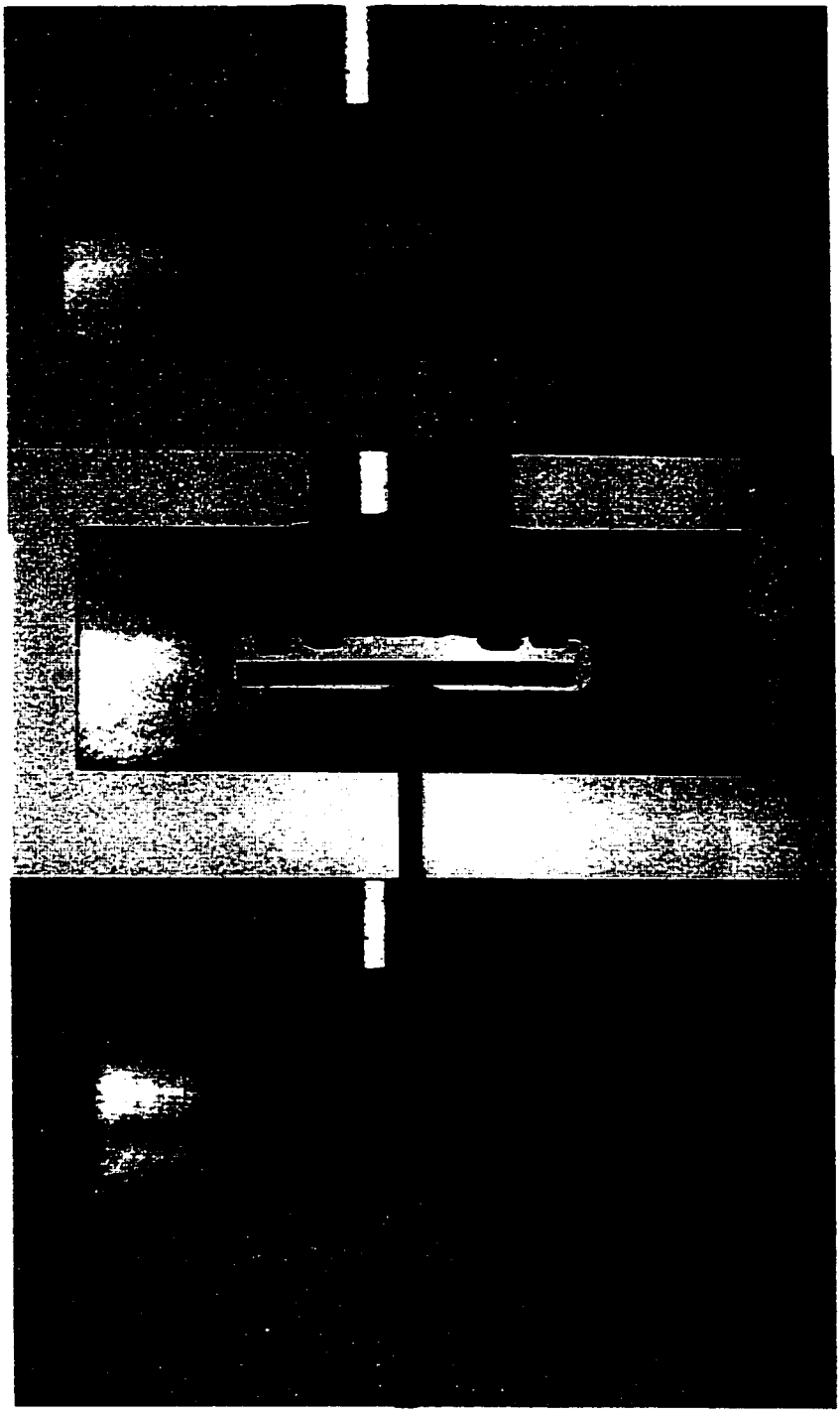

Figure 3.4 Two different T-joint testing fixtures showing sample set up for Test type a, b and c respectively. Valerie's tests were done in a holder similar to the type c fixture.

CHAPTER 4
PREVIOUS WORK ON THE WELDING OF DISSIMILAR MELTING TEMPERATURE MATERIALS

4.1 A description of amide materials

The purpose of this research is to find the weldability of high melt point nylon or several high melt temperature nylons (PPA) with nylon 6, or nylon 66.

Nylons are melt-processable thermoplastics whose chain structure features repeating amide groups. As engineering thermoplastics, they offer a combination of properties, including high strength (especially at elevated temperatures), toughness at low temperature, stiffness, wear and abrasion resistance, low coefficient of friction, and good chemical resistance.

Nylon 66 is a semi-crystalline polymer consisting of two phases: (1) an amorphous phase which can be described as being highly viscous and liquid-like with no crystalline order and (2) a crystalline phase, relating to the degree of ordered three dimensional structures. In the crystalline lattice, molecules are folded forming thin ribbon, or layer, shaped crystals called lamellae. The lamellae aggregate into spherical stacks or clusters called spherulites. The size and abundance of spherulites are dictated by a number of variables including the cooling rate of the material when it is processed; moisture and temperature effects and applied stress.

Polyphthalamide resins [17] are semi-aromatic polyamides based on terepthalic and or isophthalic acids. They are available in both semi-crystalline and amorphous versions,

with glass transition temperatures in the range of 124 C. The amorphous versions are used primarily in applications requiring barrier properties. The semi-crystalline resins are predominantly processed using injection molding, although other melt processes have been used. Semi-crystalline PPA resins have a melting point of about 332 C.

PPA resins are stronger, stiffer, much less sensitive to moisture, and much higher in thermal capability than are aliphatic polyamides. They also have significantly better creep, fatigue and chemical resistance. PPA resin is less ductile than nylon 66.

All polyamides absorb moisture to some degree, resulting in plasticization and dimensional change. For example, nylon 66 absorbs 8.9% moisture at 23 C and 100% relative humidity. This decreases its glass transition temperature from 65 C to –20 C and increases its linear dimensions by 2.3%. Under the same conditions, PPA resin absorbs approximately 6% moisture, but its Tg does not drop below + 40 C. The associated dimensional increase is less than 1.0%.

PPA resins generally exhibit excellent resistance to aliphatic, aromatic, and chlorinated hydrocarbons, esters, ketones, alcohols, and most aqueous solutions, under most environmental conditions.

From the analysis above, it is clear that the key advantages of high temperature nylons (PPA) are:

- Improved dimensional stability.
- Superior creep resistance.
- Lower thermal expansion.
- Retention of properties in the presence of moisture.
- Higher short term and long term heat resistance.
- Improved thermal and humidity aging.
- Improved electrical properties.
- Fast cycle in molding performance.

The low temperature nylons used in this research are Zytel 73G30 (PA6), 70G33 (PA66) manufactured by Dupont as well as materials from other companies. Appendix 3.1 lists the materials used in this project.

4.2 Review of previous work

Previous work on vibration welding [18,19] focused on trial welds combining different materials together to find the potential for welding dissimilar materials. These tests mainly used the same vibration welding process parameters to provide a simple survey of the joining process. Different material pairs, chosen from a material combination

matrix, were welded as Tjoint samples or as cup–welded-to-flange (CWF) specimens. The purpose was to survey how much strength can be developed in welds made from pairs of glass filled amides with dissimilar melting temperatures.

The highest weld strength, 29.2 MPa, occurred in T-joint samples with the 70G33/A1340 material combination, with the A-1340 material being the horizontal plaque (flange). This same combination but with the two materials reversed, resulted in a 26% decrease in weld strength. The second strongest welds were found to be in all following T-joint material combinations; 70G33/A-1133, 73G30/A-1133, and 73G30/A-1340, where the average weld strength was approximately 25.6 MPa. In all of these dissimilar weld pairs, the higher strength occurred when the horizontal plaque is made of a high temperature material. When the materials are reversed in position, the fracture loads decreased by 23%, 14%, and 25%, respectively for the second strongest group.

So from this previous study, carried out as a senior undergraduate project, this interesting and significant result was determined. For materials with different melting temperatures, consistently stronger welds were obtained when the web (leg) of the T weld or the cylinder on the cylinder-on-plaque welds were made from the lower melting point material. Lower strength welds always resulted when the web (T-welds) or the cylinder (WCF) was the higher melting point material. This is surprising because the latter case resulted in considerable penetration of the web (or cylinder) into the flange (or plaque) (Figure 4.1a, and Figure 4.1b).

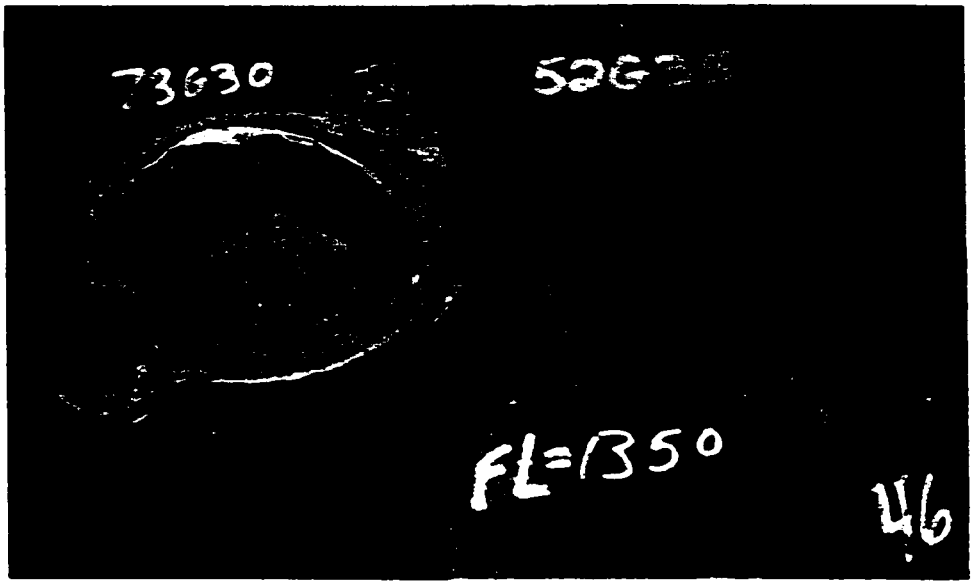

Figure 4.1a

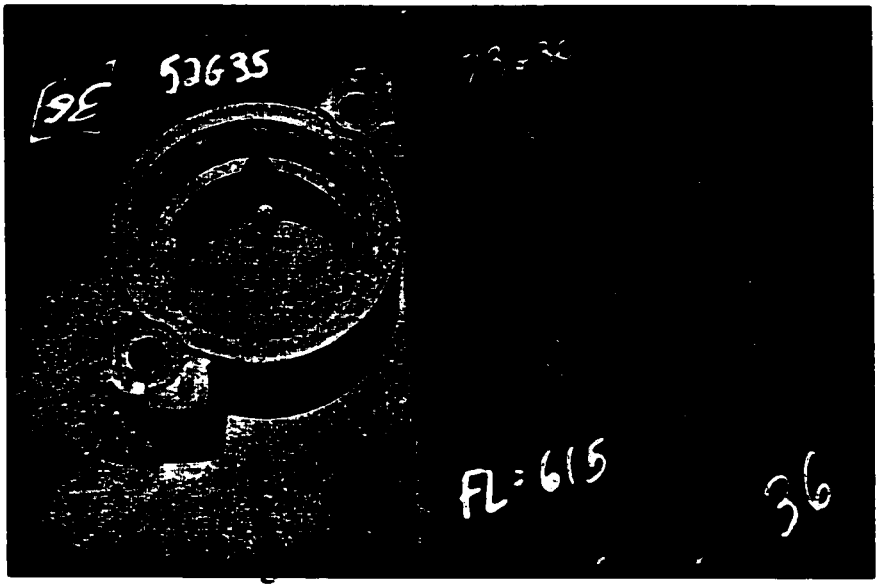

Figure 4.1 The material 73G30 is nylon 6 (T_m=223C) with 30 % glass fiber, 52G35 is a high temperature nylon (T_m=310C) with 35% glass. The is almost no penetration of the cup into the flange in Figure 1a, whereas in Figure 1b a trough more than a mm deep was created.

In the former case the lower melting temperature web or cylinder made very little ingress into the flat horizontal arms or plaque.

4.3 Shear-lap welds

Shear-lap welding was also done in the same previous study. Figure 4.2 shows the photographic results of the mounted and polished samples. The welding parameters are listed in Valerie' s report. [18] In most cases, the different shades of the materials used allow for the identification of the weld interface, and determine which materials provided the greatest contribution to the weld depth.

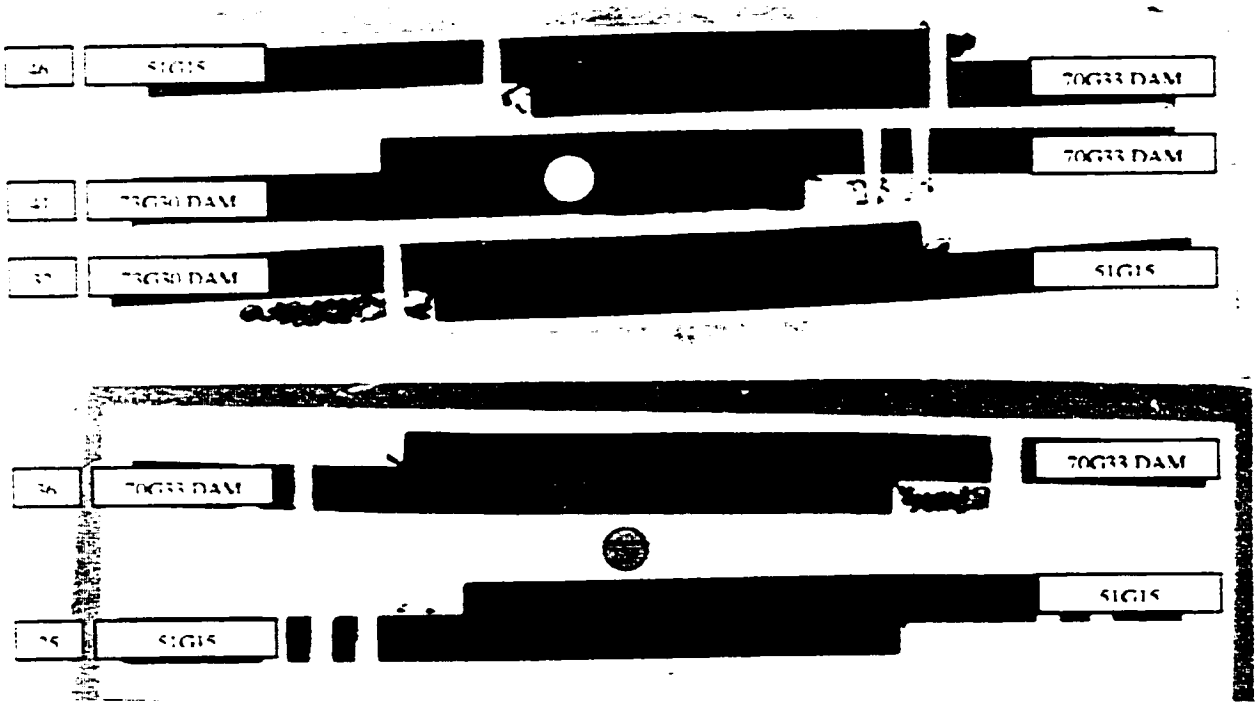

Figure 4.2 The polished cross-sectional areas of the shear lap welds provides information on the interface microstructure. The sample number is indicated in the boxes on the far left and far right hand side.

Samples 25 and 32 have the greatest melt temperature difference (78 C) and it is evident that the HTN 51G15 sank into the 73G30 and barely changed shape during the welding process. The materials of sample 46 have a lower melt temperature difference of 38 C, but still show the characteristics of the two previously mentioned samples. Sample 41, which is a weld between PA6 and PA66, having a melt temperature difference of 39 C, should also behave in the same way, but it is difficult to confirm since the weld interface is hard to identify. Looking closely at the left end of the weld, you can see the upper plaque penetrating into the lower one. This is an indication, as expected, that the lower melt temperature material contributes more to the weld depth. As for the similar material welds, the only visible weld interface is between the HTN51G15 where porosity seems to be present in the weld. Results from the scanning electron microscope confirm this (Figure 4.3) and uncover some other interesting facts. Figure 4.4 is from a different position on the same sample showing similar porosity, and also that each plaque has different glass fiber orientation.

Figure 4.3 Porosity at weld interface of 51G15 weld (Sample 25) x250

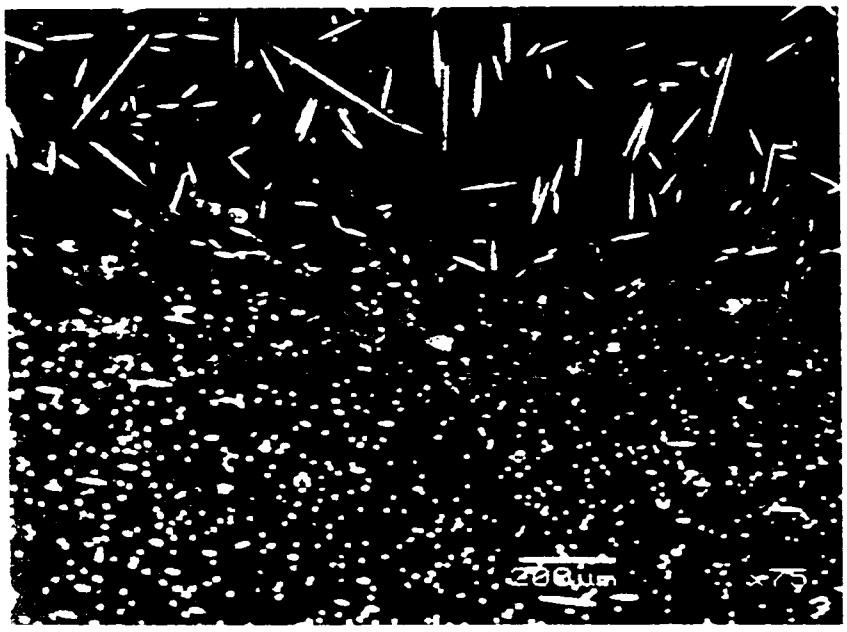

Figure 4.4 Weld interface of 51G15 material (Sample 25) x75

It is presumed that since the original plaques were cut and mismatched, one of the sections may have been at a different location relative to the injection gate than the other. Also, this magnification reveals that the glass fibers did not align with the plastic flow as did the fibers in the 70G33 similar material weld (Figure 4.5).

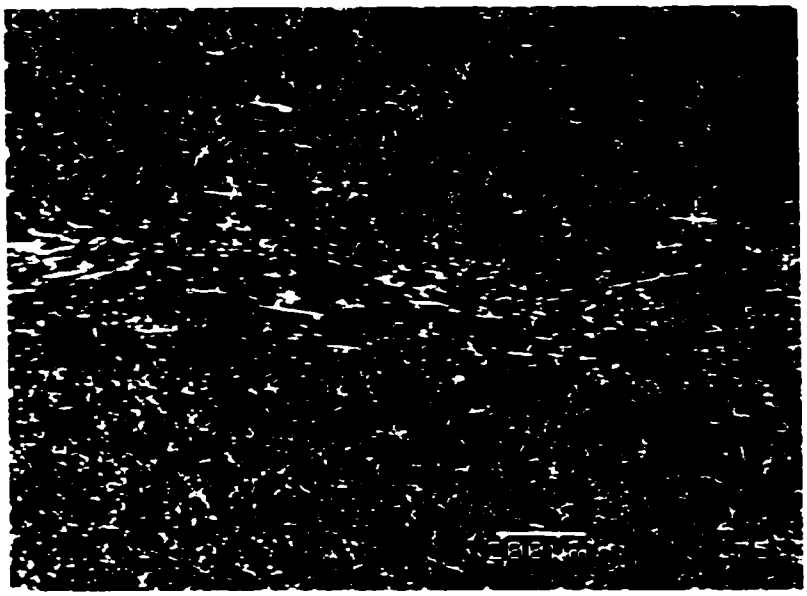

Figure 4.5 Weld interface of 70G33 material (Sample 36) x75
The direction of vibration is perpendicular to the page.

As previously mentioned, this alignment of the glass fibers parallel to the weld interface is a factor causing lowered tensile strength of glass-fiber-reinforced welds compared to that of the base material. The direction of fibers could be caused by rolling like logs during vibration, or orienting themselves with the flow of the plastic when it is forming flash. Figure 4.6 is the interface of a dissimilar material weld between 70G33 and 51G15, where there seems to be some alignment of the glass fibers with the plastic flow. The magnification of the dissimilar material weld between 73G30 and 51G15 (greatest melt temperature difference of these tests) is shown in Figure 4.7. In this case, there is minimal alignment of the glass fibers. The area shown had a much greater amount of aligned fiber than the rest of that interface.

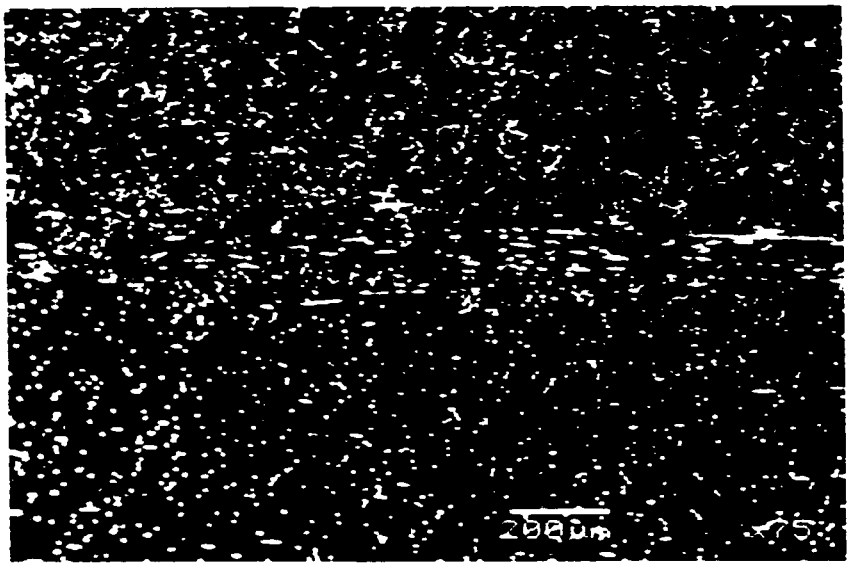

Figure 4.6 Weld interface of 70G33/51G15 weld (Sample 46) x75

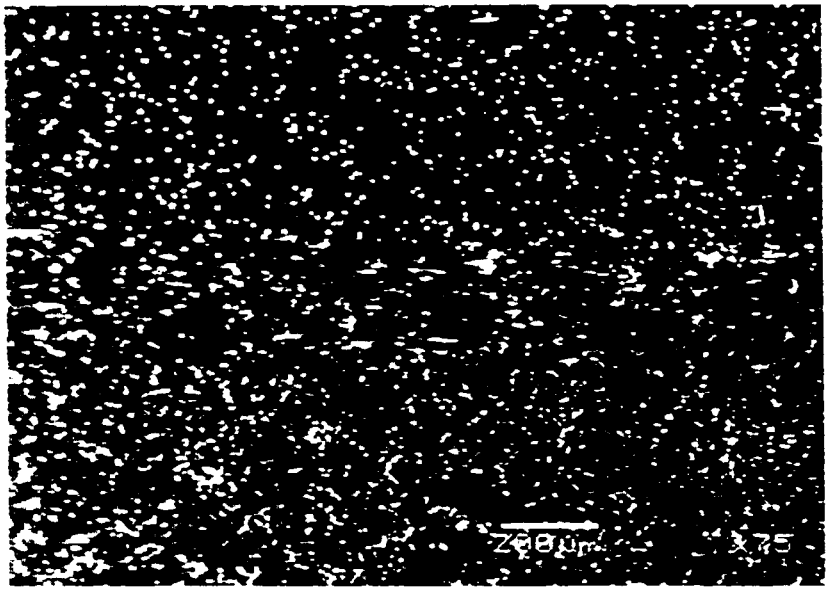

Figure 4.7 Weld interface of 51G15/73G30 weld (Sample 32) x75

CHAPTER 5
DESIGN OF EXPERIMENT TESTS RESULTS AND ANALYSES

In Chapter 2, the linear vibration welding process has been described according to the analysis of Stokes. This consists of four stages, of which the first three are mechanisms for heating:

- Friction heating in which the solid surfaces are rubbed against each other under the clamping pressure
- A brief transitional phase in which some of the interface has melted, and which is complete when the interface is completely melted to a stable thickness
- A steady state period in which the vibration heats the interface through viscoelastic hysteresis losses.

The final stage consists of holding the two parts together under pressure with no relative motion (other than meltdown), so that the molten material can freeze so as to make the weld.

For high performance LVW joints, certain processing and weld interface parameters are critical. The independent process parameters that can be adjusted are:

- Welding amplitude (A), in inches (or mm);
- Weld pressure (P), in psi (or MPa);
- Welding time (Wt) (which includes all three heating phases), in seconds;
- Hold time (Ht), in seconds.

Note that the relative amount of time spent in each of the heating phases is a dependent parameter, and will vary with clamping pressure and welding amplitude. Other important process parameters that are not (easily) adjustable include:

- Temperature;
- Stable thickness of the heated viscoelastic layer at the interface during steady state heating (Stage 3), in microns;
- Meltdown, which is governed by the rate at which liquid is squeezed out of the interface in the steady state phase;
- Vibration frequency, in Hz (typically in range from 120 to 240 Hz) which is fixed by the natural oscillation frequency of the upper fixture;
- Direction of oscillation/linear vibration (parallel or perpendicular to thickness of wall/bead, or other angle). This is controlled by the contours of the weld interface.

Of these, the meltdown rate is obviously a function of the temperature and thickness of the interface layer, and of the clamping pressure. The temperature is governed by the balance between the heat generated from interfacial movement, conduction loss to the adjoining plastic, and material loss through meltdown.

In this chapter, an attempt has been made to correlate the quality of welds produced with the independent process parameters listed above, and also with the meltdown.

The objective is to determine the relationships among the process parameters and the quality of the welds produced for a given plastic, so that the weldability of that material

can be included in the design of a part [20]. Assessing material performance in the vibration welding process, so as to define the weldability for use as an evaluation reference tools, is done making use of the Design of Experiments (DOE) method[21-23]. DOE provides two tenets: 1) the reduction in variation (improved quality) of a product or process represents a lower scrap loss, and 2) the proper development strategy can intentionally reduce variation.

Weldability includes the following definitive components:

- Weld strength
- Location of the failure surface of the welded tensile test
- Marking on class A surface, or non-aesthetic flash discharge
- Machine power requirement for welding.

If the last mentioned criterion is above a certain level, it can result in a machine over-load condition, or in non-economic energy usage.

In the present work, a DOE study was performed to determine the optimal welding process parameter set-up conditions for several types of polyamides, using weld strength as the quality attribute. Optimal vibration welding conditions for the material, robustness of the optimal set-up conditions, and the average weld strength with different types of polyamides with different fiberglass contents are determined.

5.1 Design of experiments (DOE) and materials used

There are three groups of dissimilar materials combinations. The TA, TB, and TC materials combinations are 70G33/HTN, 70G33/A1133, and 70G33/AS4137 respectively.

5.1.1 DOE matrix and results for the TA group

The DOE consisted of 18 runs with four control factors: weld pressure, weld time, vibration amplitude, and hold time with each factor having three levels as shown in Figure 5.1, Table 5.1 and Table 5.2. The responses that were measured included tensile strength, melt down distance, and flash weight.

The materials used for the welds are Zytel 70G33 (PA66, 33% glass) and HTN 52G35 (containing terephthalic acid). The dimension of the plaques before welding into the T sample configuration were 51x102x3.2 mm for the 70G33 and 51 x 102 x 6.5 mm for the HTN. The melting points were 262 C and 310 C respectively, giving a melt temperature difference between these two materials of 48 C.

A three level, four parameter, eighteen experiment orthogonal matrix was chosen to examine the effects of weld pressure, welding time vibration amplitude and holding time. The initial values were chosen from a preliminary general survey of welding dissimilar materials.

Weld Parameters	Low Level	Medium Level	High Level
Weld Pressure (MPa)	0.98	1.44	1.97
Weld Time (Seconds)	4	6	8
Weld Amplitude (mm)	1.27	1.52	1.78
Weld Holding Time (Seconds)	3	6	9

Figure 5.1 Weld parameters of DOE

From other previous work on dissimilar T-sample tests, the highest strengths were found when the high melting temperature material is in the horizontal flange position, and lower melting temperature material is in the vertical web position [18]. The welding set-up therefore had the 70G33 in the vertical position being held stationary on the lower table of the welder. The horizontal HTN plaque was balanced on the vertical web such that when the table was raised, the horizontal plaque was pressed against sandpaper backing on the vibration fixture to keep it from sliding on the fixture during the welding process.

Table 5.1 is the DOE matrix used in this process. The orthogonal matrix has 18 experiments. Experiment 19 is an extra test in which the adjustable process parameters are all set to the high values. Table 5.2 gives the Taguchi matrix +1 extra test with regression results. UTS1 through UTS6 represent the UTS estimated by different regression analyses as discussed below.

DOE	Load	Amplitude	Weld Time	Hold Time	UTS	Meltdown	Flash Weight
ID	LB	0.001*in	Seconds	Seconds	MPa	mm	G(Ave,6s)
1	L 75	L 50	L 4	L 3	11.62	0.29337	0.0038
2	L 75	L 50	M 6	M 6	14.20	0.92964	0.0098
3	L 75	M 60	M 6	M 6	17.06	0.88392	0.0260
4	L 75	M 60	H 8	H 9	22.10	1.55956	0.0893
5	L 75	H 70	H 8	H 9	26.38	2.08661	0.0905
6	L 75	H 70	L 4	L 3	19.87	1.17094	0.0441
7	M 110	L 50	M 6	H 9	17.60	0.70231	0.0430
8	M 110	L 50	L 4	H 9	10.10	0.34544	0.0103
9	M 110	M 60	H 8	L 3	24.62	1.77927	0.1968
10	M 110	M 60	M 6	L 3	22.67	1.30302	0.1287
11	M 110	H 70	L 4	M 6	19.50	0.80518	0.0248
12	M 110	H 70	H 8	M 6	30.88	2.5146	0.0497
13	H 150	L 50	H 8	M 6	23.79	1.4351	0.1385
14	H 150	L 50	H 8	L 3	22.33	1.49098	0.1405
15	H 150	M 60	L 4	H 9	17.56	0.67183	0.0680
16	H 150	M 60	L 4	M 6	18.13	0.6223	0.0440
17	H 150	H 70	M 6	L 3	28.84	1.83642	0.1878
18	H 150	H 70	M 6	H 9	30.75	2.00406	0.1768
19	H 151	H 70	H 8	H 9	31.98	2.82702	0.2760

Table 5.1 L18 (4^3) Taguchi matrix +1 extra test with regression results

P	Am	Wt	Ht	UTS 1	UTS 2	UTS 3	UTS 4	UTS 5	UTS 6
MPa	mm	Sec	Sec	MPa	MPa	MPa	MPa	MPa	MPa
0.98	1.27	4	3	9.93	10.308	11.053	9.98	9.84	10.81
0.98	1.27	6	6	13.88	13.813	15.423	13.96	13.86	14.70
0.98	1.52	6	6	18.49	18.4	18.168	18.21	18.45	18.94
0.98	1.52	8	9	22.44	22.218	23.452	22.19	22.47	21.85
0.98	1.78	8	9	27.23	27.315	27.258	27.41	27.23	27.08
0.98	1.78	4	3	19.33	19.027	14.787	19.44	19.20	17.27
1.44	1.27	6	9	15.72	15.61	18.088	15.84	15.71	16.77
1.44	1.27	4	9	11.30	11.529	13.439	11.40	11.22	12.34
1.44	1.52	8	3	25.70	25.743	26.954	25.44	25.70	24.94
1.44	1.52	6	3	21.28	21.349	21.391	21.00	21.22	21.62
1.44	1.78	4	6	21.18	20.824	17.452	21.32	21.05	19.71
1.44	1.78	8	6	30.02	30.264	30.481	30.20	30.01	30.91
1.97	1.27	8	6	23.29	23	26.407	23.43	23.32	21.54
1.97	1.27	8	3	23.76	23.576	26.686	23.89	23.78	21.54
1.97	1.52	4	9	18.58	18.537	18.661	18.34	18.48	17.71
1.97	1.52	4	6	19.05	19.113	18.94	18.79	18.94	17.71
1.97	1.78	6	3	28.74	28.853	27.637	28.91	28.65	29.84
1.97	1.78	6	9	27.79	27.701	27.079	28.00	27.73	29.84
1.97	1.78	8	9	32.22	32.42	27.079	32.44	32.21	34.42

Table 5.2 L18 (4^3) Taguchi matrix +1 extra test with regression results.

5.1.2 Interactions Between Weld Strength, Meltdown and Flash Weight

In this welding process, the four process parameters that can be adjusted are welding pressure, welding time, vibration amplitude and hold time. The ultimate tensile strength, meltdown and flash weight are the measurable responses to the process. Figure 5.2 shows the experimental relationship between the UTS with Meltdown, and Figure 5.3, UTS with Flash weight. As expected, the strength increases with both meltdown and flash weight increase. During the welding process, when the meltdown increases, the material squeezed out also increases. A successful weld requires that such material melting and expulsion takes place.

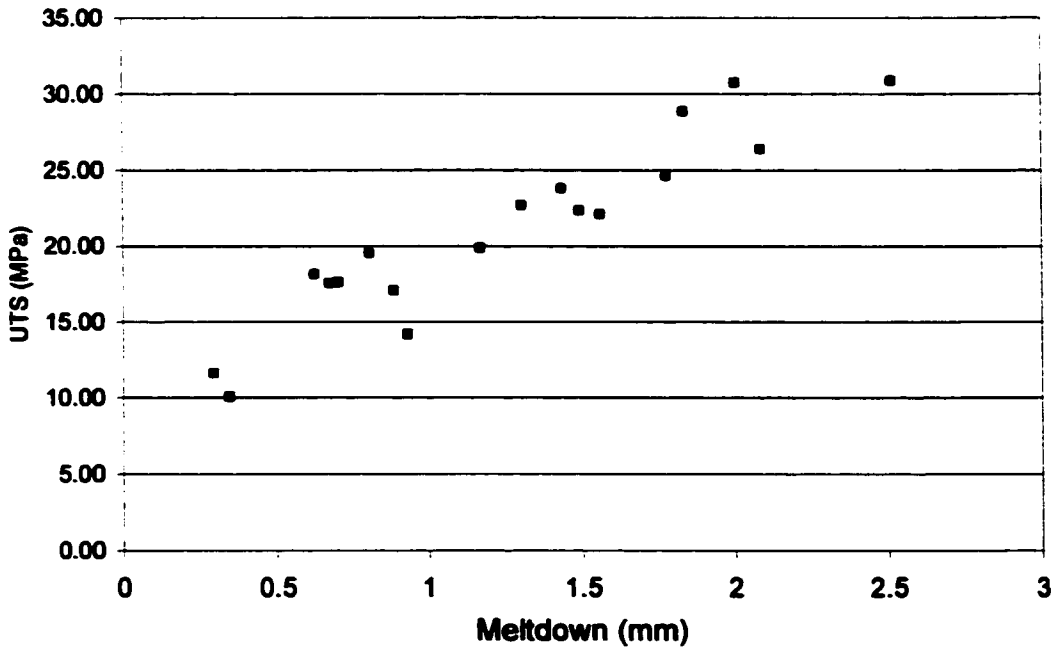

Figure 5.2 Experimental values for UTS vs. Meltdown

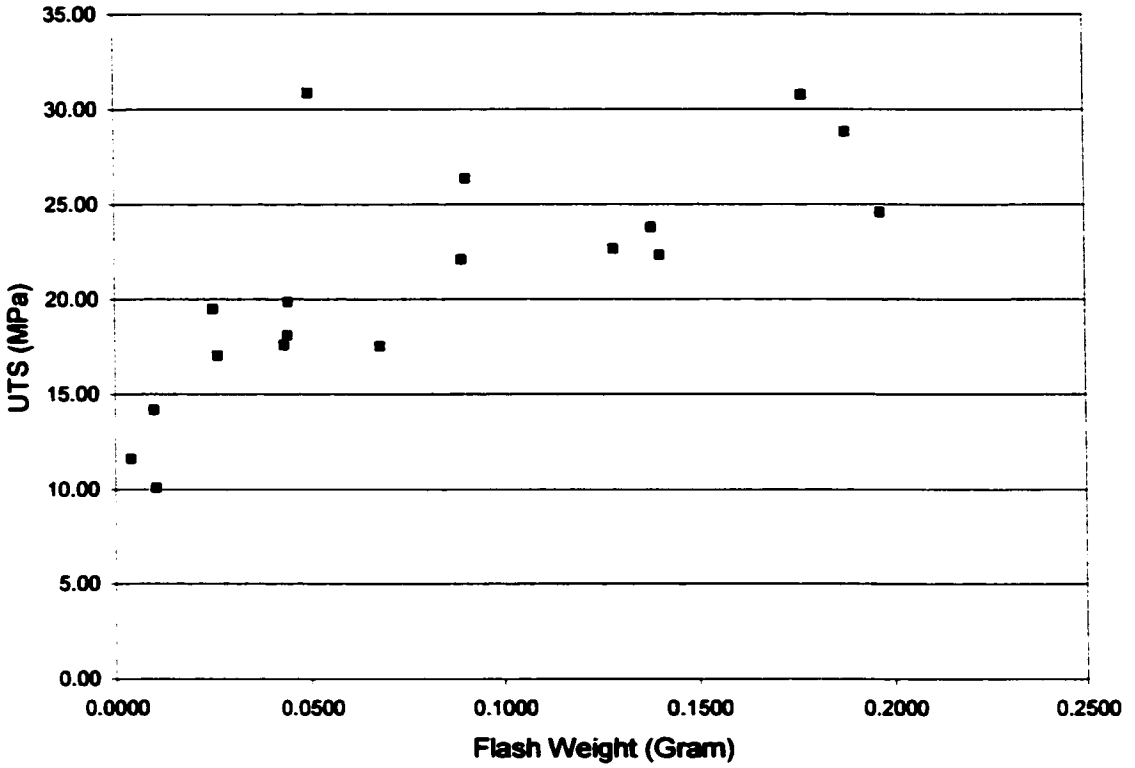

Figure 5.3 Tensile strength as a function of Flash weight

5.1.3 Predictive Mathematical Models for Weld Strength

The simplest way to analyze the results is to find the mean value of ultimate tensile strength (UTS) for all tests done at a given setting for one of the adjustable variables in the tests. Using the values from the 18 orthogonal experiments Figure 5.4 shows the mean value for the UTS for each setting of weld pressure. The leftmost set of points on the graph represents the mean value of UTS, for the 6 experimental settings, which had the Weld Pressure at 0.98 MPa. (See Table 5.1) As the Weld Pressure increases, the UTS increases; the difference between the highest mean UTS and the

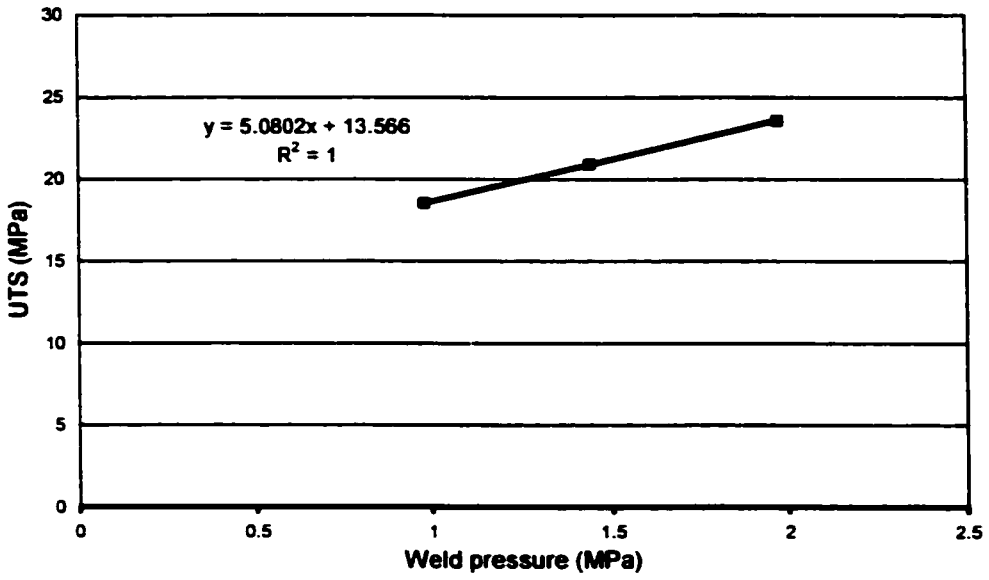

Figure 5.4 UTS vs. weld pressure

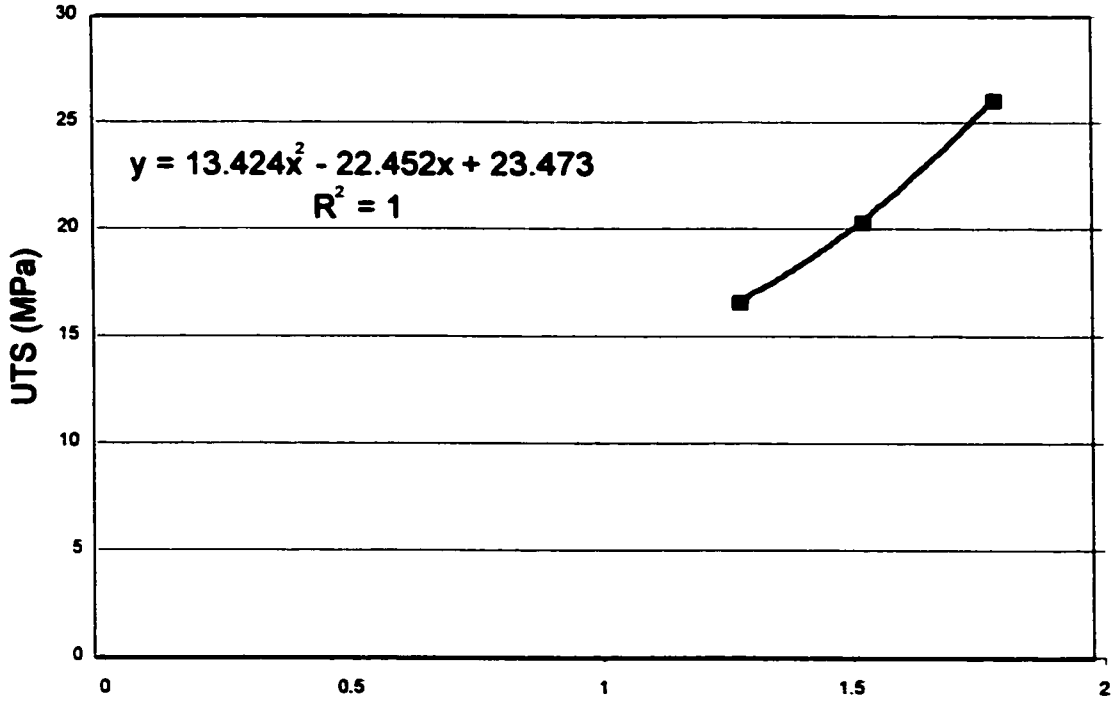

Figure 5.5 UTS vs. weld amplitude

lowest is 5.03 MPa. Figure 5.5 similarly shows that the mean UTS increases by 9.43 MPa as the Vibration Amplitude increases. In Figure 5.6, increasing the Weld Time also gives a mean UTS increase of 8.89 MPa. Changing the Hold Time has very little effect on the UTS, at least in the experimental range used in these tests (Figure 5.7).

This is the standard method for estimating the sensitivity of the weld strength to the adjustable process parameters. It clearly predicts that Vibration Amplitude and Weld Time are the most important parameters affecting the weld strength. The Hold Time (beyond 3 seconds) is not significant. When the mean result for UTS is plotted for a given setting the results seem well defined. The reason it is permissible to plot the mean UTS values is that the DOE matrix is orthogonal. This means that for each of the three different levels of Weld Pressure (P) there is an identical number of similar parameters (2 each of low, medium, high) settings for the other three parameters (Vibration Amplitude (A), Weld Time (Wt) and Hold Time (Ht). The way in which these other parameters are combined at each setting of Weld Pressure is different, so that the matrix can also be made orthogonal for each of them.

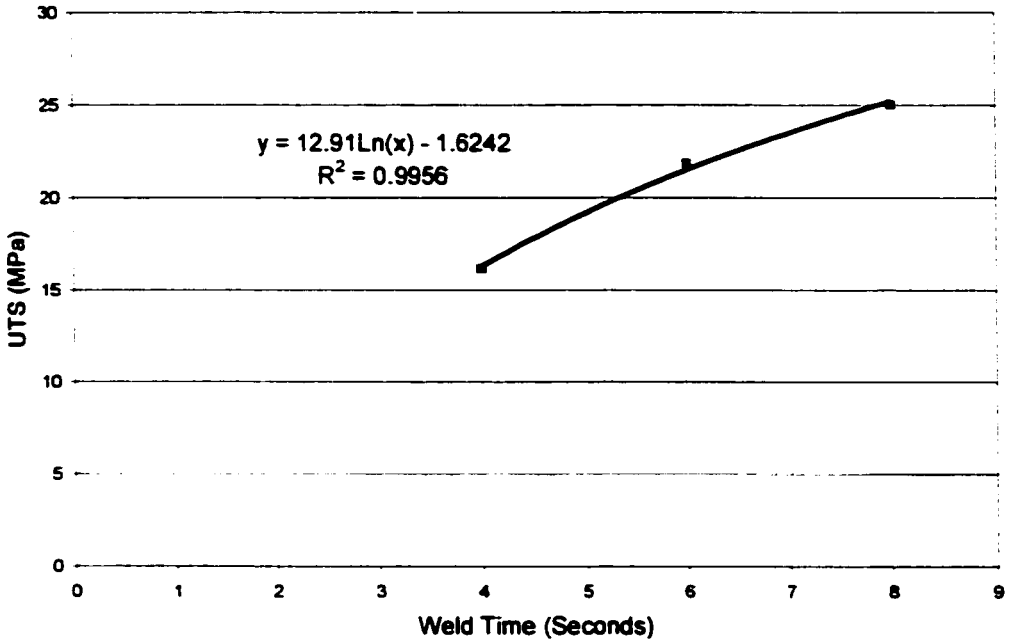

Figure 5.6 UTS vs. weld time

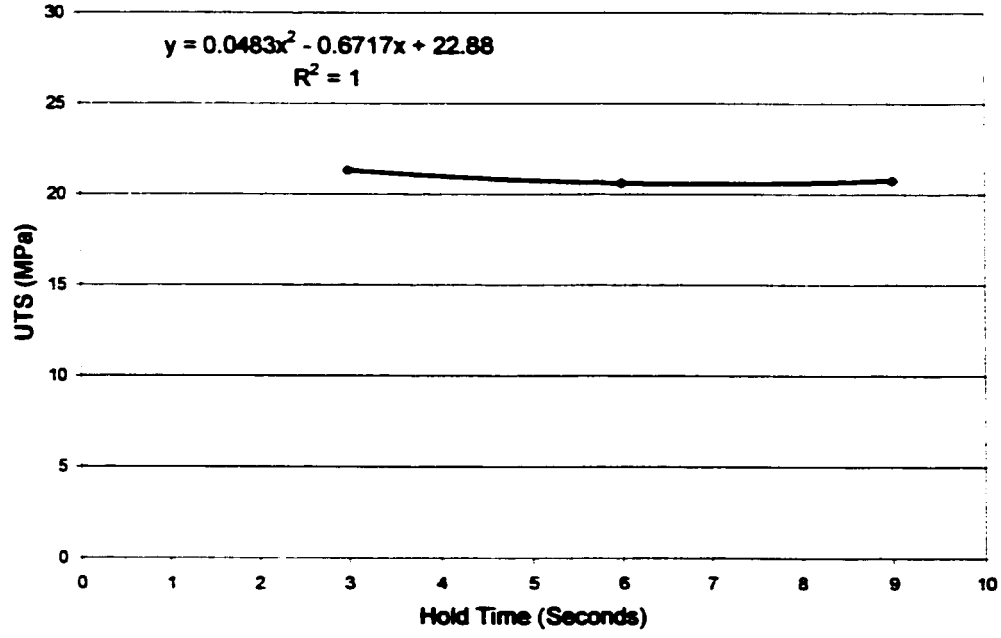

Figure 5.7 UTS vs. weld hold time

It is of some interest to plot the same results, but in this case all of the mean values for each of the individual experiments are shown as in Figures 5.8, 5.9, 5.10 and 5.11. Note that the range of these results at a given level does not indicate the experimental scatter. Each point on each graph represents the mean value of 6 tensile tests, three tests on each of the duplicate samples made at each experimental weld parameter setting. These figures show that while the mean values, shown in Figures 5.4 to 5.7, and discussed in the previous paragraphs, give a rapid estimate of sensitivity of the process to the adjustable parameters. They also give guidance with respect to optimum settings. However, they are not adequate for creating a mathematical model that will help in understanding the process at a more fundamental level. To do this it is necessary to look at the physics of the process and to do a more informative regression analysis.

The DOE orthogonal matrix in Table 5.2 is taken from the book by Taguchi [26]. The results in Table 5.2, shows that Experiment 12, which had medium welding pressure, long welding time, high vibration amplitude and medium holding time produced the strongest weld (30.88 MPa) of the DOE set of tests. Experiment 18, which had high pressure (P), high welding vibration amplitude (A), medium welding time (Wt) and long holding time (Ht), gave a similar result of 30.75 MPa

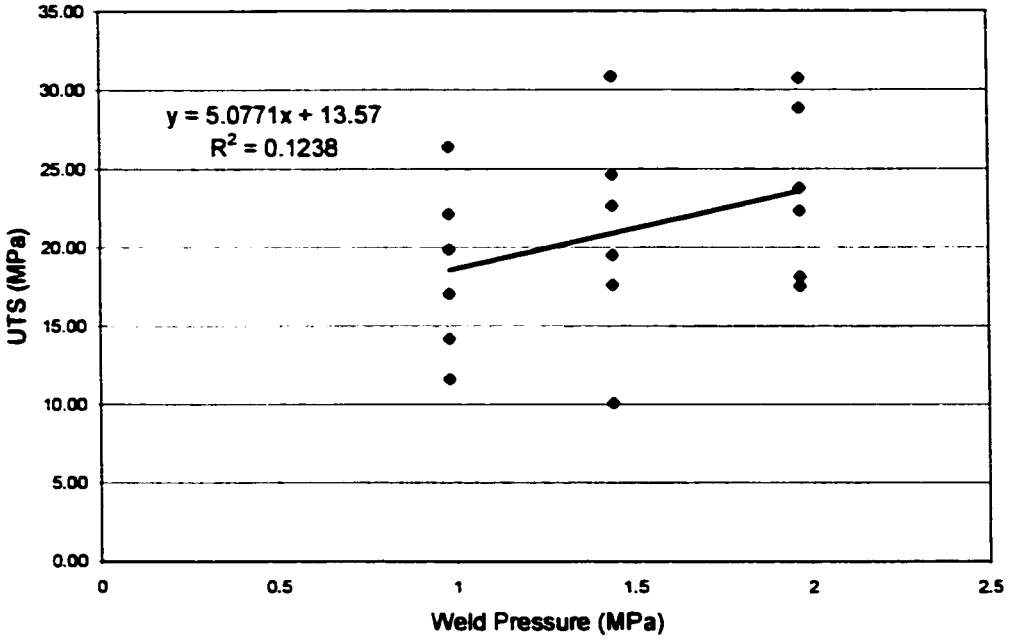

Figure 5.8 Individual data for UTS vs. weld pressure

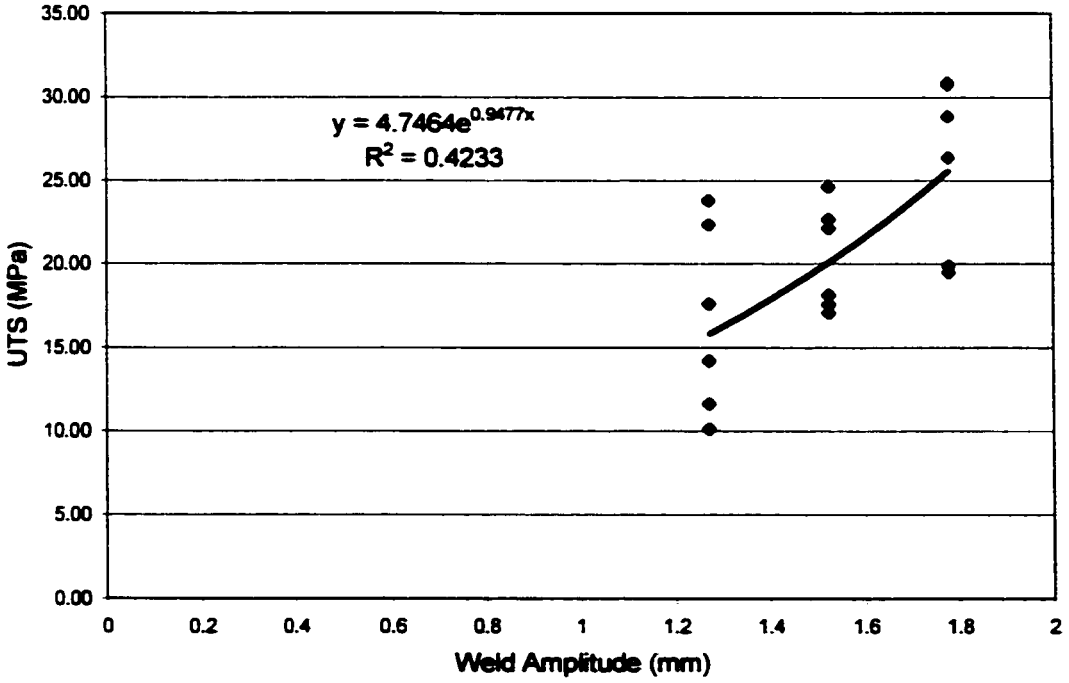

Figure 5.9 Individual data for UTS vs amplitude

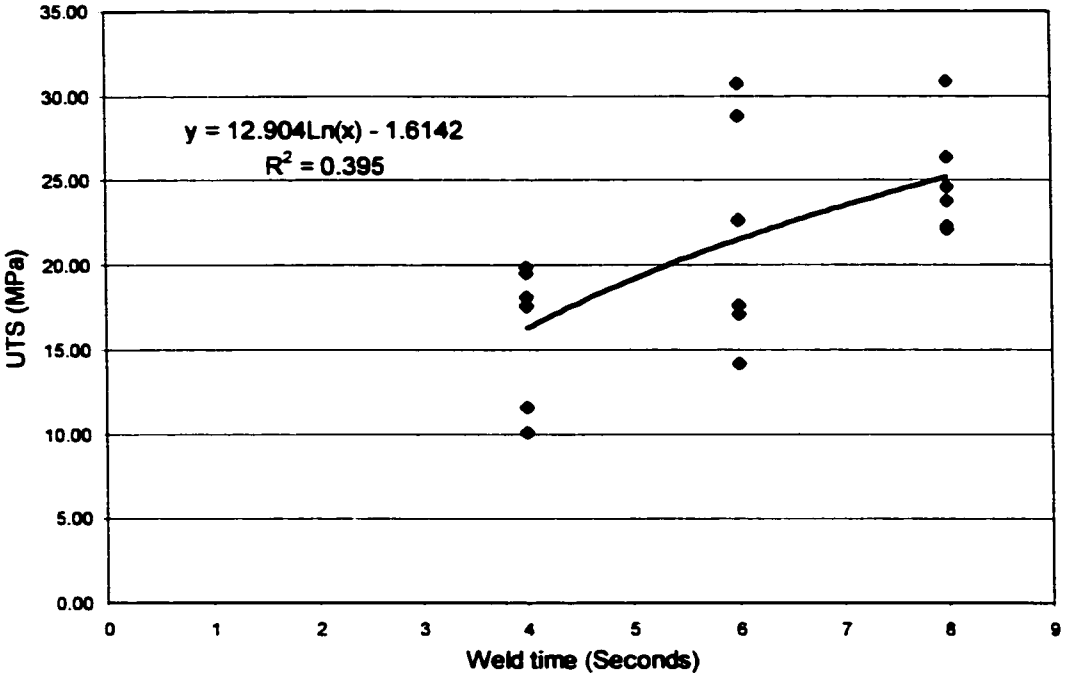

Figure 5.10 Individual data for UTS vs. weld time

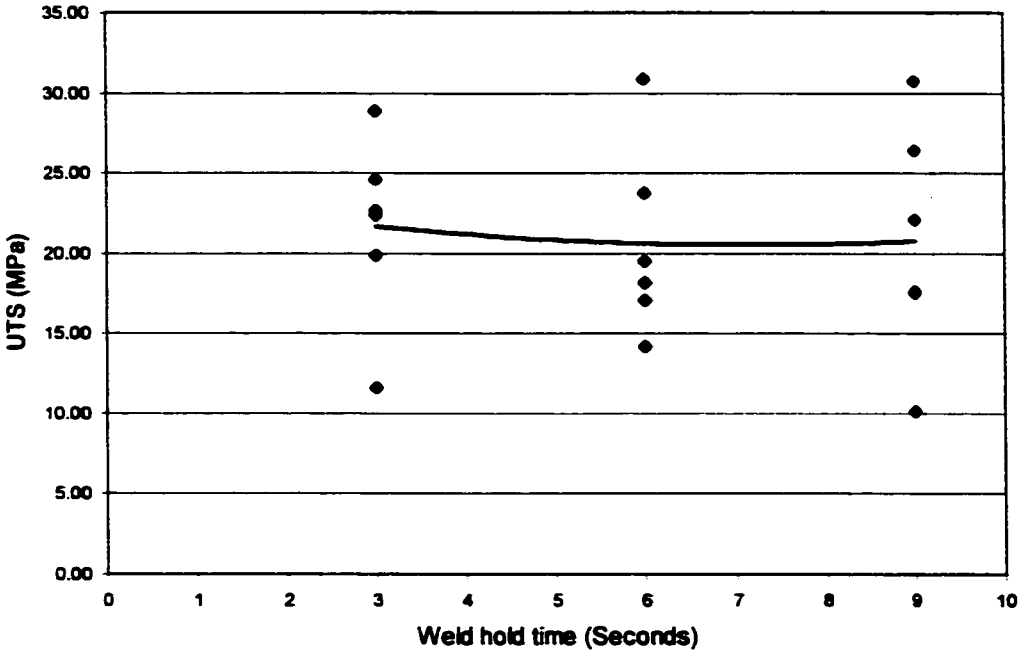

Figure 5.11 Individual data for UTS vs weld hold time

From the physics of the welding process, it is expected that increasing P, A and Wt would increase the amount of liquid produced. This might help to make a better weld. Therefore, immediately after completing the DOE set of experiments, it was noted that the matrix chosen did not contain the combination of high values for all of Pressure, Amplitude, Weld time, and Hold time. Therefore, an extra set of duplicate samples was welded with these settings, giving experiment 19 in Table 5.2. This produced the strongest weld of all those made; 31.98 MPa. Note that this result does not appear in Figures 5.4 to 5.11 because it would make the matrix non-orthogonal. However it can be included in any multivariate regression analysis done on the data.

Analysis of the physics of the process shows that the total sliding distance over which the surfaces to be welded move is $D = 4A\omega * Wt$ (mm), where A is the vibration amplitude (mm/0.25 cycle), ω is the frequency (Hz), and Wt is the welding time in seconds. Because the oscillation frequency is fixed and is set by the machine architecture, then A*Wt can represent D to demonstrate the relationship between the UTS and sliding distance. The experimental results plotted in this way are given in Figure 5.12.

To further examine the physics of the process, it is necessary to treat separately what happens in Stokes' Phase I, from the processes, which occur in Phase III. In Phase I, the power (energy dissipation rate) is given by $P = f * v$, where v is the relative

velocity of the two faces being welded and the shear force $f = \mu * F$ where μ is the coefficient of friction and F is the weld force applied normal to the faces being welded. This gives an average energy dissipation (power input to the weld) of $P_{ave} = 2\mu FA\omega/\pi$. In Phase III, the surfaces ride on a layer of viscous fluid, and so energy dissipation is

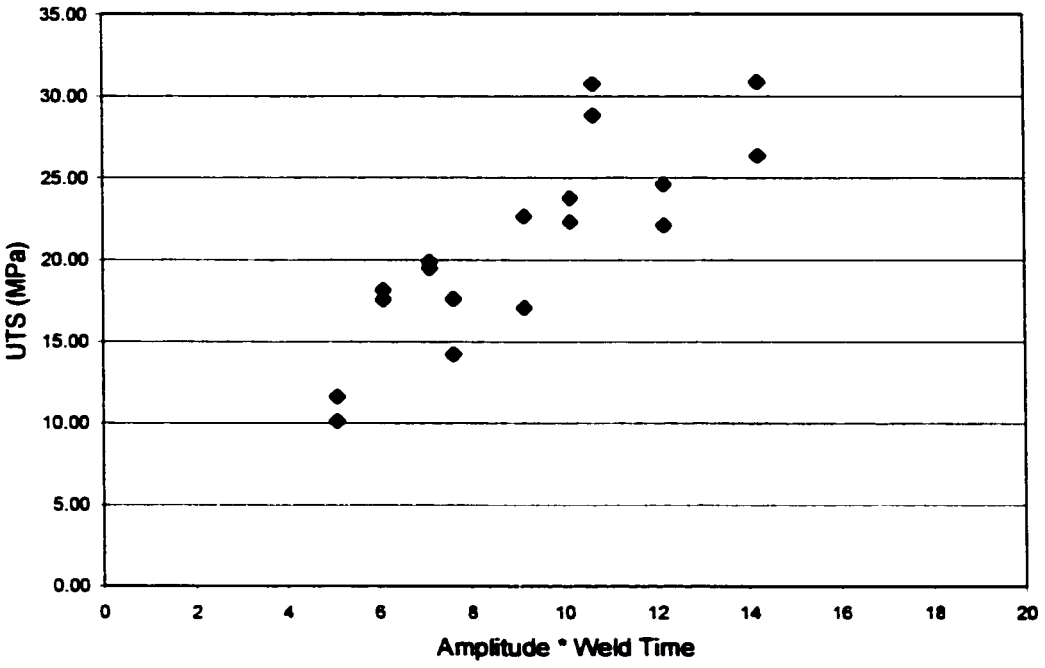

Figure 5.12 UTS vs. weld time * amplitude (total sliding distance)

through viscous heating. The average energy dissipated per unit area of weld surface is $q_{ave} = \eta A^2\omega^2 / 4h$ where η is the viscosity, A is the vibration amplitude, ω is the vibration frequency and h is the thickness of the liquid layer.

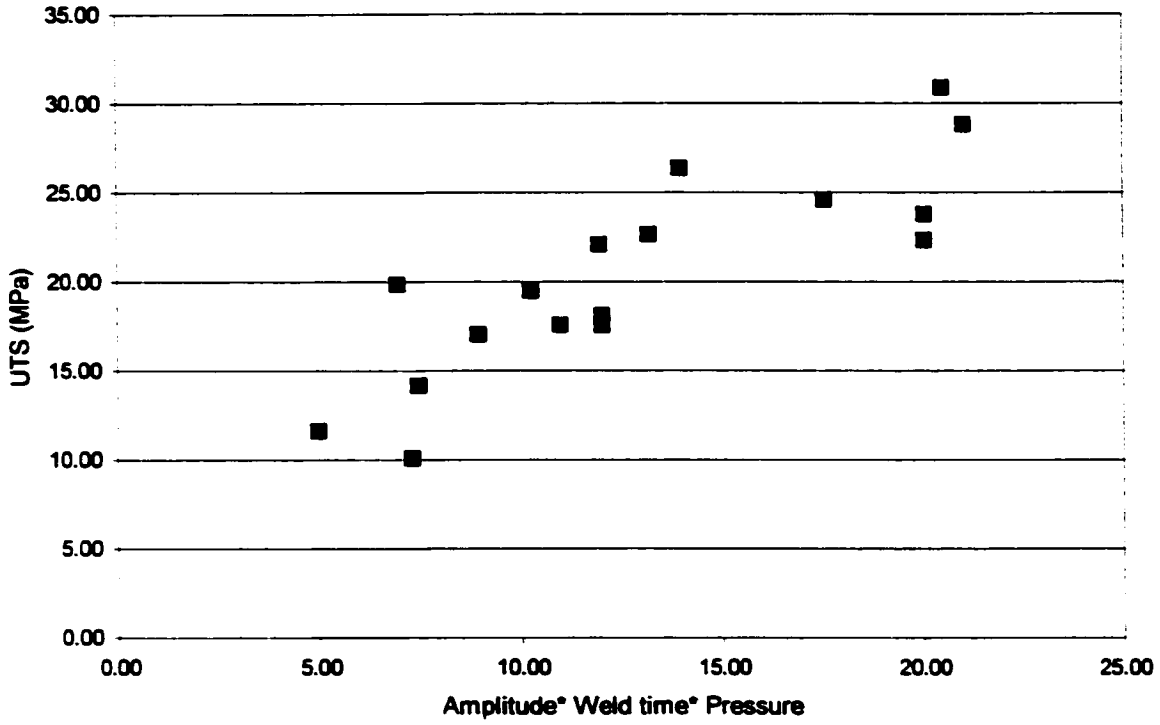

Figure 5.13 UTS vs. pressure * weld time * amplitude

Note that in Phase I heating, the weld force P contributes directly to the heating through its effect on the shear force. In phase III, the weld forces act to squeeze the liquid layer out of the weld faying surface. This decreases h, which is a small number in the denominator, and therefore can contribute significantly to the power dissipation. Therefore it is of interest to plot the UTS values against A * Wt * P. Figure 5.13 shows that there is an obvious relationship between weld strength and the product of these three parameters.

5.1.4 Regression Analysis

Multivariate regression analysis was performed in an attempt to find a predictive mathematical relationship for the UTS, based on the adjustable welding parameters.

The simplest form of regression analysis uses an equation of the form

$$UTS1 = aP + bA + cWt + dH + e$$

where a, b, c, d and e are coefficients to be determined by the regression. This gave **UTS1 = 5.035 P + 18.436A + 2.211Wt - 0.158Ht -26.786** which had a Standard Error of Estimate of 1.3069 MPa, and $R^2 = 0.9577$. The results are shown in Figures 5.14a and 5.14b. In Figure 5.14a, the experimental points are plotted as diamond shaped points, whose y value is the experimental result, and whose x value is the UTS1 value calculated for the appropriate P, A, Wt and H values. A perfect fit would have all the points lying along the diagonal line.

In Figure 5.14b, the triangular points represent the experimental results y, and the nearest circular dot is the value y' calculated using UTS1. The standard error of estimate is calculated as $\{(y-y')^2/n-1\}^{1/2}$ for these n results, and is based on the vertical distance between corresponding points on this figure.

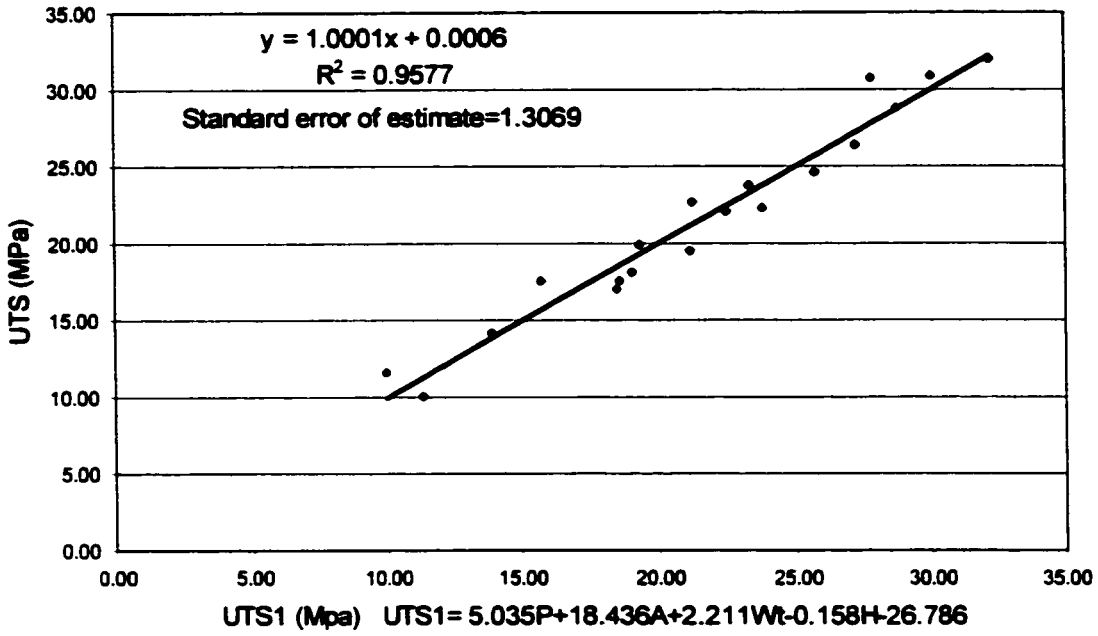

Figure 5.14a Experimental UTS vs. formula UTS1

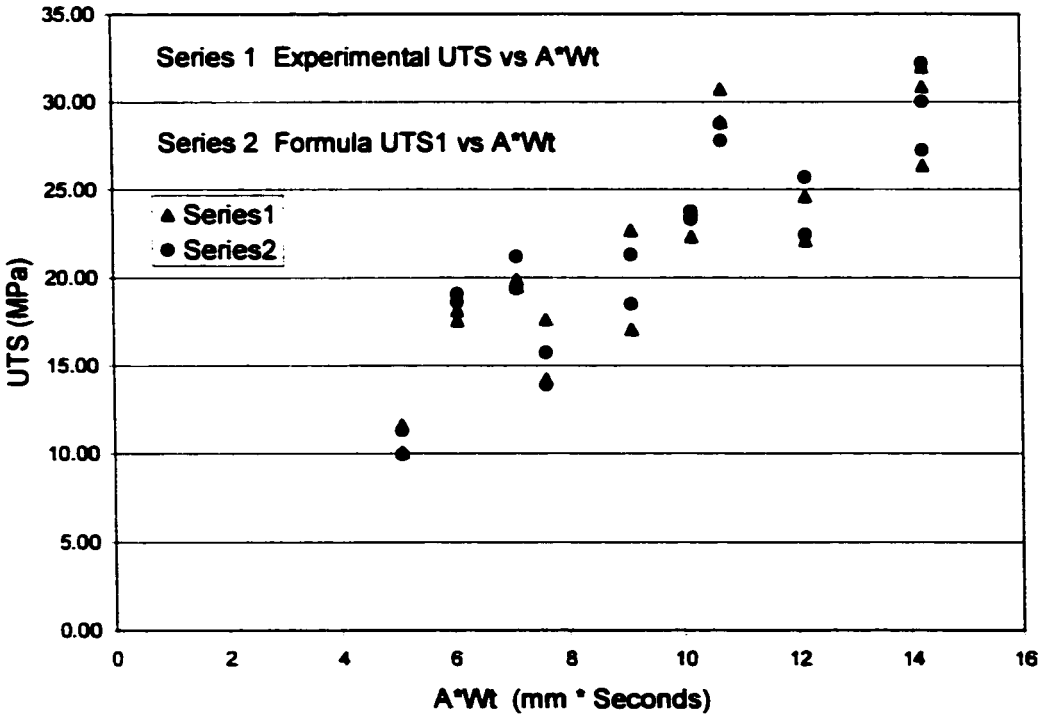

Figure 5.14b Experimental UTS and formula UTS1 vs. A*Wt

. Which of the adjustable process parameters has the greatest influence in determining the UTS ? The median experimental values of P, A, Wt, and H are 1.44 MPa, 1.52 mm, 6 s and 6 s respectively. Multiplying these by their respective regression coefficients shows that their relative contributions to the calculated values of UTS were (P) 7.25 MPa, (Am) 28.02 MPa, (Wt) 13.27 MPa, (Ht) 0.95 MPa and -26.786 MPa is the y intercept with all process parameters at zero. This indicates that the vibration amplitude dominates the contribution to the strength.

All of this shows that this regression equation fits the test results quite well, especially at the lowest values of UTS (Figure 5.14b).

The formula for UTS1 is a simple linear additive equation, which makes no

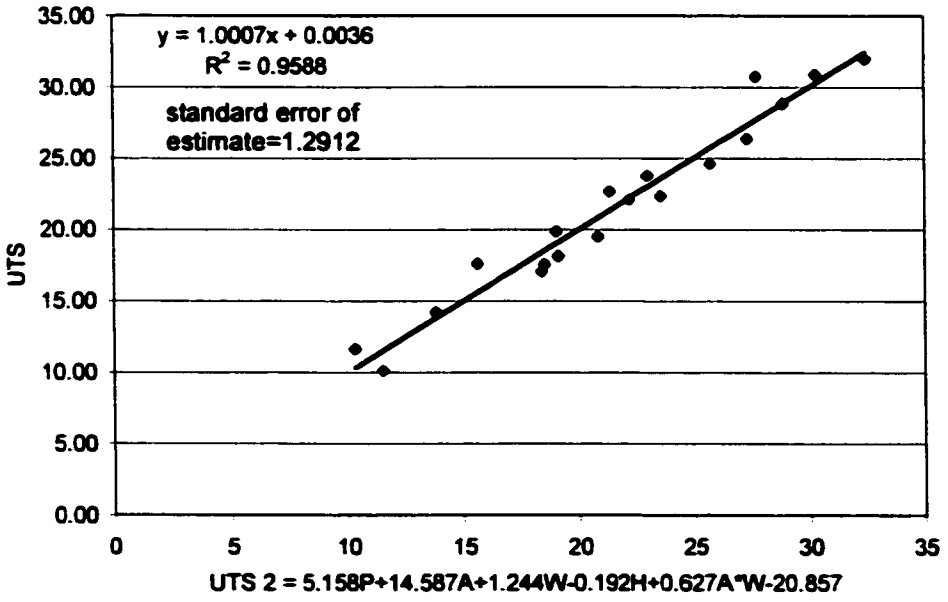

Figure 5.15a Experimental UTS vs. formula UTS2

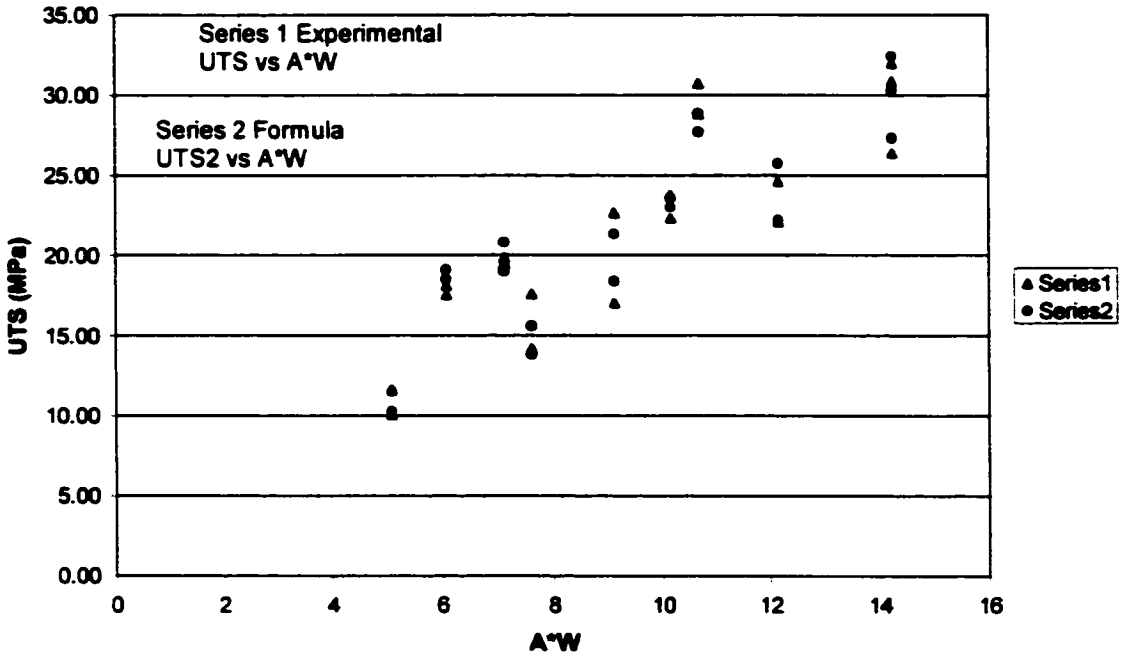

Figure 5.15b Experimental UTS and formula UTS2 vs. A*Wt

allowance for synergistic effects between the parameters. Stokes analysis of the process shows that the total distance traveled by the surfaces sliding over each other is proportional to A*Wt. So an additional term was added to UTS1 to allow A and Wt to contribute independently as their product. This gave **UTS2 = 5.158P + 14.587A + 1.244Wt - 0.192Ht + 0.627A*Wt - 20.857.** The standard error of estimate is 1.2912 MPa, which is a very slight improvement over UTS1, and $R^2 = 0.9516$. The results are plotted in Figures 5.15a and 5.15b. The median value for Am*Wt is 9.12, so for UTS2, the relative contributions are (P) 7.43, (A) 22.17, (Wt) 7.46, (Ht) 1.15, (A*Wt) 5.72 and the intercept is –20.86. So again the individual contribution of the vibration amplitude dominates.

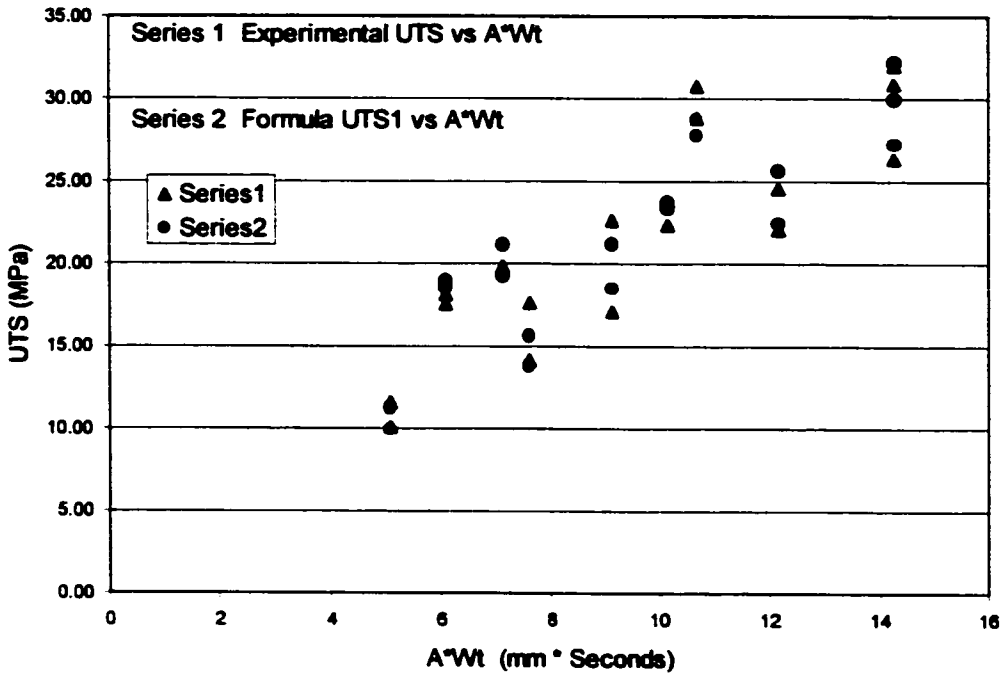

Figure 5.16 Experimental UTS and UTS3 vs. sliding distance.

Out of curiosity, expecting that A*Wt, which is directly related to the total sliding distance during welding, should really be the dominant parameter, the equation

UTS3 = 6.4P + 1.83A*Wt - 0.093Ht - 4.236

was examined. The Standard error of estimate was 2.59 MPa and $R^2 = 0.8337$. So this gives a poorer fit to the data. Figure 5.16 illustrates the results.

Next it is assumed that the heat input is most important in Phase III heating, so the equation for UTS1 is modified to allow the fit to be with vibration amplitude squared, rather than simply with the amplitude on its own. The rationale is that in Phase III, the power dissipated varies as $\eta A^2\omega^2 /4h$, and since ω is fixed, and h is governed mainly by P, this change is closer to the physics of the process. All this gives

UTS4 = 5.077P + 6.083Am^2 + 2.22Wt - 0.152Ht - 13.23,

which has a standard error of estimate of 1.259, and an R^2 value of 0.9605 (Figures 5.17a and 5.17b). These are the best results to date. The median experimental values of P, A^2, Wt, and Ht are 1.44, 2.31, 6 and 6 respectively. Multiplying these by their respective coefficients shows that their relative contributions to the calculated values of UTS were (P) 7.31 MPa, (A^2) 14.05 MPa, (Wt) 13.32 MPa, (Ht) 0.91 MPa and –13.23 MPa is the y intercept with all process parameters at zero. This implies that vibration amplitude and weld time contribute about equally.

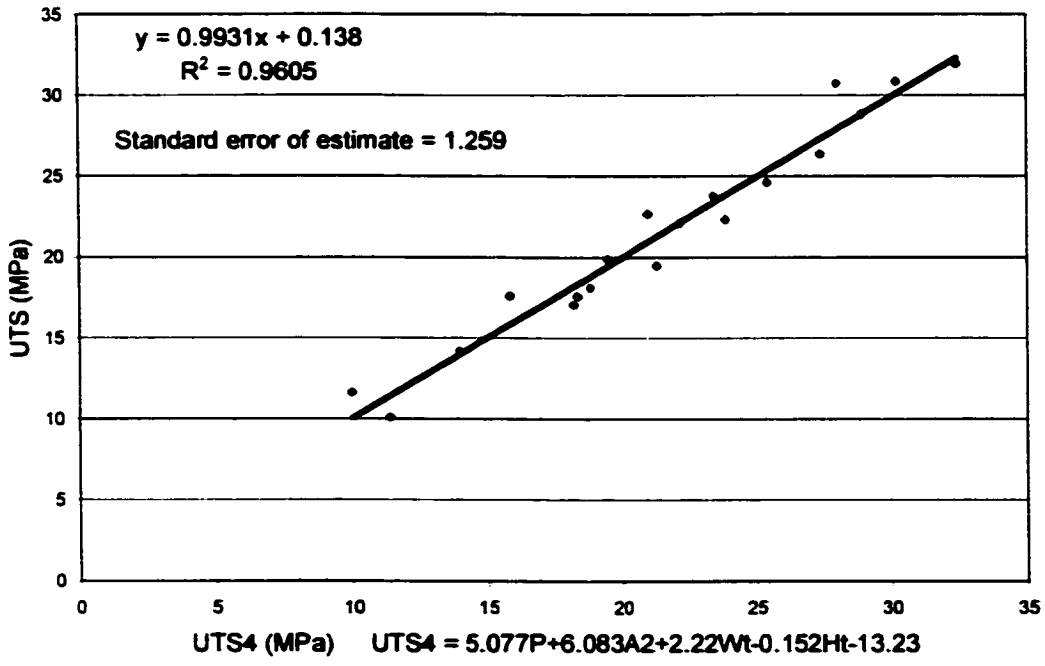

Figure5.17a Experimental UTS vs. formula UTS4

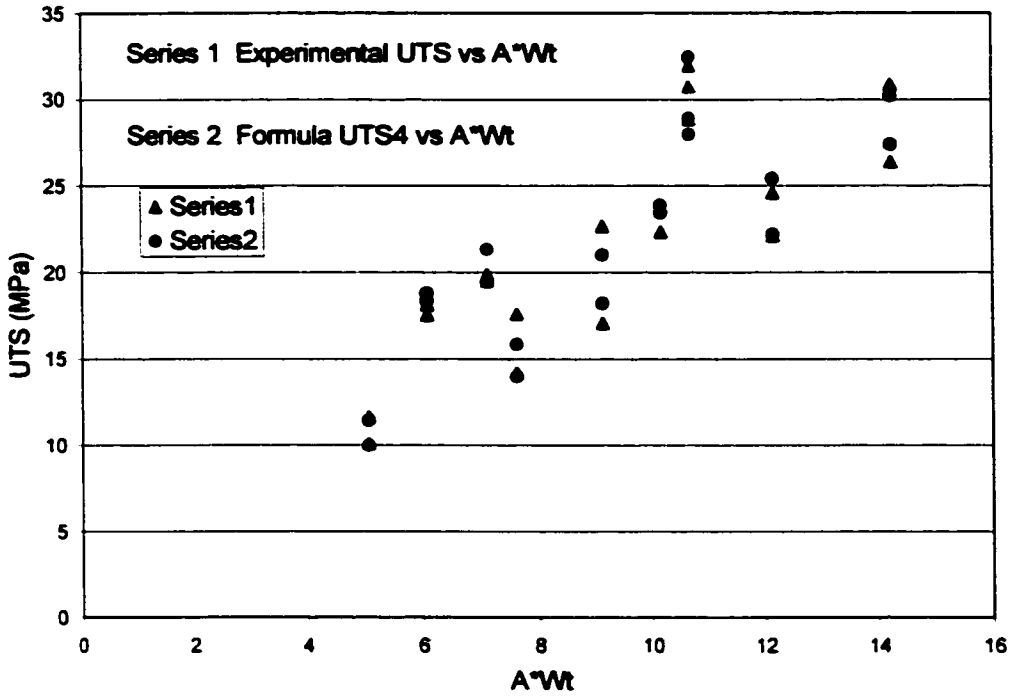

Figure 5.17b Experimental UTS and formula UTS4 vs. A*Wt

The power dissipated is the energy dissipated per second. Therefore the product A^2 Wt is a measure of the total energy dissipated. This leads to

UTS5 = 5.025P+18.38A+2.245Wt - 0.154Ht - 0.0017A^2Wt - 26.94

which has a Standard Error of estimate of 1.307 MPa, and an R^2 value of 1.31, see Figures 5.18a and 5.18b. The median experimental values of P, A, Wt, A^2Wt and Ht are 1.44, 1.52, 6, 13.86 and 6 respectively. Multiplying these by their respective coefficients shows that their relative contributions to the calculated values of UTS were (P) 7.24 MPa, (A) 27.93 MPa, (Wt) 13.47 MPa, (Ht) -0.924 MPa, (A^2Wt) - 0.024 MPa and –26.94 MPa is the y intercept at all parameters at zero. The negative and negligible contribution of the energy dissipation term is troubling at its median level, the vibration amplitude on its own contributes a term almost as big as the largest measured UTS value, and this forces some other terms to take on negative values. Although the Standard error of estimate and

R^2 value indicate a good fit, the large coefficient for amplitude seems unrealistic. At the high level setting for amplitude (1.78 mm), it would contribute 32.71MPa., which is slightly higher than the largest observed UTS value. The large negative value for the y intercept term has the effect of creating sets of combinations of positive values of P, A, Wt which will predict a no-weld situation (UTS = 0 or UTS<0). This is realistic. The large coefficient (18.38) of vibration amplitude contributes 23.34 MPa at the lowest level (1.27 mm) used in these experiments. With the other parameters at their median level, UTS5 predicts 16.16 MPa. This setting did not exist in this test set, but it is close to Tests 2 and 7. If the vibration amplitude is lowered to 0.39 mm, then with the other parameters at their median values, UTS5 predicts a strength of -0.008 MPa.

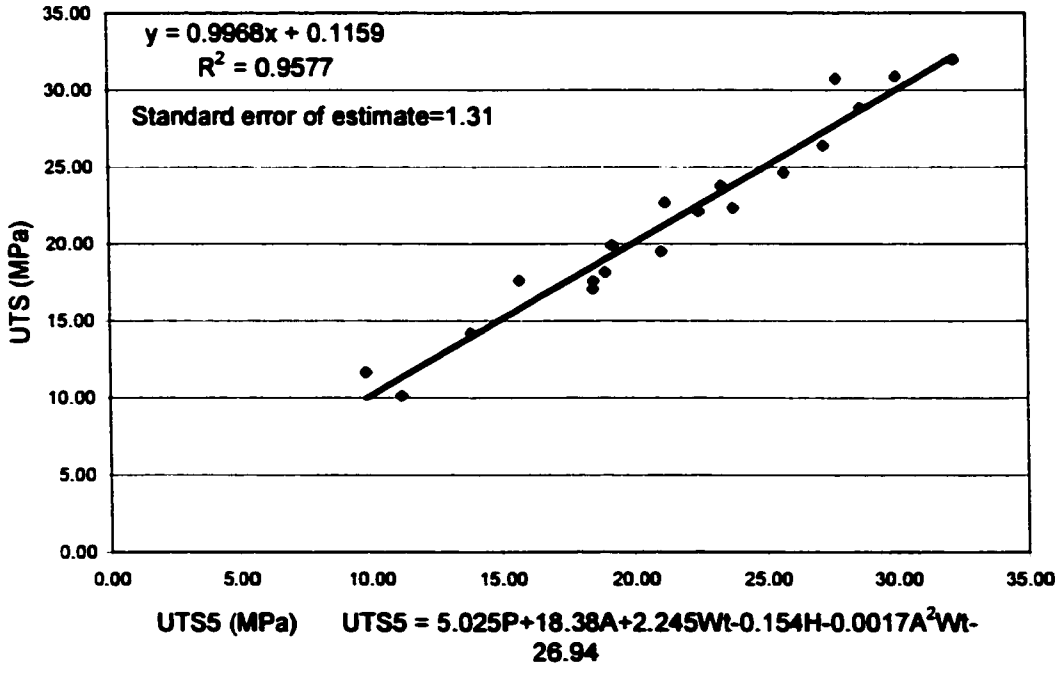

Figure 5.18a Experimental UTS vs. formula UTS5

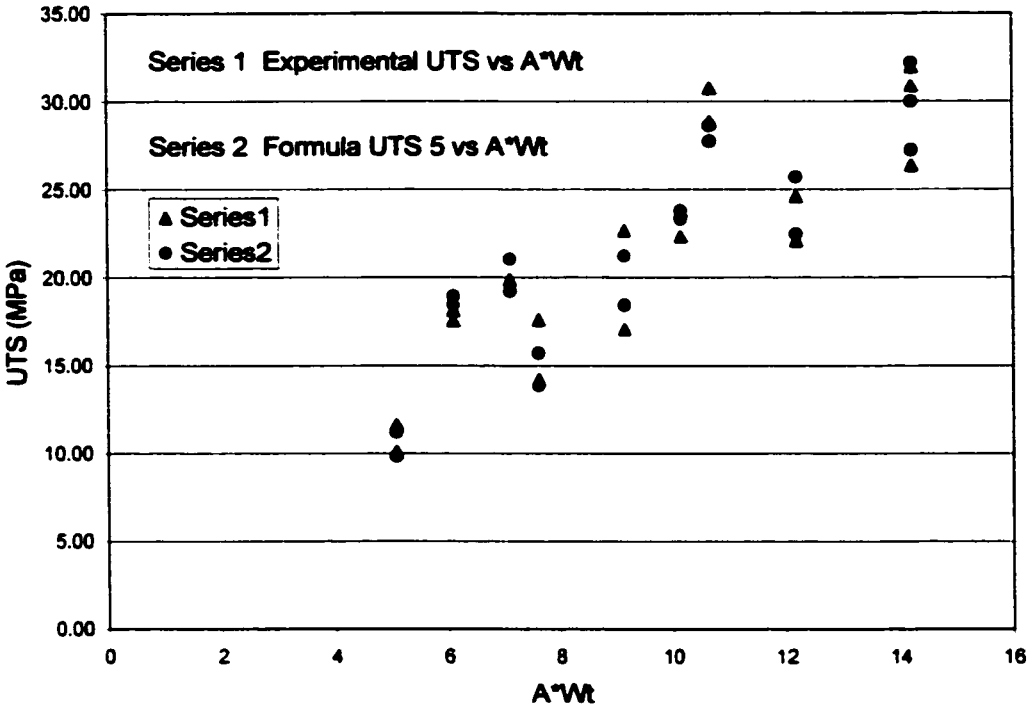

Figure 5.18b Experimental UTS and formula UTS5 vs. A*Wt

All of the above regression analysis assumed that the adjustable welding parameters act together in an additive fashion. But the analysis of the physics of the process predicts that the average power dissipation in Phase III will be $q_{ave} = \eta A^2\omega^2/4h$. In this formula, the parameters clearly have a multiplicative interaction. It is possible to use the same sort of regression analysis if the following procedure is used.

The general equation that $\mathbf{UTS6 = P^a * A^b * (Wt\text{-}t1)^c * d}$ where a, b, c, and d are coefficients to be determined. This equation also can be written as **lnUTS6 = aLnP + b LnA + cLn (Wt-t1) +d**. Note that t1 is to represent the time used in the solid/solid frictional Phase I. It is assumed that the time spent in Phase I does not contribute to the

UTS. To estimate t1, different t1 values were tried, and the standard error of estimate was calculated for each t1 value. These results are plotted against t1 to determine a minimum value giving Figure 5.19. This shows that when t1=3 seconds, the formula has the best fit for the test results. This method gives **UTS6 = 0.3434LnP +1.3926Ln A+0.2794Ln (Wt-3) + 2.0547, or UTS6 = 7.804 P $^{0.3434}$ * A $^{1.3926}$ * (Wt-3) $^{0.2794}$.**

This gives a Standard error of estimate is 1.34 MPa and $R^2 = 0.9575$. (See Figures 5.20a and 5.20b). This formula has a predictive ability comparable to the additive equations.

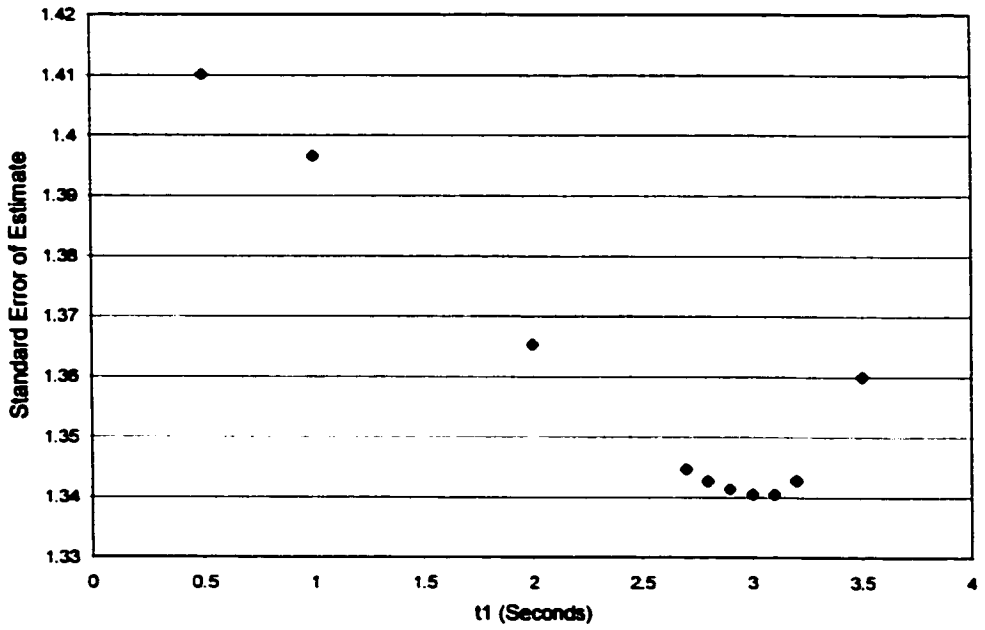

Figure 5.19 Standard error of estimate vs. t1

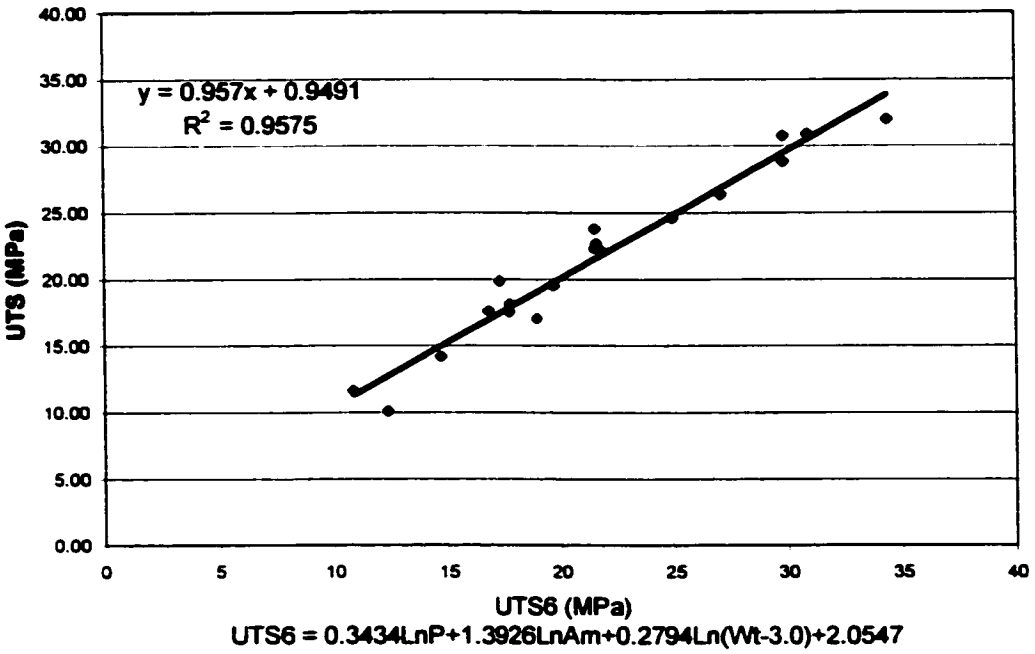

Figure 5.20a Experimental UTS vs UTS6

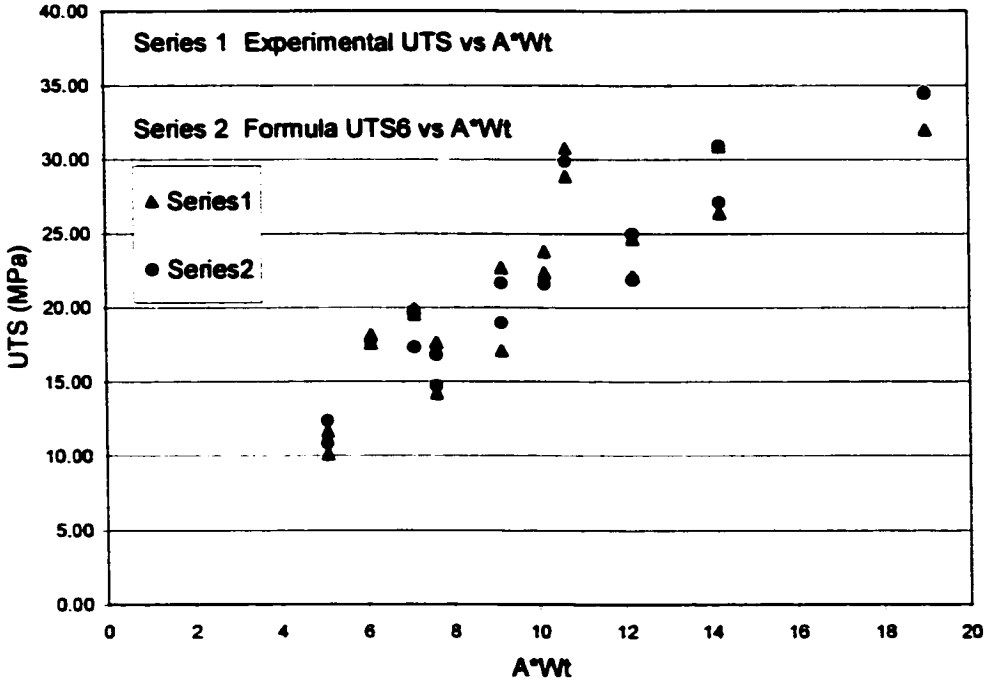

Figure 5. 20b Experimental UTS vs. formula UTS6

It is of interest to compare the predictive capabilities of these equations with the reproducibility of experimental values as previously measured on duplicate weld samples. In general, each of the given experimental UTS results is the mean value of 6 tensile T tests. Some samples produced zero or close to zero strength indicating a no-weld condition. In Table 5.3, the experimental conditions which produced these samples, are omitted from the calculation of the Experimental Standard Deviation.

Experiment	Average UTS	of Zero Values	Standard Deviation	UTS Model	Standard Error of Estimate
NO.	MPa	<1 MPa	MPa	NO.	
1	7.92	2	7.18	UTS1	1.31
2	11.85	1	6.3	UTS2	1.29
3	17.06		1.14	UTS3	2.59
4	22.1		1.34	UTS4	1.26
5	26.38		1.65	UTS5	1.31
6	19.87		1.37	UTS6	1.34
7	17.60		0.95		
8	10.06	1	4.15		
9	24.62		2.07		
10	22.67		3.01		
11	19.5	Only 3 samples	4.60		
12	30.88		1.91		
13	23.9		1.80		
14	22.33		2.90		
15	17.56		1.96		
16	18.13		1.97		
17	28.84		1.77		
18	30.75		1.31		
Average SD (excluding tests 1,2,8,11) = 1.7964					

The standard error of estimate of all models except UTS3 is smaller than the average standard deviation of the measured duplicate UTS value

Table 5.3 Summary of TA result

Perhaps all that this general analysis shows is that with 18 test results, and with five or more adjustable regression coefficients, almost any type of equation will give a good fit. Note also that the ability of these equation to predict behaviour outside of the test data range is not proven.

5.1.5 On the Co-dependence of UTS and Meltdown

Figure 5.21 showed that as meltdown increased, the UTS also increased.

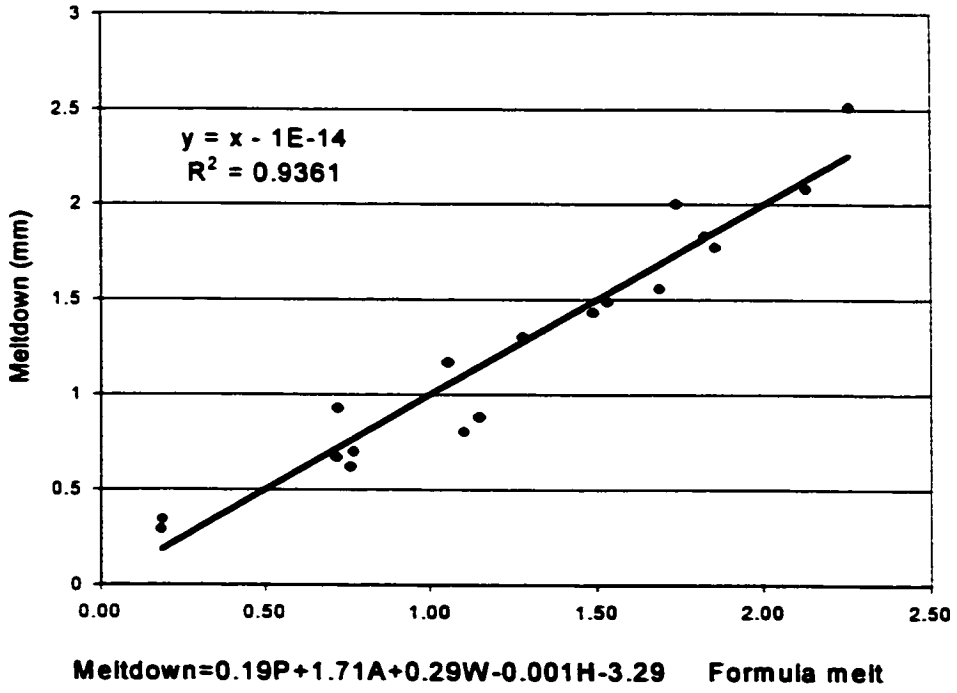

Figure 5.21 Experimental meltdown vs. formula meltdown

In previously reported work, some tests were done on a machine which had an adjustable Meltdown setting [18]. So, finding a regression equation between meltdown and the other welding parameters may also be meaningful to determine the optimal weld pressure, weld time and vibration amplitude to predict meltdown during a manufacturing process. Meltdown has the potential to be a control factor for designing weld joints and for conducting quality control. Therefore, another regression analysis was performed to find **Meltdown = 0.19P + 1.71A + 0.29Wt - 0.001H - 3.29** for the data shown in Figure 5.21 and in detail in Figure 5.2a. Figure 5.21 plots the experimental meltdown values versus the meltdown predicted by this formula. This gives R^2 = 0.9361, and standard error of estimate = 0.16. This regression describes the process very well. Once again vibration amplitude is the main factor controlling the meltdown distance.

5.2 Experimental design set TB

A second set of DOE experiments was done using a different pair of dissimilar materials. The other major difference in this DOE is that one of the orthogonal process parameters is the product of the vibration amplitude and the welding time (A * Wt). This parameter is proportional to the total welding sliding distance

5.2.1 Experimental results for the TB Group

The TB DOE used A-1133 as the upper flange, and 73G30 as the lower web material. The melting temperature difference between these two materials is 87 ^{0}C.

DOE	Weld P	A*W	Amp	Wt	Ht	Meltdown	UTS
Experiment Number	MPa		Mm	Sec	Sec	mm	MPa
TB 1	0.98	5.6	1.02	5.50	3.00	0.34	8.26
TB 2	0.98	8.4	1.40	6.00	5.00	1.25	11.57
TB 3	0.98	11.2	1.78	6.30	7.00	2.30	20.67
TB 4	1.57	5.6	1.40	4.00	7.00	0.37	9.67
TB 5	1.57	8.4	1.78	4.70	3.00	1.74	15.70
TB 6	1.57	11.2	1.02	11.00	5.00	2.33	10.31
TB 7	2.25	5.5	1.78	3.10	5.00	1.42	15.45
TB 8	2.25	8.5	1.02	8.30	7.00	2.11	10.01
TB 9	2.25	11.2	1.40	8.00	3.00	3.28	12.92
Plus10	0.98	11.2	1.02	11.00	5.00	1.78	9.15
Plus11	0.98	11.2	1.02	11.00	10.00	2.03	11.07
Plus12	0.98	11.2	1.40	8.00	10.00	2.29	12.97
Plus13	0.98	15.4	1.40	11.00	10.00	2.11	10.70

Table 5.4 The experimental matrix for welding parameters with meltdown and strength results for Test Set TB

Table 5.4 summarizes the DOE settings, and the mean values for the experimental results. The orthogonal DOE is the first 9 experiments, with three levels of P, A*Wt and

Ht. An additional four experiments, tests Plus 10 to Plus 13 were conducted at the same time as the orthogonal set TB, in the hope of shedding further light on the results.

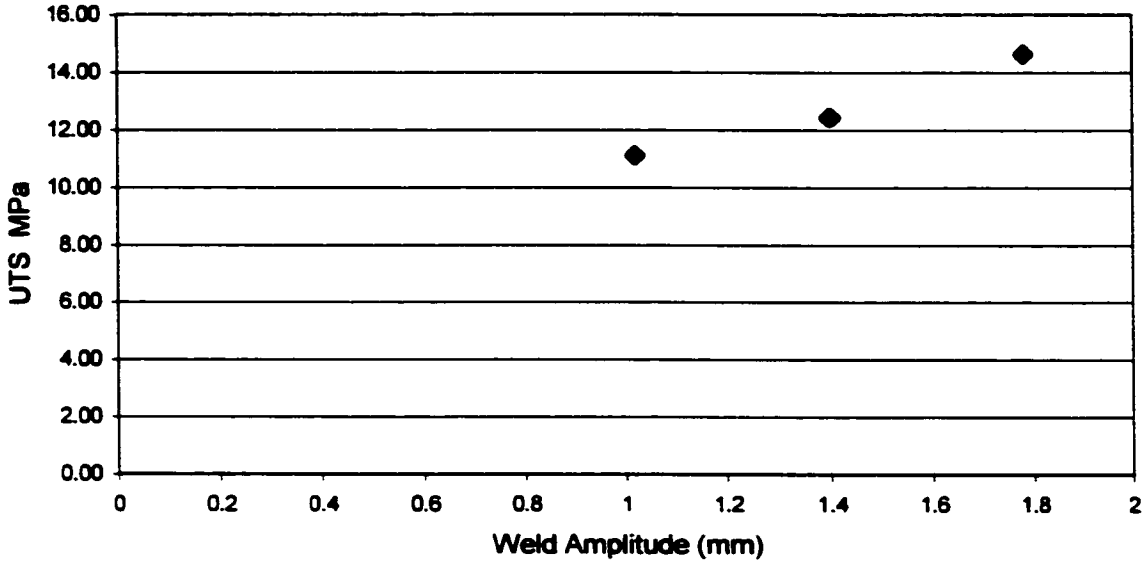

Figure 5.22 TB group, UTS vs. weld amplitude

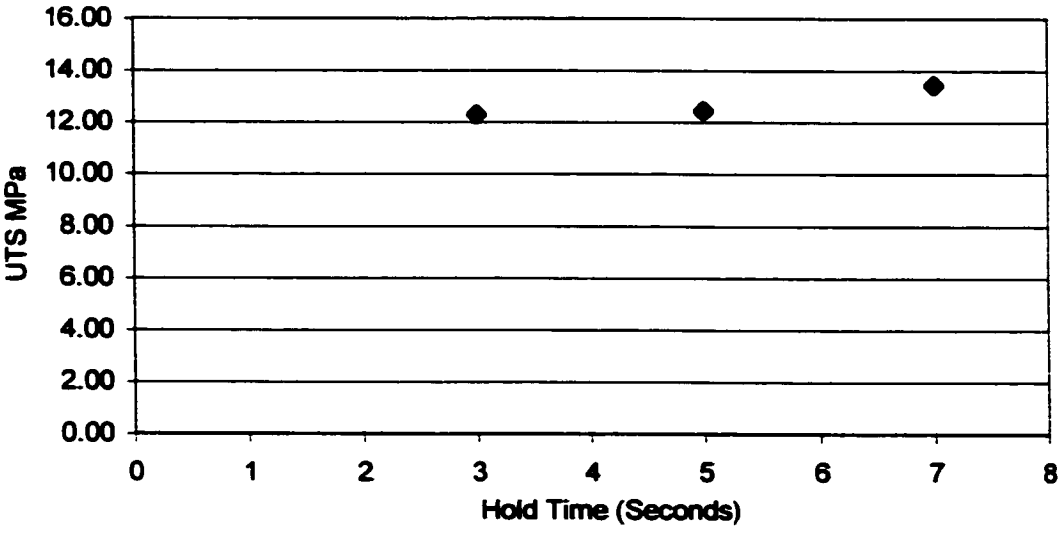

Figure 5.23 TB group, UTS vs. hold time

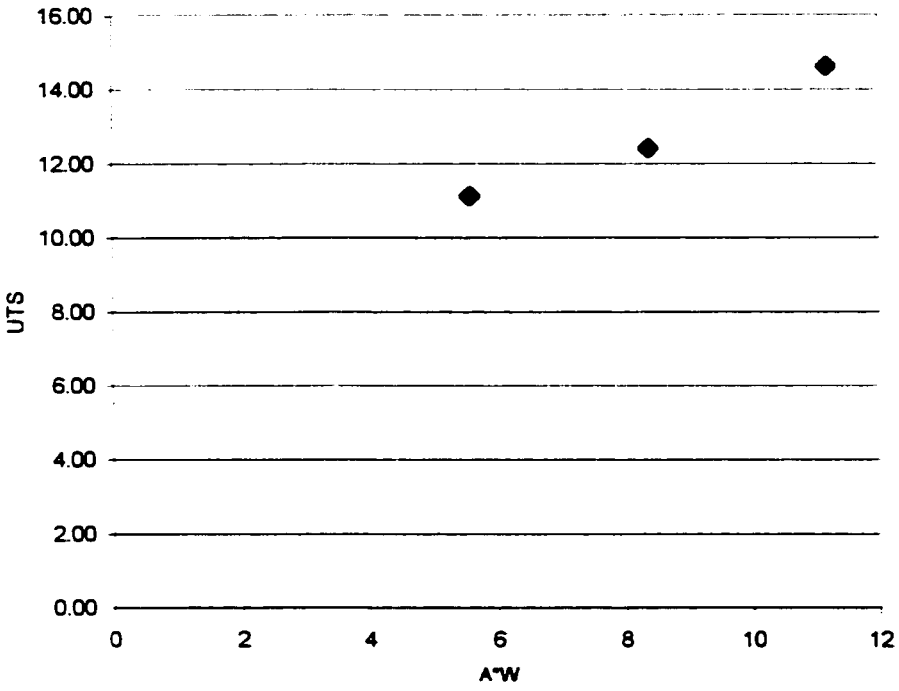

Figure 5.24 UTS vs. vibration amplitude times welding time

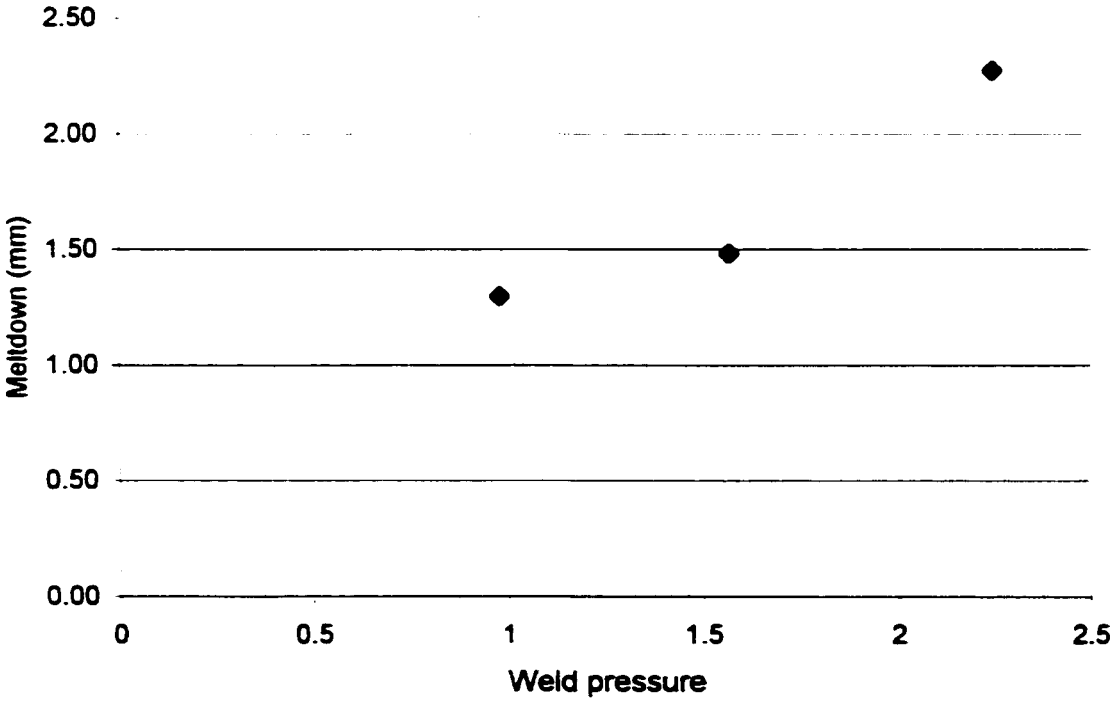

Figure 5.25 Meltdown vs. weld pressure

Figures 5.22 to 5.25 confirm the general trends found for DOE Set TA. As the weld pressure, vibration amplitude, welding time, sliding distance increase the UTS and meltdown distance increase. The maximum strength, 20.67 MPa, was observed for Experiment 3 which used P = 0.98 MPa (low), A= 1.78 mm (high), Wt = 6.3 s and Ht= 7 s (high). This experiment had the third highest value for meltdown at 2.3 mm. The maximum meltdown of 3.28 mm occurred for Experiment 9 where P=2.25 MPa (high), A=1.4 mm (med), Wt = 8 s (high) and Ht = 3 s (low), but this gave a relatively low value of 12.92 MPa for the UTS. Both these tests had an A*W sliding distance factor of 11.2, which is the highest level used in the DOE set. By having tests that have a common sliding distance factor (A*Wt), but made up of different welding times and vibration amplitudes, the individual contributions of these latter factors can be clarified.

Experiment No.	P MPa	Slide Dist A*W	Am mm	Wt sec	Ht Sec	UTS MPa	Meltdown Mm
TB3	0.98	11.2	1.78	6.3	7	20.67	2.3
Plus12	0.98	11.2	1.4	8	10	12.97	2.29
TB9	2.25	11.2	1.4	8	3	12.92	3.28
Plus11	0.98	11.2	1.02	11	10	11.07	2.03
Plus13	0.98	15.4	1.4	11	10	10.7	2.11
Plus10	0.98	11.2	1.02	11	5	9.15	1.78

Table 5.5 Experiments with A*W = or > 11.2 arranged in ranked order of UTS.

Figure 5.24 makes it clear that as the sliding distance increases, the UTS increases. What Table 5.5 makes clear is that for a given sliding distance factor, A*W,

(11.2 mm), the strength decreases as the welding time increases. The corollary of this is that as the welding amplitude increases, the strength increases. These results confirm the importance of vibration amplitude, previously determined in the regression analyses on Test Set TA.

5.3 Experimental Design Set TC

In this group, a set of DOE experiments was run to find the maximum fracture strength of the weld between the AS4137 and 70G33. From the table we find the maximum strength is 12.2MPa. This strength is very low. It means that the combination of AS4137/ 70G33 is not a good choice, even after the DOE. Individual data is listed in Appendix I

5.4 Correlation of flash parameters with the strength of the welds.

Attempts were made to correlate the shape and amount of the flash with the strength of the individual welds in DOE sets TB and TC. There was no obvious relationship between the flash characteristics and strength. Details of this work are given in Appendix II.

CHAPTER 6
THE EFFECT OF TEST FIXTURE DESIGN ON THE TENSILE STRENGTH OF T JOINTS

6.1 Measurement of curvature in T-joint flanges

An earlier study by another student[18,19] showed surprising results when dissimilar melting point materials were made in a T-joint test, or in a cup-welded-to-flange configuration. These tests had in common a vertical element, the web or cup wall, pushed against a horizontal planar surface being the flanges or flange.

When the horizontal flange (or the flange) was the higher melting point material, then the vertical web (or cup) just mashed against the flange (or flange) without achieving significant penetration. The only visible effect was that a lot of flash spread out from the interface. When the flanges (or the flange) were from the lower melting point material, then significant penetration did take place, also with the production of a lot of flash.

The surprising (to most observers) result was that, the tests which were characterized by having significant penetration were, without exception for the same pair of materials, weaker than the tests with minimal penetration.

The key to the understanding of this result came with the observation that those T-joint samples which had a lot of penetration, also had flanges which bent downward, as if there was a plastic hinge above the web.

To quantify the bending, a dial gage was attached to the vertical axis spindle of a Bridgeport milling machine. To the end of the dial gage indicator was attached a slightly dulled needle. The T-joint samples were clamped to the Bridgeport x-y table in a common tool vise. Height readings were then taken on the upper flange surfaces of 14 different 100mm long by 50 mm wide by 50 mm high T-joint samples left from the work of a previous student. The samples were clamped with the webs in the x-z plane, where the z direction is vertical. Using the manual x and y screw drives, the samples were moved in the y direction in 5 mm steps at a constant x position, recording x and y positions from a digital position indicator and the z position from the dial gage. Effectively, the Bridgeport mill had become a CMM (co-ordinate measuring machine). Every sample is measure 4 times. Figure 6.1 shows the author of the present thesis taking readings on these samples.

The results from these measurements are listed in Table 6.1. There are three different types of welding material combinations; same materials, higher temperature material in the flanges, lower temperature materials in the flanges. Welds numbered 5, 8, and 17 all belong to the group where flange and web are from the same material. Welds numbered 34, 35, 46, and 49 are dissimilar materials combination with the low melting material in the web position and high melting materials are in flange position. Weld samples 29, 42, 66, 84, 94, and 96 are dissimilar materials with the higher temperature materials in the web. These samples are from a test program where the welding parameters were kept constant, only the materials were changed from test to test.

Figures 6.2a and 6.2b show some typical examples of these measurements on dissimilar materials. In each figure the two materials remain the same, but the blue symbols represent the case where the lower melting point material is in the flange. Complete results from these tests are shown in Appendix III.

Figure 6.1 Bridgeport milling machine temporarily converted to measure the curvature in the flanges of T-joint welds.

Material Web/Flange	Weld Combination Number	Melting Temperature Difference (web-flange)	Curvature Depth (mm)
A1340/A1340	5	0	0.1355
A1133/A1133	8	0	0.2000
AS4133/AS4133	17	0	0.2460
70G33/73G30	29	39	0.2500
73G30/70G33	34	-39	0.2558
73G30/70G33	35	-39	0.2575
A1133/70G33	42	48	0.2755
70G33/A1133	46	-48	0.3014
73G30/A1133	49	-87	0.3083
A1133/73G30	56	87	0.4200
A1340/70G33	66	48	0.4334
A1340/73G30	84	87	0.4480
AS4133/73G30	94	104	0.4635
AS4133/73G30	96	104	0.6064

Table 6.1 Curvature measurements for the upper flanges of T-joint samples

From Table 6.1 it can be seen that when the low melting temperature is in the flange position, the value of curvature is bigger than when the high temperature material is in the flange.

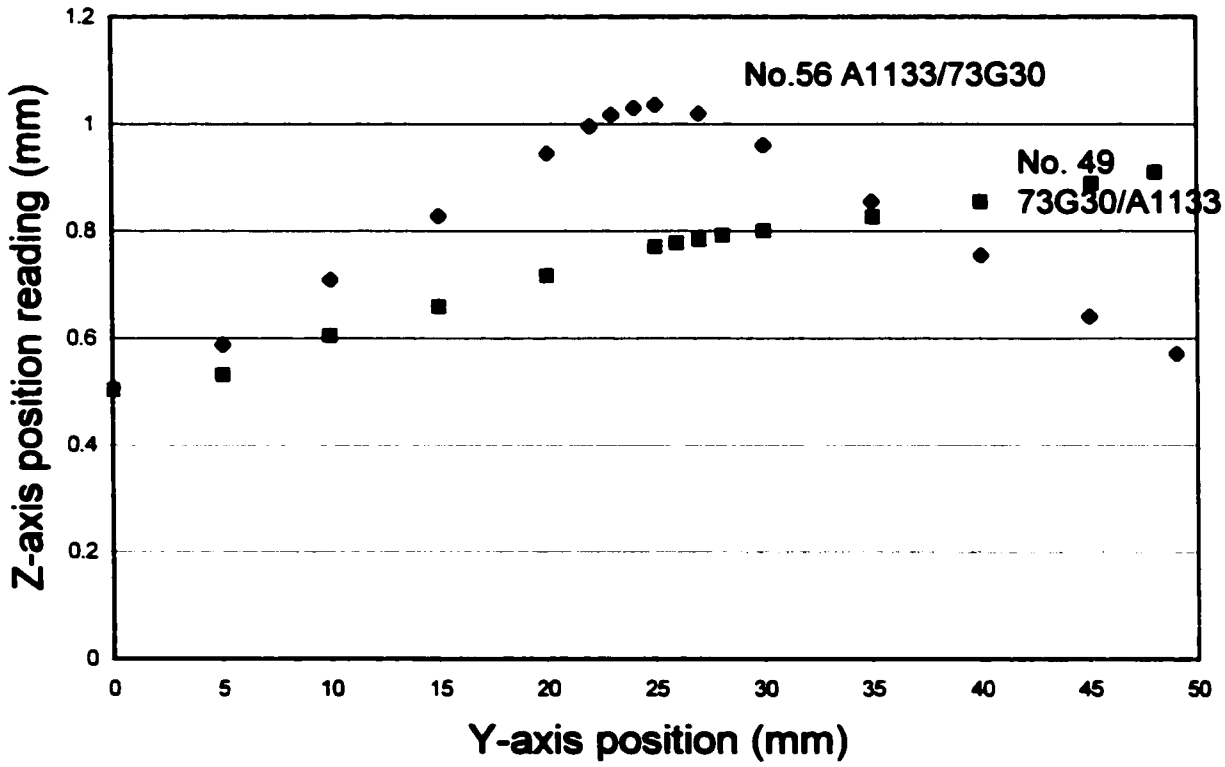

Figure 6.2a Curvature measurements for welds 56 and 49. These samples are for a high temperature amide A-1133 welded to nylon 6.

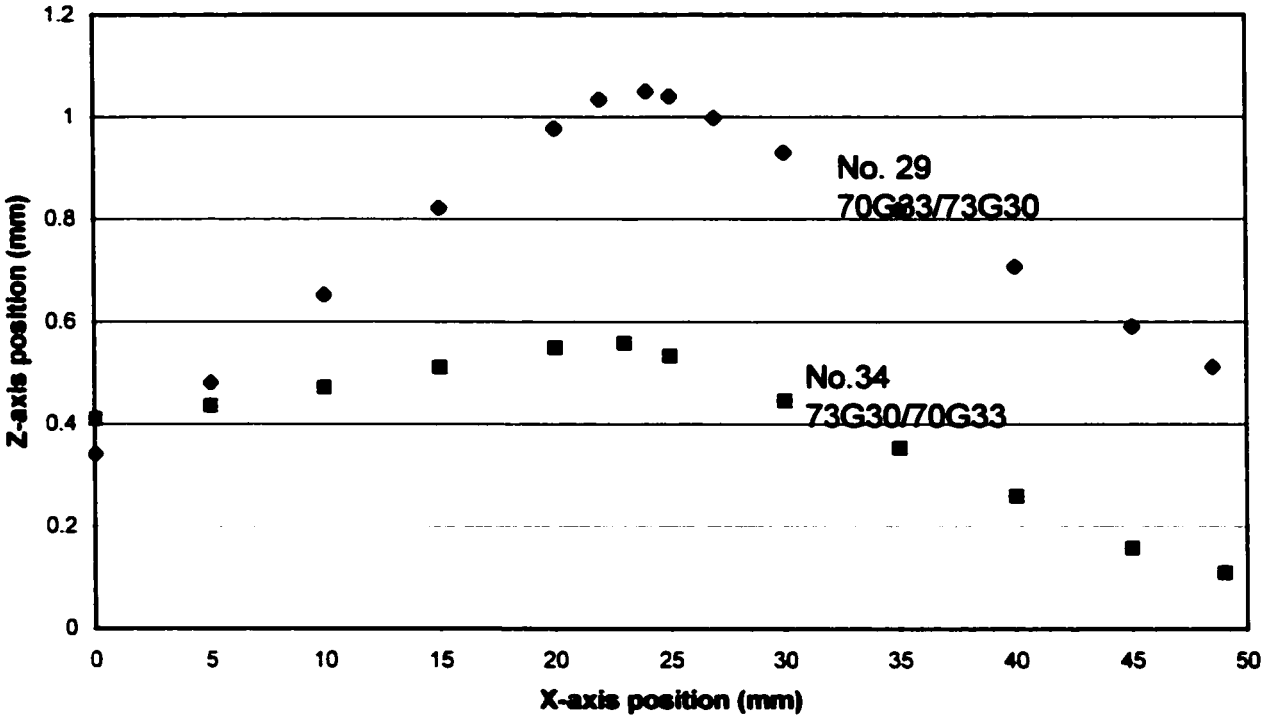

Figure 6.2b. Curvature measurements for tests 29 and 34. These samples are for nylon 6 welded to nylon 66.

In Table 6.1 and Figures 6.2a and 6.2b, the curvature is defined as the difference between the z-position of the highest point on the flange minus the mean value of the z-positions of the two ends.

In Figure 6.2 the pink symbols represent the low melting material in web position, and high melting material in flange position. Blue is the reverse. The average[#] curvature for the pink symbols is 0.2792 mm, while for the blue symbols it is 0.325 mm.

6.2 Effects of Curvature on Tensile Strength Measurement

The curvature that exists in the T-welded samples indicates that a residual stress must exist in the samples causing them to bend. Closer examination of Figures 6-2a and 6-2b shows that the bending is confined to a region very near to the junction with the web.

This can be seen by simply placing a straight edge parallel to the z-position values for the flanges of any of the samples in Figure 6-2 or in Appendix III.

The source of the curvature can be explained as follows. For a sample where the flange is made from the high temperature material, the weld zone is formed against the lower face of the flange, and excess liquid escapes relatively easily to the outside of the weld interface as flash. When the flange is made of the lower melting point material, then the web penetrates a significant distance into the flange. It is now more difficult for the liquid to escape, but a lot of it does by moving down the sides of the web.

The interesting part of the process is what happens as the liquid plastic freezes, and undergoes a significant contraction. When the flange is made from a higher melting point material, then the liquid layer at the faying surface is very thin, and any mushy viscoelastic zone is contained mainly in the web. The thin layer at the surface will develop tensile stresses, but such a thin layer will only exert a small tensile force acting to cause bending. When the flange is made from the lower melting point material, then the thickness of the liquid zone in the z direction is greater, and so tensile stresses are

created acting in all directions as the liquid and mushy zone cool. Because the liquid zone is thicker in the vertical direction than the previous case, the total tensile force available to cause bending is also greater. It will have a shorter moment arm in the flange, and some bending may be constrained by the presence of the stiffer web remnant. However the measurements in Table 6.1 show that the greater bending occurs when the liquid zone freezes in the interior of the flange.

Whatever the detailed explanation for the cause of these stresses, consider the consequences of doing tensile tests on these samples. There are no official standards for the design of gripping fixtures for T-joint tests. The common way to test them is to make a fixture that has horizontal surfaces to support the lower faces of the flanges, and then to grip the web and pull on it to failure. Often the flanges are clamped flat against the horizontal surfaces to counteract the natural tendency of the flanges to bend upward during testing(Stokes). It has previously always been assumed that the flanges are initially straight.

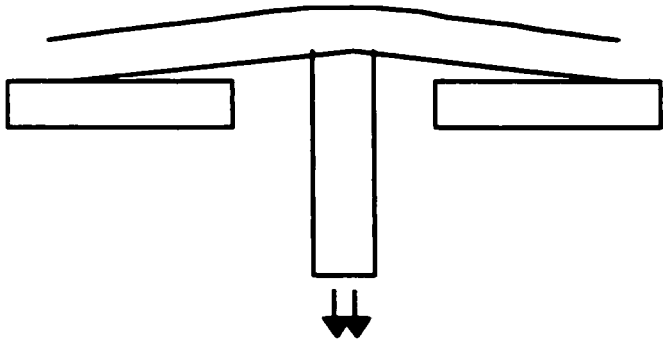

Figure 6.3. The consequences of pulling a sample with bent flanges against a holder with flat horizontal surfaces.

Figure 6.3 shows what will happen when a T-joint sample with bent flanges is put into an ordinary T-joint test fixture. The only part of the sample touching the fixture support surface is the tips of the flanges. These flanges behave as cantilever beams. When the web is pulled downward, the flanges are bent upward to their straightened position putting a high horizontal tensile stress into the lower surfaces of the flanges, stretching the flanges away from the junction with the web. If the fixture is such that the sample is first clamped flat before the web is pulled, then the act of clamping it will flatten the sample and so produce the same horizontal stress in the flanges at the junction with the web.

To see if the flange straightening had a significant effect on the strength of the welds, a slightly different type of sample holder was created. In this fixture (Figures 6.4a and 6.4b), the sample is supported only at the region very close to the junction with the web, the rest of the flange does not contact the lower surface of the sample holder. In this version of its use shown in Figure 6.4a, grub screws are brought down so that they just make light contact with the flanges. This prevents the flanges from rotating, and eliminates the horizontal x direction tensile stress caused by flange straightening. In the version in Figure 6.4b, the grub screws are raised so that the flanges can move upward. However, because the support points are so close to the web, the actual bending moment causing the flanges to rotate upward is significantly smaller than in 6.4c.

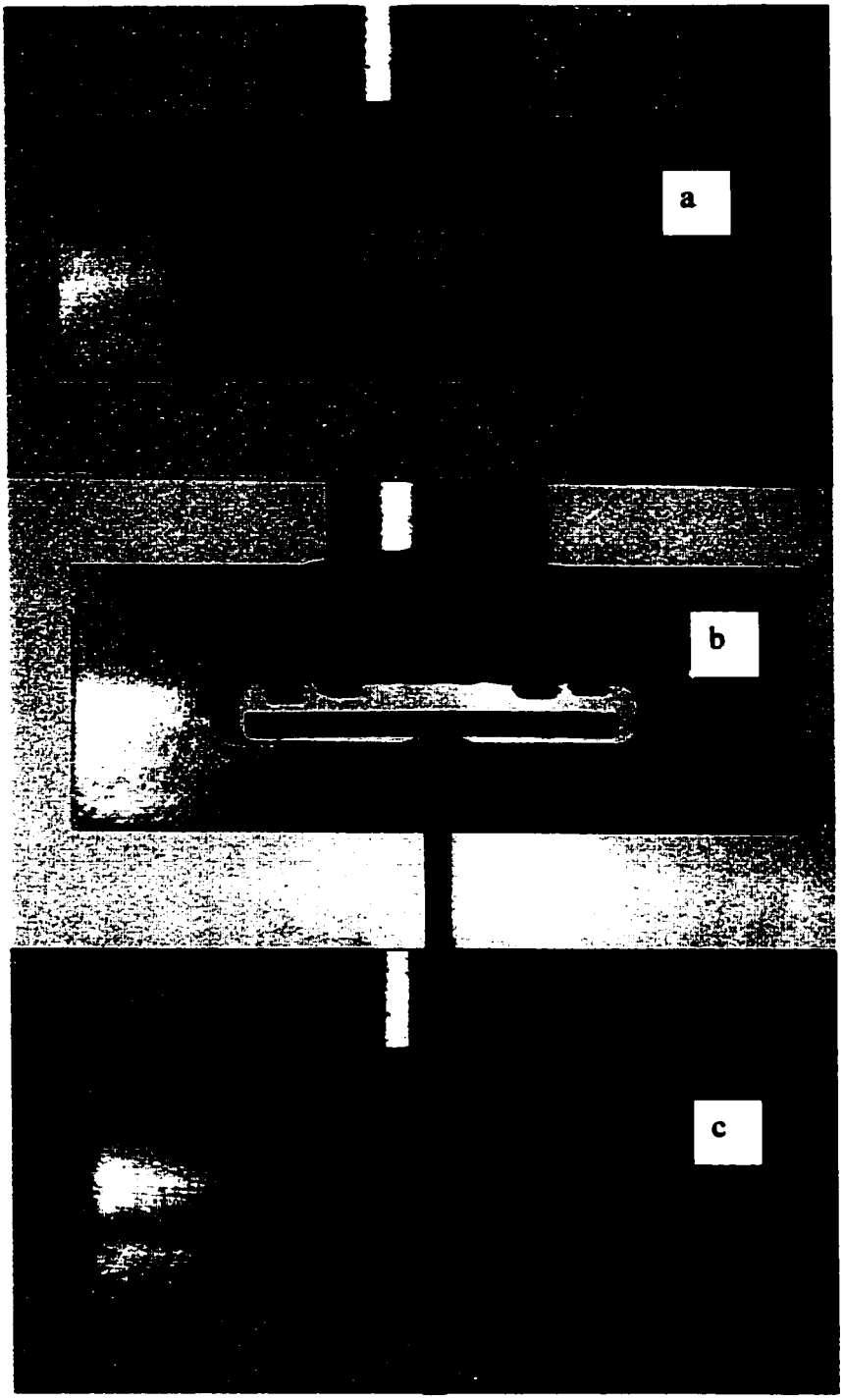

Figure 6.4 Test fixtures of types a, b and c. Tester type c was also used for Valerie's samples.

In 6.4a and 6.4b, the width of the slot is 3.6 mm, giving a total clearance between the web and the fixture of 0.42 mm, while in the case of 6.4c the slot width is 6.47 mm, giving a clearance of 3.29 mm. This clearance difference will contribute to the stretching of the underside of the flange of the sample in the x direction along the weld line, but the main difference is that the flanges are not bent back straight before testing. This controversial conclusion is based on the observation here by a previous student that putting an 3.2 mm thick aluminum shim above the sample in the 6.4c version sample, and clamping it down with the grub screws shown did not affect the test results compared with just pulling the sample held as shown in Figure 6.4c. This result is different than some others have experienced, as reported verbally in the discussion after a presentation at an SPE ANTEC paper. They claimed an improvement in strength measured of about 15% in samples that were clamped. The geometry of their fixtures was unknown.

To determine the effects of the residual stress bending and fixture type on the measured strengths, three T-joint samples 24.5 mm wide were cut from each the measured 100 long samples listed in Table 6.1. One of these samples was pulled in each of the fixtures as shown in Figures 6.4a to c. The results are listed in Table 6.2 below.

Duplicate samples for each of the material combinations listed in Table 6.1 had previously been pulled to failure for samples formed at the same time under the same welding process parameter settings. These previously measured results were also tested using the holder shown in Figure 6.4c, and are listed as V (for Valerie) in Table 6.2.

The results in Table 6.2 dramatically show the effects of test fixture geometry. Looking at columns headed a, b and a-b, it is clear that, with or without the grub screws engaged before testing, the fixture shown in Figure 6.9a and 6.9b produced values that were much higher than those tested in fixture 6.9c (column headed c). Compare the results for column averages and median results as well as individual test results. For angle-measured samples tested in fixture 6.9c (column c), the strengths matched closely the results from the previous worker (columns headed c, v, and c-V). Note that the numbers for columns a, b and c are for only one sample per result; those from V are the average of three results. Because columns headed c and V give similar results, and column V represents many more test results, the comparison between fixtures 6.9a and 6.9c are calculated in the columns headed a-V, a/V and [a-V]/V. None of the differences (a-V) or the ratios (a/V or [a-V]/V) are constant, but the value for tests done in fixture a is always greater than that for Valerie's tests V done in fixture c.

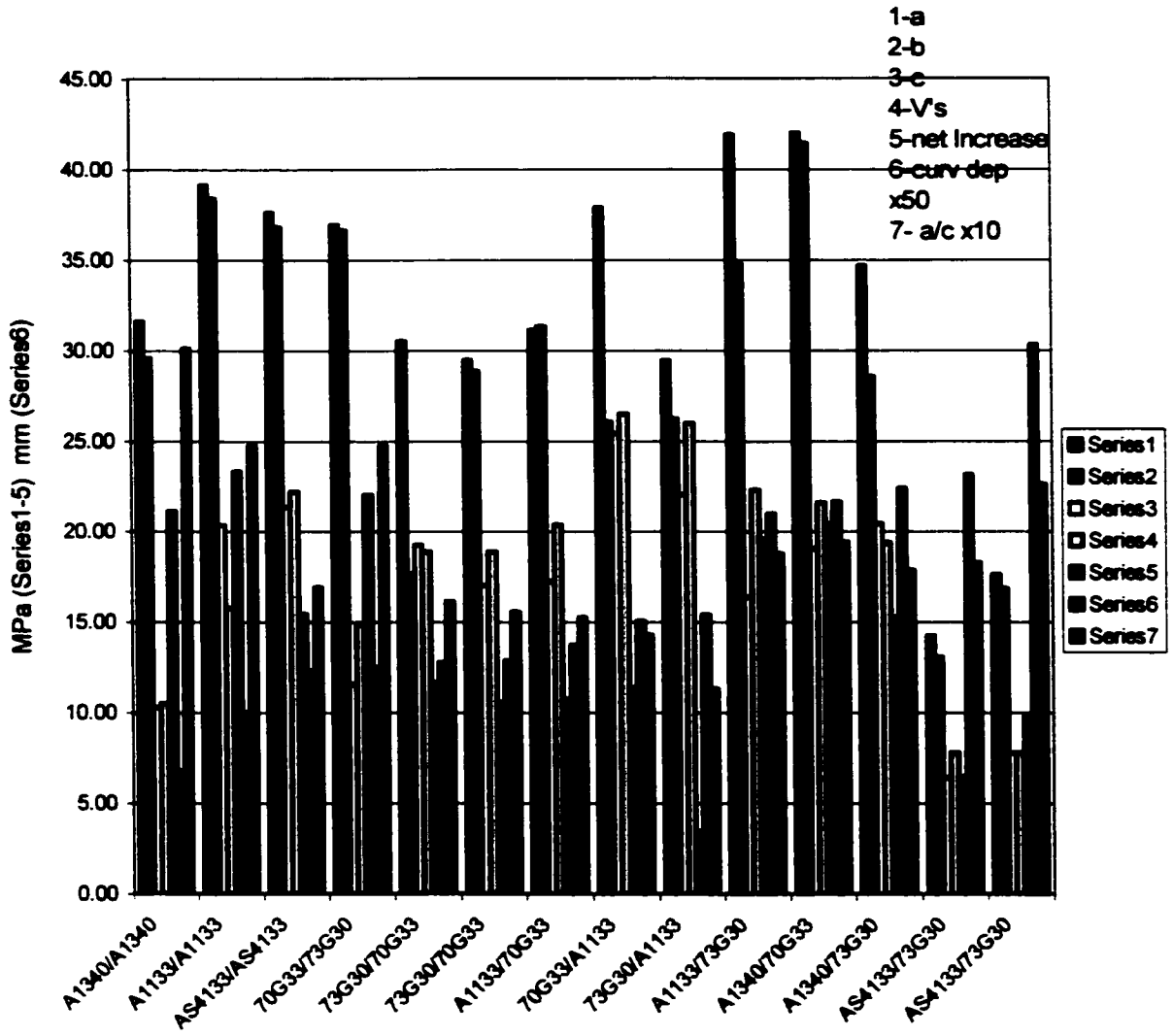

Figure 6.5 Histographic summary of Tables 6.1 and 6.2

Series1, blue, represents the tensile strength as tested by fixture a; while Series 2, dark red is from fixture b. The average value of Series 1 is little higher than that of Series 2, and both are higher those of Valerie's samples. The net value increase between test fixture a relative to V is shown in Series 5 (black). The curvature depth (mm times 50) as Series 6 shows not much correlation with strength. This is better observed in Figure 6.6 Series 7, (dark blue) is the ratio between Series 1 and 4. The average ratio is around 1.92.

Weld Materials	Weld Test Number	Fixture Type a	Fixture Type b	Fixture Type c	Valerie's V	a-b	c-V	a-V	Melt Temp Diff	A / V	(a-V / V)
Web/Flange		UTS MPa	MPa	MPa	MPa				C		
A1340/A1340	5	31.62	29.59	10.29	10.5	2.02	-0.21	21.12	0	3.01	2.01
A1133/A1133	8	39.14	38.39	20.37	15.8	0.75	4.57	23.34	0	2.48	1.48
AS4133/AS4133	17	37.64	36.81	21.37	22.2	0.83	-0.83	15.44	0	1.70	0.70
70G33/73G30	29	36.95	36.64	11.57	14.9	0.31	-3.33	22.05	39	2.48	1.48
73G30/70G33	34	30.54	17.70	19.27	18.9	12.84	0.37	11.64	-39	1.62	0.62
73G30/70G33	35	29.49	28.87	17.02	18.9	0.62	-1.88	10.59	-39	1.56	0.56
A1133/70G33	42	31.15	31.36	17.24	20.4	-0.20	-3.16	10.75	48	1.53	0.53
70G33/A1133	46	37.90	26.06	25.41	26.5	11.84	-1.09	11.40	-48	1.43	0.43
73G30/A1133	49	29.45	26.23	22.06	26	3.22	-3.94	3.45	-87	1.13	0.13
A1133/73G30	56	41.92	34.80	16.40	22.3	7.12	-5.90	19.62	87	1.88	0.88
A1340/70G33	66	42.02	41.44	19.06	21.6	0.58	-2.54	20.42	48	1.95	0.95
A1340/73G30	84	34.70	28.55	20.44	19.4	6.14	1.04	15.30	87	1.79	0.79
AS4133/73G30	94	14.26	13.09	6.43	7.8	1.17	-1.37	6.46	104	1.83	0.83
AS4133/73G30	96	17.65	16.87	7.76	7.8	0.77	-0.04	9.85	104	2.26	1.26
Ave		30.04	27.29	16.97	18.071	3.43	-1.31	14.39		1.90	0.90
Median		33.16	29.23	18.15	19.15	1.00	-1.23	13.47		1.81	0.81
Minimum		14.26	13.09	6.43	7.8	-0.20	-5.90	3.45		1.13	0.13
Maximum		42.02	41.44	25.41	26.5	12.84	4.57	23.34		3.01	2.01

Table 6.2 Strength results using different test fixtures on nominally identical samples.

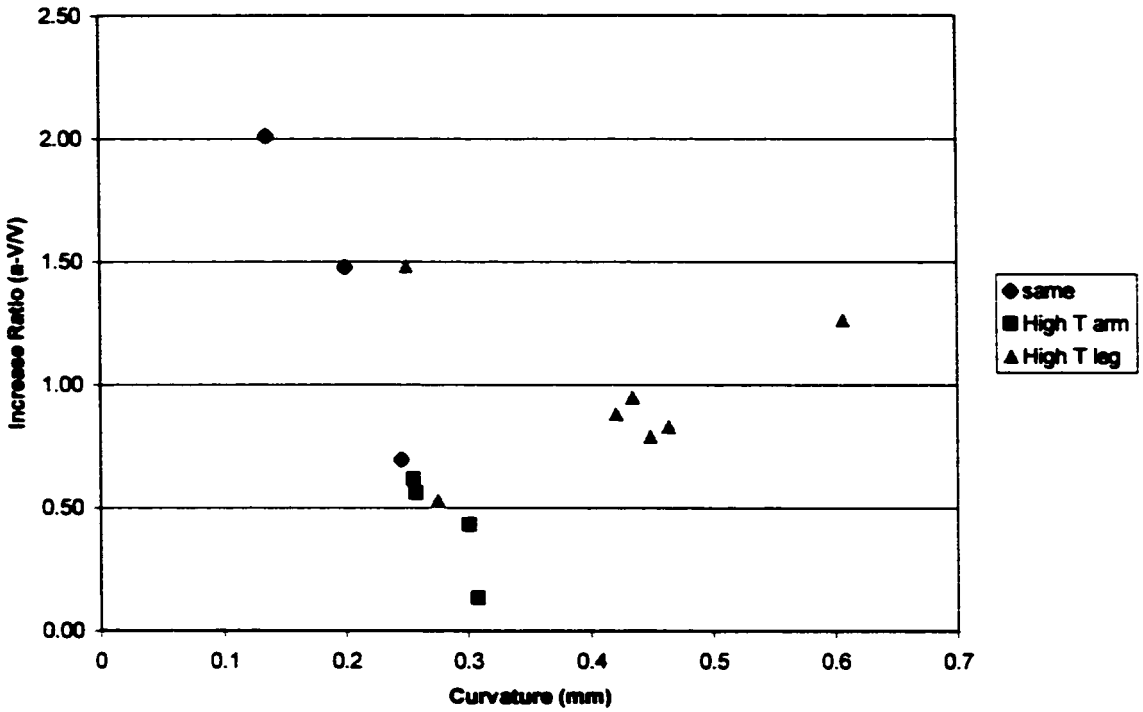

Figure 6.6 Correlation between the tensile strength ratio (between fixtures a and V as a-V/V) versus the depth of curvature.

The correlation between the increase in measured strength as a function of curvature surprisingly shows a negative trend for high temperature amides welded to themselves, as does those samples which have the high temperature material on the flange. The samples which have the high temperature material on the web, which are those most likely to have embedded liquid zones, do show a positive trend for all except for test set 29, which is the only sample in this group with a nylon 66 as the web. All the others have high temperature amides as the web material. This latter group sub-group has a higher difference in temperature between the flange and web than Test 29. It is interesting that the two highest values of increase ratio are for the two high temperature samples welded to themselves. The next highest is for nylon 6 welded to nylon 66, where the temperature difference is only 39^0C.

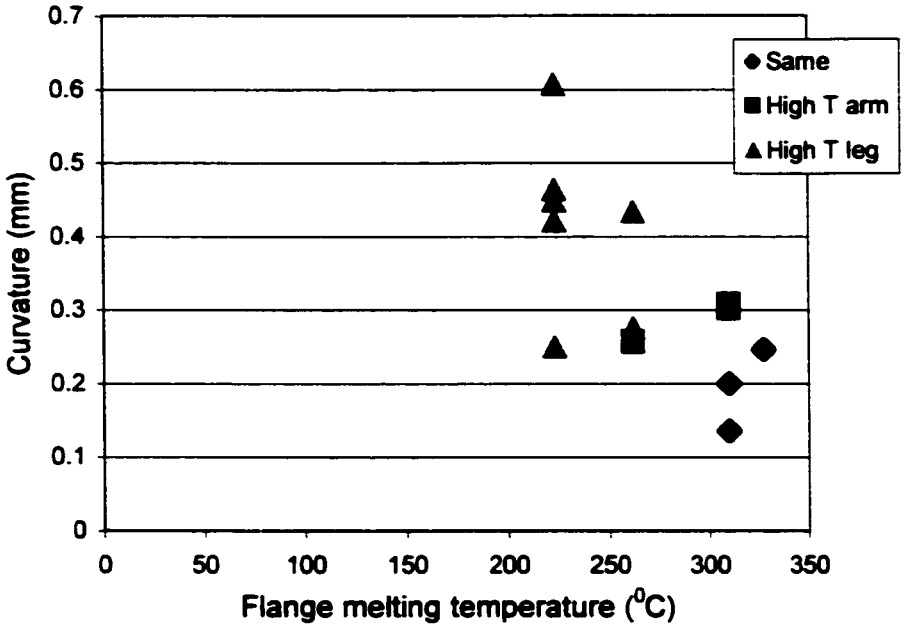

Figure 6.7 The relationship between curvature and the melting temperature of the flange

There is a correlation between curvature and the melting temperature of the material in the flange. This can be attributed to having less penetration of the web into the flange. The higher melting temperature also implies that there will be a stiffer material in the flange, so that a higher stress level must be achieved for the same level of curvature. This may help to explain the large values for strength ratios at relatively low curvature for the high temperature amides welded to themselves as shown in Figure 6.6.

CHAPTER 7
RESULTS FOR BUTT WELD JOINT TESTS

A series of butt welds has been made by linear vibration welding. Its intent was to do a preliminary survey of welding potential. No attempt was made to optimize the welding parameters for these material combinations. The tensile strength of welded butt joint is one of the most important mechanical performance parameters for critically stressed under-the-hood components. For non-reinforced thermoplastics (polypropylene, polyester, etc), the percentage of tensile strength retention with different welding techniques is in the range of 30-90%. For non-reinforced nylon 6 (and for nylon 66), a butt weld joint strength is nearly equivalent to the strength of the base material[24]. However, for fiberglass-reinforced thermoplastics, the maximum achievable weld strength is usually 70-80% of the strength of the base matrix material.

7.1 Tensile Strength

Materials used in these tests were HTN 52G35, 70G33, A1133 (white), A1133 (black), AS1466, AS1933, AS4133, A1565 and AS1133. The different combination of the welds and temperature difference are listed along with the average weld tensile strength in Table 7.1

Sample Group	Material	Melt Temper-ature	Material	Melt Temper-ature	Temp Difference	Average Strength
		°C		°C	°C	MPa
BA3-BA6	70G33	262	70G33	262	0	50.52
BA7-BA10	HTN 52G35	310	70G33	262	48	27.8
BA11-BA16	HTN 52G35	310	HTN 52G35	310	0	24.1
BA17-BA20	70G33	262	A1133 W	310	50	46.93
BA21-BA24	70G33	262	A1133 B	310	50	49.39
BA25-BA28	70G33	262	A1340	310	50	43.01
BA29-BA32	70G33	262	AS1466	310	50	28.44
BA33-BA36	70G33	262	AS1933	310	50	44.06
BA37-BA40	70G33	262	AS4133	327	65	31.96
BA41-BA44	70G33	262	A1565	310	50	31.25
BA45-BA48	70G33	262	AS1133	310	50	39.78
BA49-BA52	70G33	262	70G33	262	0	36.7

Table 7.1 Butt joint combinations for which welds have been made.

Test groups BA1 to BA2 were used to find usable welding parameters. For groups BA3 to BA16, where the samples were 6 mm thick, the welding parameters were kept at the same values: Amplitude 0.07 in (1.78mm) , weld force 100lb (470N), weld time 8 seconds, hold time 20 seconds. From BA17 to BA52, the samples were 3 mm thick, and the welding parameters were adjusted to a different set of common values: Amplitude 0.07 in (1.78 mm), weld force 100 lb(470 N)), weld time 4.5 seconds, hold time 20 seconds.

The individual experimental values for tensile strength and meltdown, as well as the welding parameters are listed in Appendix IV. Table 7.1 gives the average fracture strengths and meltdown values, based on a sample size that varied between 4 and 6 samples per test group. This means that every weld test parameter group had 12 to 18 tests. Sample BA14 was not tested. It was set aside for reasons discussed later in this section.

Figure 7.1 The black sample (70G33) and the "natural" sample (A1133) have been butt welded together.

7.2 Tensile Strengths in 6 mm Thick Samples

The highest average weld strength in 6 mm thickness samples was 50.52 MPa. This occurred in the 70G33/70G33 materials combination. The second strongest welds were found in the materials combination HTN/70G33, where the average weld strength was 27.8 MPa. The welds between HTN and itself produced the poorest results. Their average tensile strength was only 24.10 MPa.

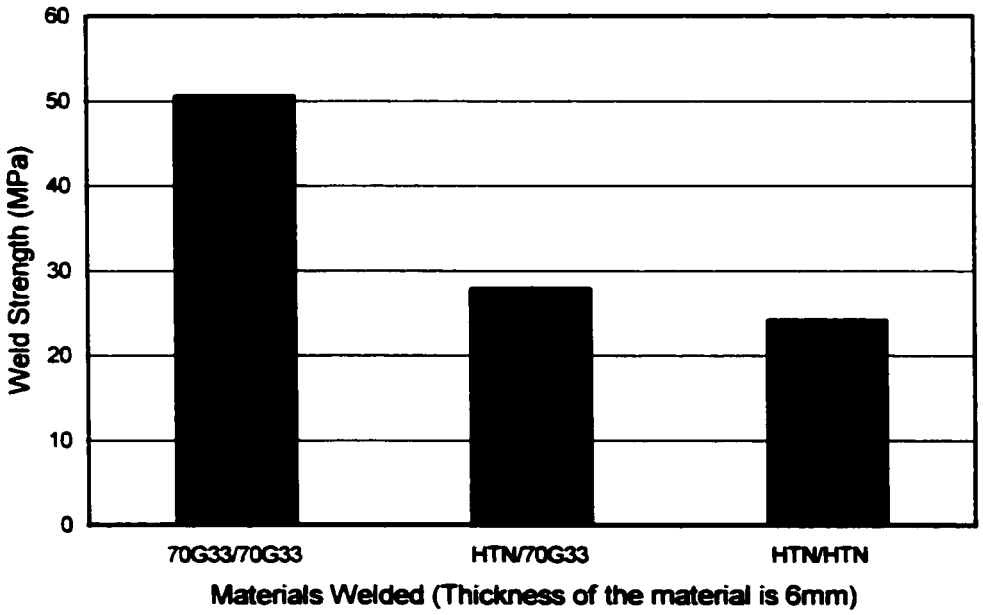

Figure 7.2 Tensile strength of 6 mm thickness butt joints.

Why is the strength of the HTN/HTN combination so low? In Table 7.1, the column headed "Melt temperature" shows that HTN is a high melting point temperature amide (310^0C). These welds were made using the process parameters which were found

to make for good welds with combinations using the low temperature nylon 70G33. It appears that the energy dissipated using these parameters does not melt enough material when only HTN is present. In HTN (or any other thermoplastic) only when the meltdown distance reaches a critical penetration threshold, can the weld achieve its maximum strength.

For test groups BA3 to BA6, there were12 welds. For these samples, the welding process parameters were set to the same values, but Figure 7.3 shows that the weld strength distributions are different.

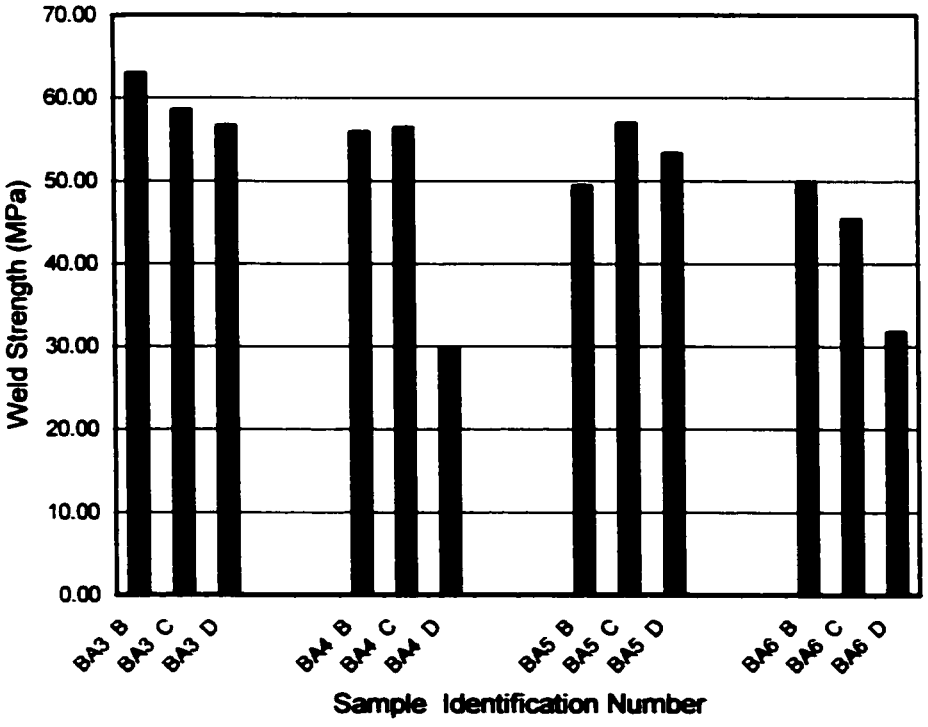

Figure 7.3 Individual test sample weld strength variation of samples of HTN/70G33. The ID numbers are in the same order that they were located in the welded sample.

In BA3 and BA6, there is a continuously decreasing strength from test sample B to D. In groups BA4 and BA5, the maximum tensile strength appears in the middle sample. For these samples all the other process parameters were set the same, the only obvious process variation is pressure along the weld interface. When the sample was mounted into the holding fixture, it was difficult to make sure the surfaces to be welded were exactly parallel to each other. Figure 7.4 is a photograph of BA14D. It can be seen the right hand side of the sample is welded, but on the left hand side, the two parts do not touch each other.

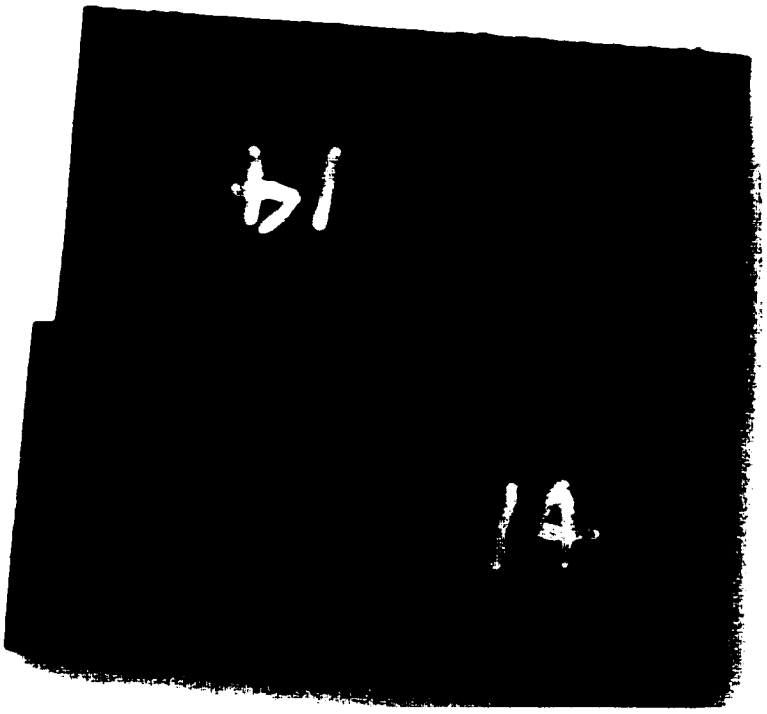

Figure 7.4 Unsuccessful butt joint for BA14, HTN to HTN.

Most of the tensile samples broke at the weld surface. But in some samples the fracture occurred in the parent materials. In Appendix IV, samples marked with a black

dot represent test specimens where fracture happens in the base material. Samples BA3C and BA4B, which is a 70G33/70G33 combination, broke in the 70G33 base material. Samples BA12B and BA12D, both HTN/HTN combinations, broke within the HTN base material. Samples BA7B, BA7D, BA9B, BA9C and BA10B, all of which were HTN/70G33 combinations, all broke within the HTN base material. Figure 7.5 shows the failure running through the HTN high temperature material in BA10B.

From the listed material properties, HTN should be stronger than 70G33. The tensile strength of HTN is 241 MPa (dry as molded) and 210 MPa (50% RH). The tensile strength of 70G33 is 210 MPa (DAM), 150MPa at 50% RH. The strength of fiberglass reinforced materials is strongest along the injection molding direction, because the fibers line up along this direction. For the HTN/70G33 samples mentioned above, the fibers in the HTN base materials may be parallel to the plane of the fracture.

Figure 7.5 Tensile sample BA10B has broken in the HTN base material.

7.3 Tensile Strengths in 3mm Thick Samples

There are nine groups of weld combinations in the 3mm thickness materials, all of which have 70G33 on at least one side of the weld. Figure 7.6 shows that the highest weld strength at 49.39 MPa, occurs in the 70G33/A1133 materials combination, in which A1133 is black in colour. The next highest strength is also 70G33 welded to A1133, but the latter has a white (or natural) colour.

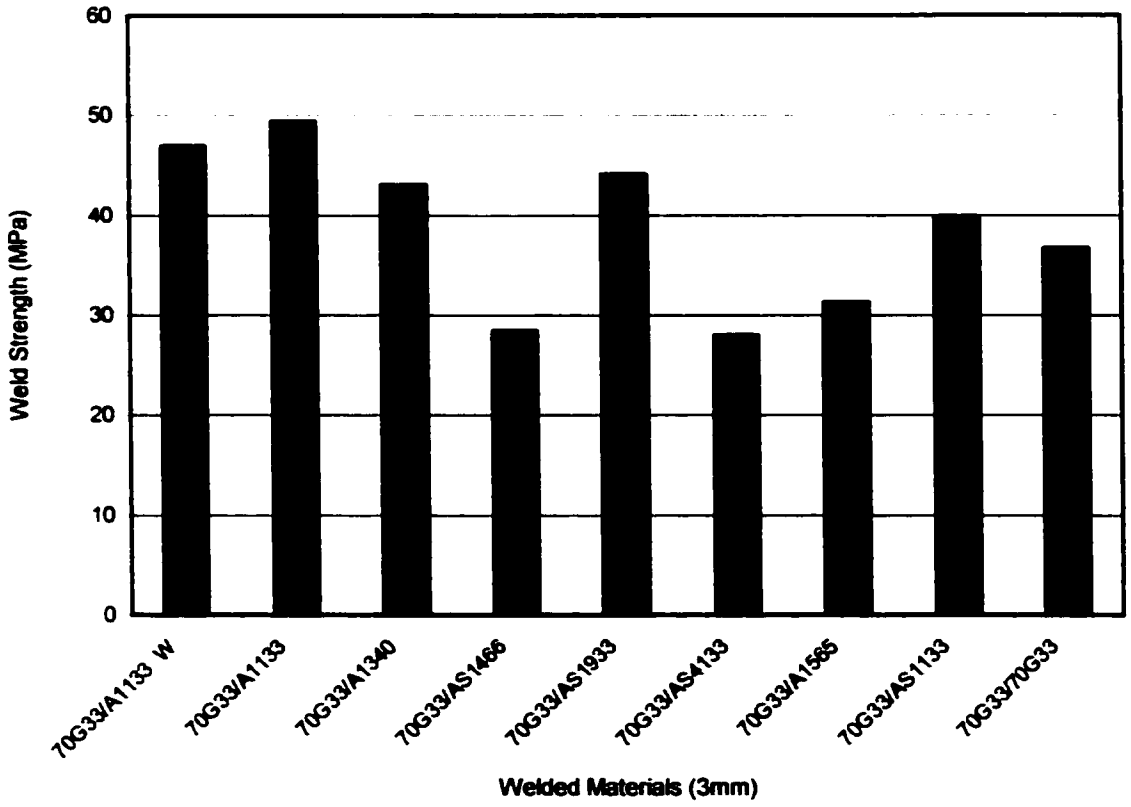

Figure 7.6. Tensile strength of 3mm thick material combinations.

There are three other weld combinations with a tensile strength greater than that of 70G33/70G33 (36.7MPa), which was the strongest of the 6 mm butt welds at 50.52 MPa.

The weakest average weld strength in the 3 mm samples was 70G33/A1466 at 28.44 MPa. The samples with the highest temperature difference (70G33/AS4133) had a strength of 31.96 MPa.

Figure 7.7 shows the meltdown distance (penetration) for each material combination.

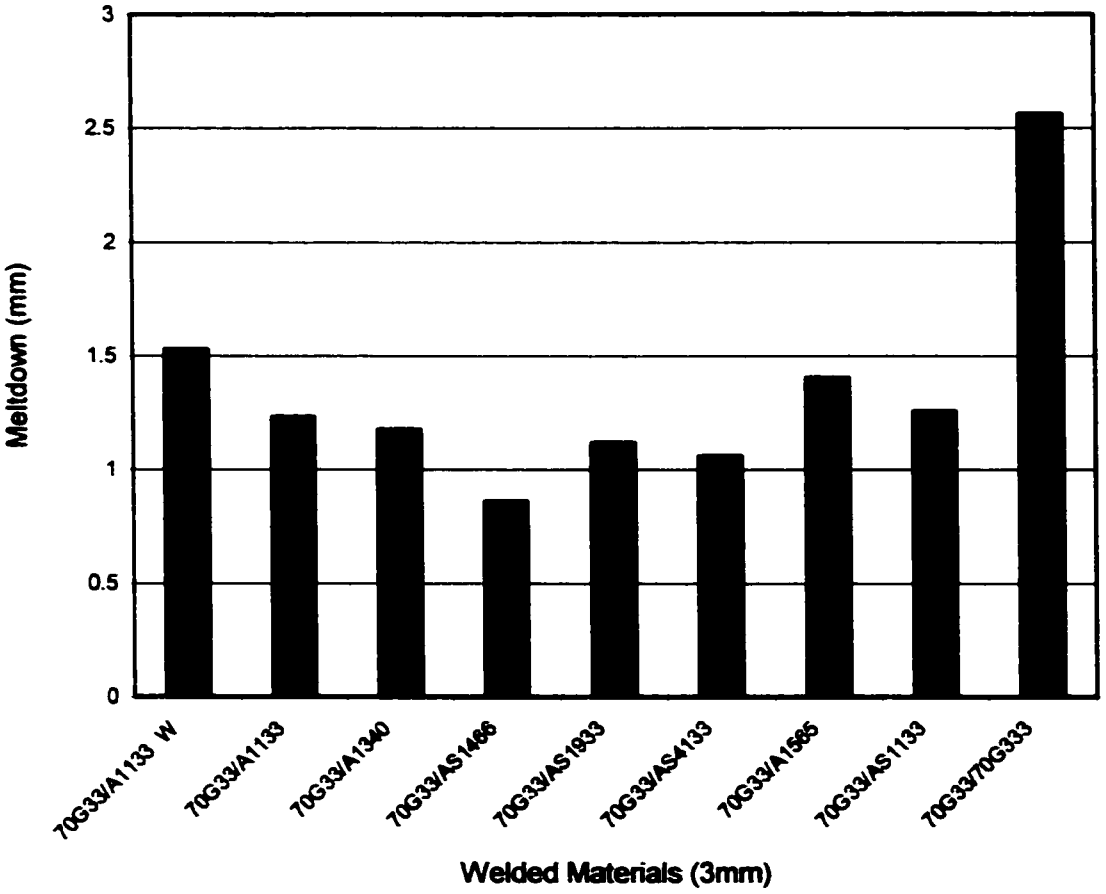

Figure 7.7 Meltdown distance for different combinations of materials in 3 mm thick butt welds.

Figure 7.8 shows that there is a weak correlation between strength and meltdown distance for the 3 mm thick samples which have a high temperature amide welded to 70G33.

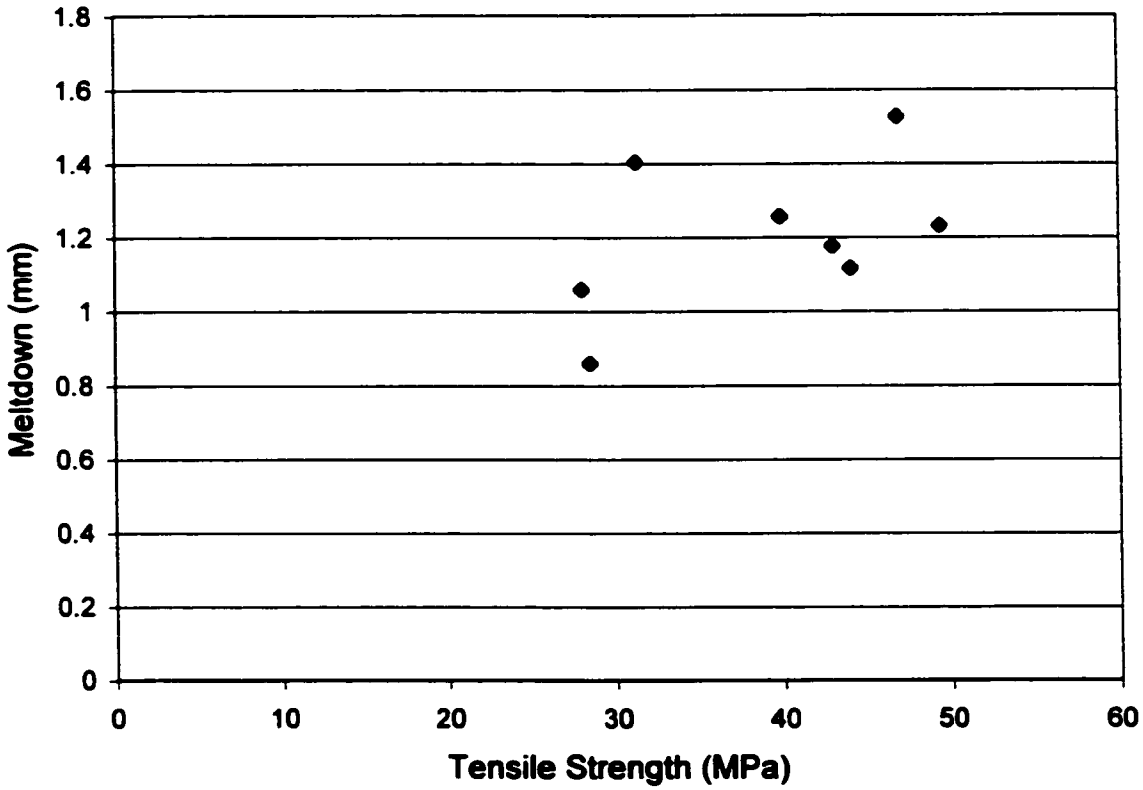

Figure 7.8 Meltdown distance vs strength for 3 mm samples excluding 70G33/70G33.

7.4 Further Discussion

The only material combination used in both 6 mm and 3 mm thick samples was 70G33 welded to itself. Comparison of the results for these two sets of samples is of interest.

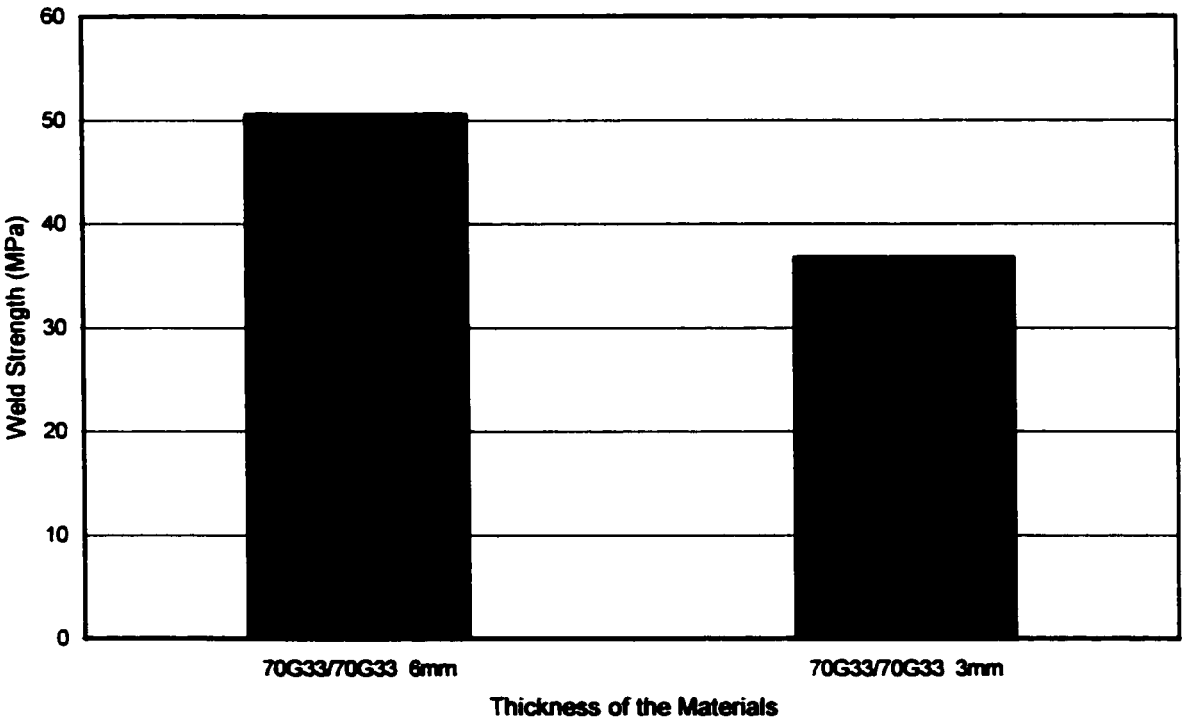

Figure 7.9 Strength comparison for 6 mm thick samples and 3 mm samples of 70G33/70G33 butt welds

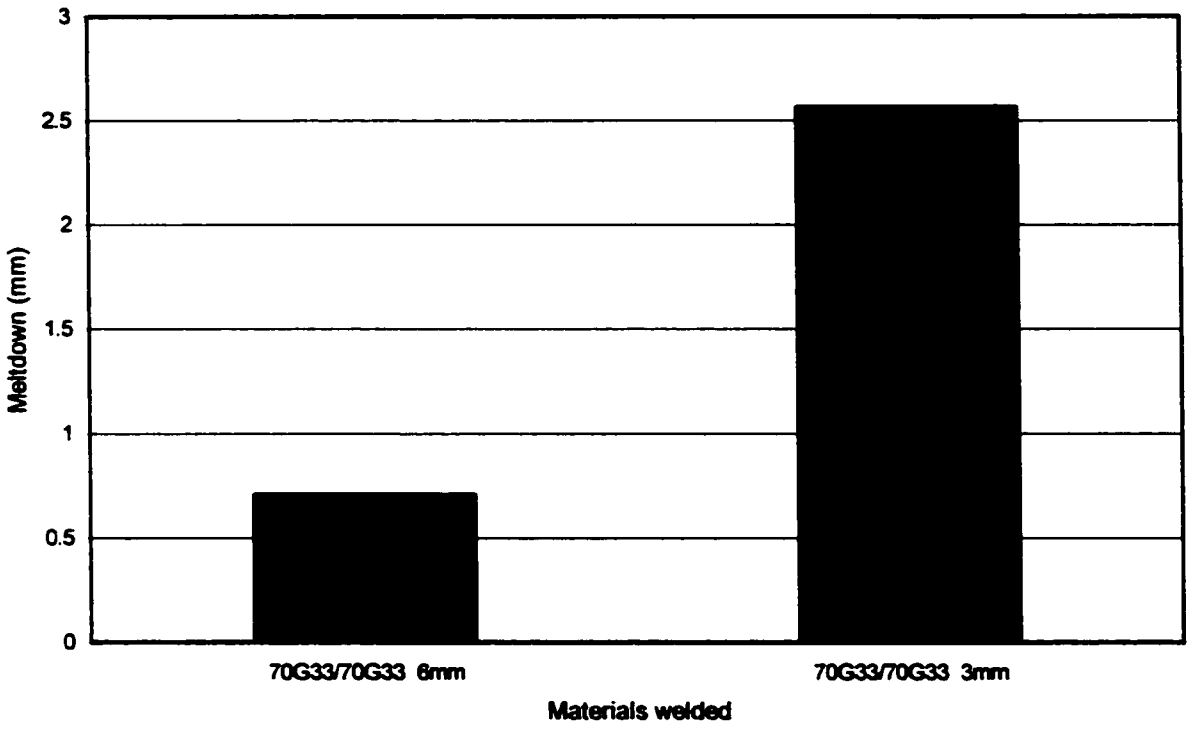

Figure 7.10 Meltdown distances for 6 mm thick samples and 3 mm samples of 70G33/70G33 butt welds

Figures 7.9 and 7.10 show that although the meltdown distance for the 3 mm thick samples of 70G33/70G33 is greater than that for the 6 mm samples for the same material combination, the thicker sample has a much higher strength. The weld strength for a thickness of 6 mm is 50.52 MPa and 3 mm is 36.7 MPa. So, the weld strength of a butt joint is apparently affected by the thickness of part.

Theoretically, when the process parameters and materials are the same, the butt welds should have the same strength, independent of the thickness. One factor that might help to explain the difference which has been observed is shown in Figures 7.11 and 7.12.

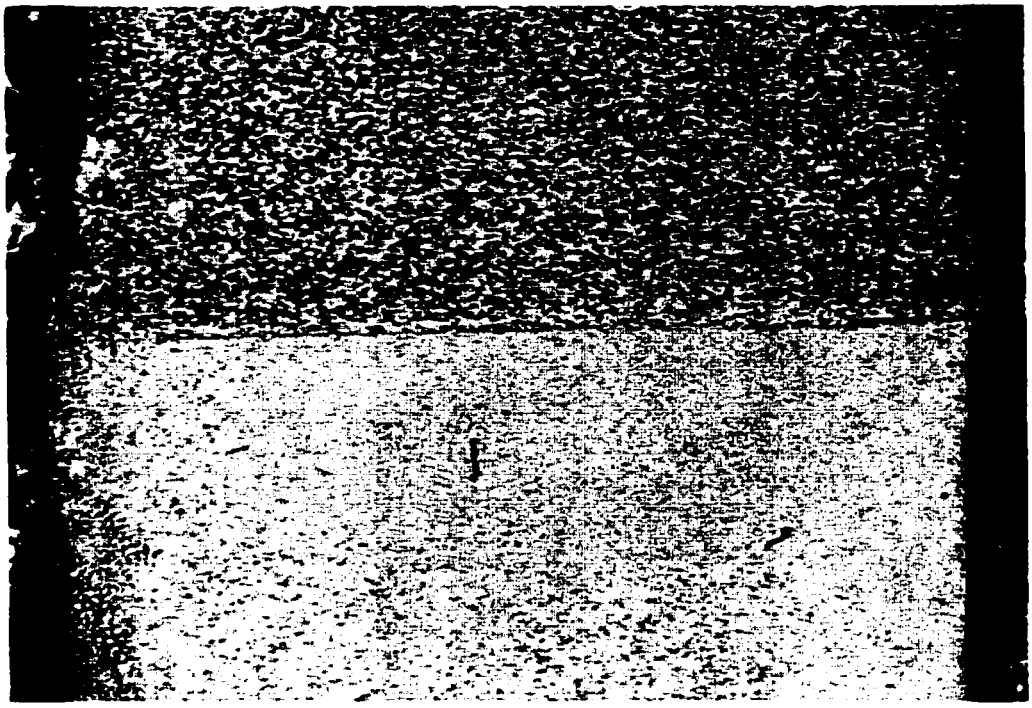

Figure 7.11. Geometry of the BA40E 3 mm cross-section.

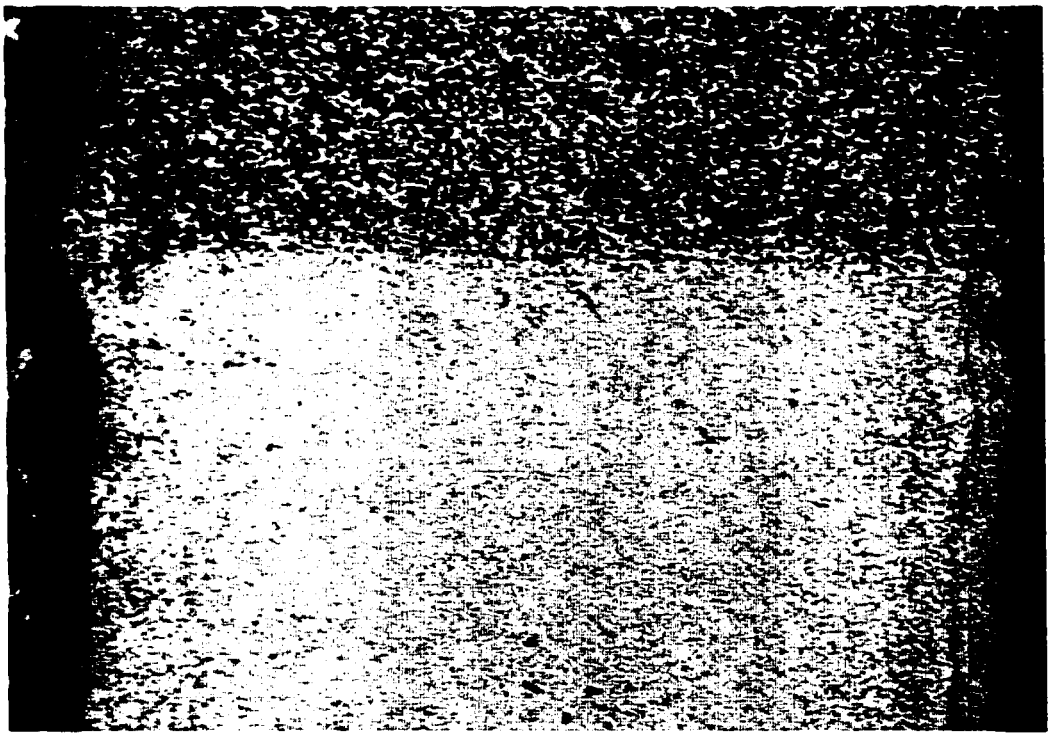

Figure 7.12. Another 3 mm weld cross-section.

In both of these figures, the two welded parts are not aligned with each other. This means that total width of the weld is smaller than that of width of the part. The unaligned edges may also act as local stress raisers. This misalignment occurs when the sample is loaded into the holding fixture. It is difficult to make sure the weld surfaces are parallel to each other, and share the same centerline. Moreover, as the welding proceeds, a liquid layer forms , allowing the two faces to slide sideways with respect to each other. This defect makes up a higher percentage of 3 mm thick width, than that of the 6 mm width. Earlier in this chapter, Figure 7.4 showed sample BA14, an even more extreme example where the two halves of the weld did not even make contact a one end of the sample.

CHAPTER 8
MICROSTRUCTURAL OBSERVATIONS

It has been reported that for unreinforced materials, weld strengths nearly equivalent to the strength of base material can be attained [24]. However, in glass fiber reinforced thermoplastics, the maximum weld strength achievable is usually thought to approximately equal to or less than that of the unreinforced base material. In the present research work, all the weld strengths are lower than that of the base materials. This lowered tensile strength is attributed to a change in the glass fiber orientation at the welded joint, where the fibers align along the weld line, perpendicular to applied stress in the tensile test strength measurement. In this configuration, they act as stress raisers rather than reinforcements.

8.1 Weld Microstructures Observed In T-Joint Samples

Three shapes of T weld interface are shown in Figure 8.1a, b, and c. When the lower temperature material is in web position, there is no penetration. When the same material is welded itself, or when a lower temperature material is in flange position, the weld shapes vary from triangular to semi-circular to square (see Figure 8.1).

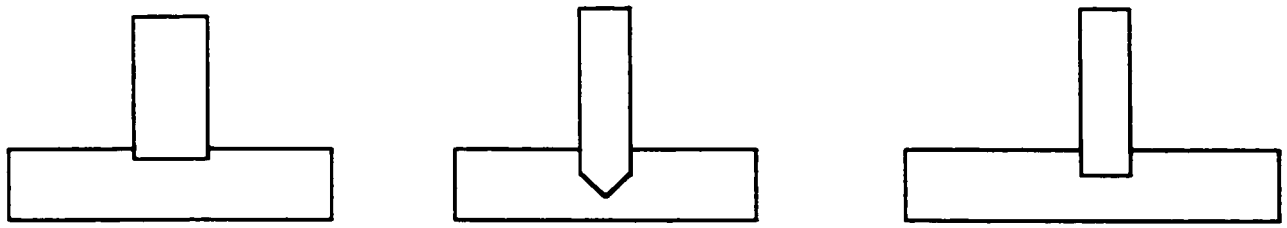

Figure 8.1 Typical weld interface shapes

In Figure 8.2, the high melt temperature web (upper left hand side) has penetrated into the lower right hand side) flange in all three micrographs.

This has created the flash in the right hand side of Figure 8.2a with its associated porosity at the interface.

Figure 8.2b and Figure 8.2c are about in the positions with respect to each other that they occupied in the original sample.

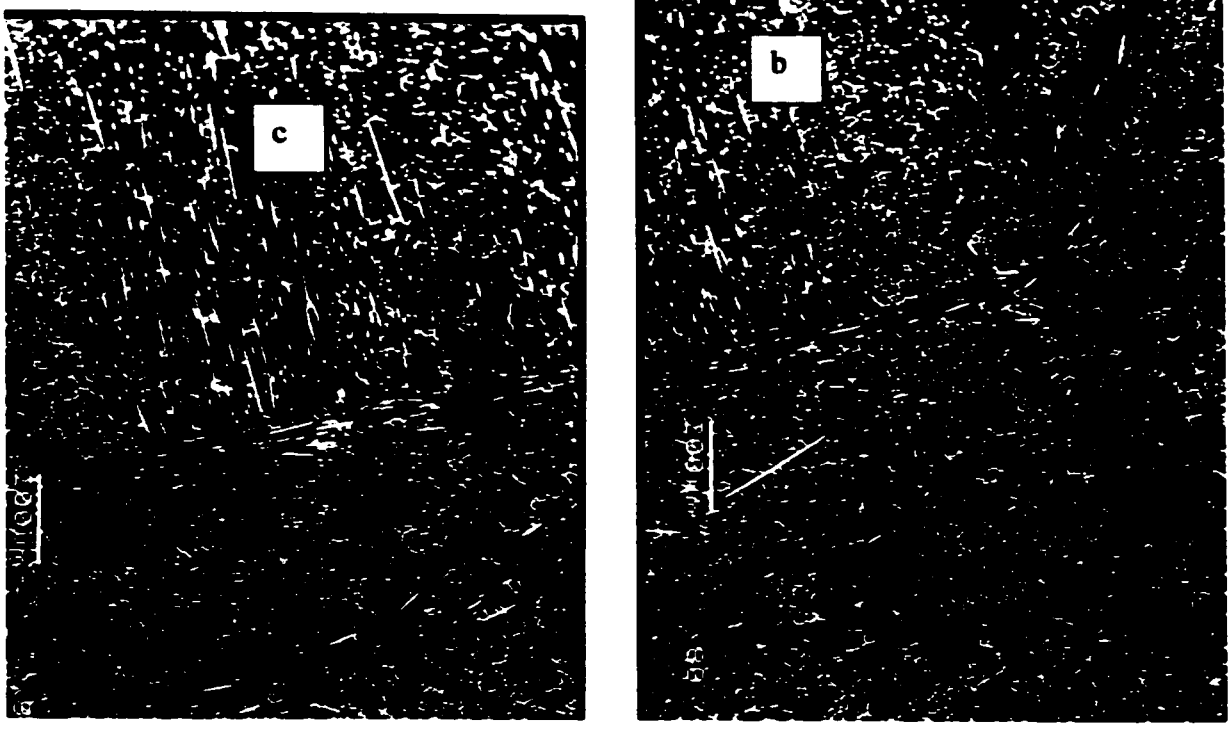

Figure 8.2 High temperature part penetrate into low temperature material (SEM x 80)

The microstructures shown in Figure 8.2 are from test set 96, in which the web material is AS4133, and flange material is 70G33. The melt temperature difference is 38 C. There is an obvious interface between two materials, and the glass fiber orientation is rotated into the weld interface. Figure 8.2a shows that there is no bonding at the flash at the edge of the weld.

8.2 Observations On Cap-Welded-to-Flange Joints

The test sample geometry is shown in Figure 8.3. In this group only, long fiberglass material, Vernon F-7007, was used.

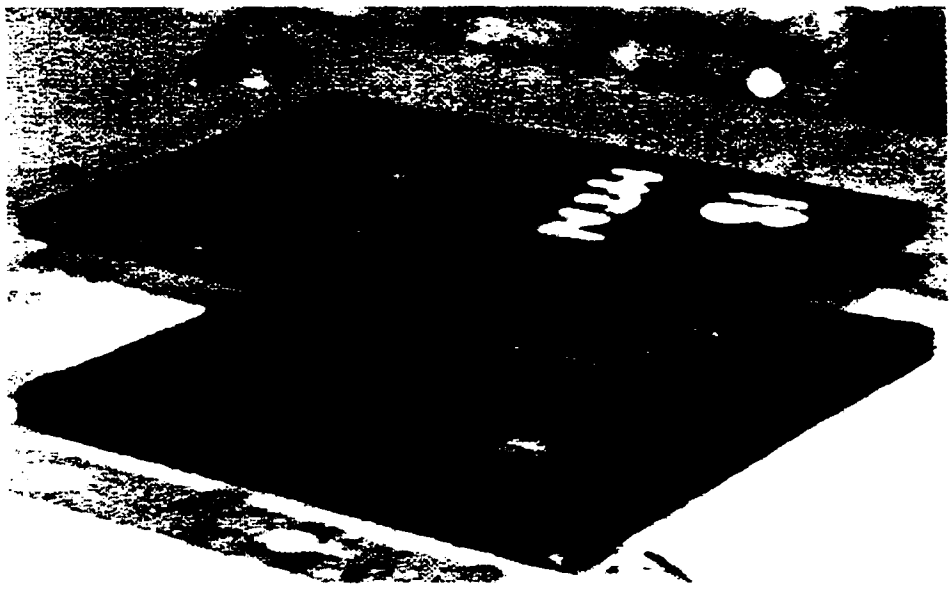

Figure 8.3 Geometry of Cap-Welde –to Flange samples

CWF Sample 65, with long fiber RF-7007 cup, and HTN 52G35 plaque had an average strength of 4.67 MPa. For this sample, the welding parameters were: Amplitude 0.071 in (1.78 mm), weld force 1200lb (5.7 KN), weld time 2.72 second and the hold time was 3 seconds.

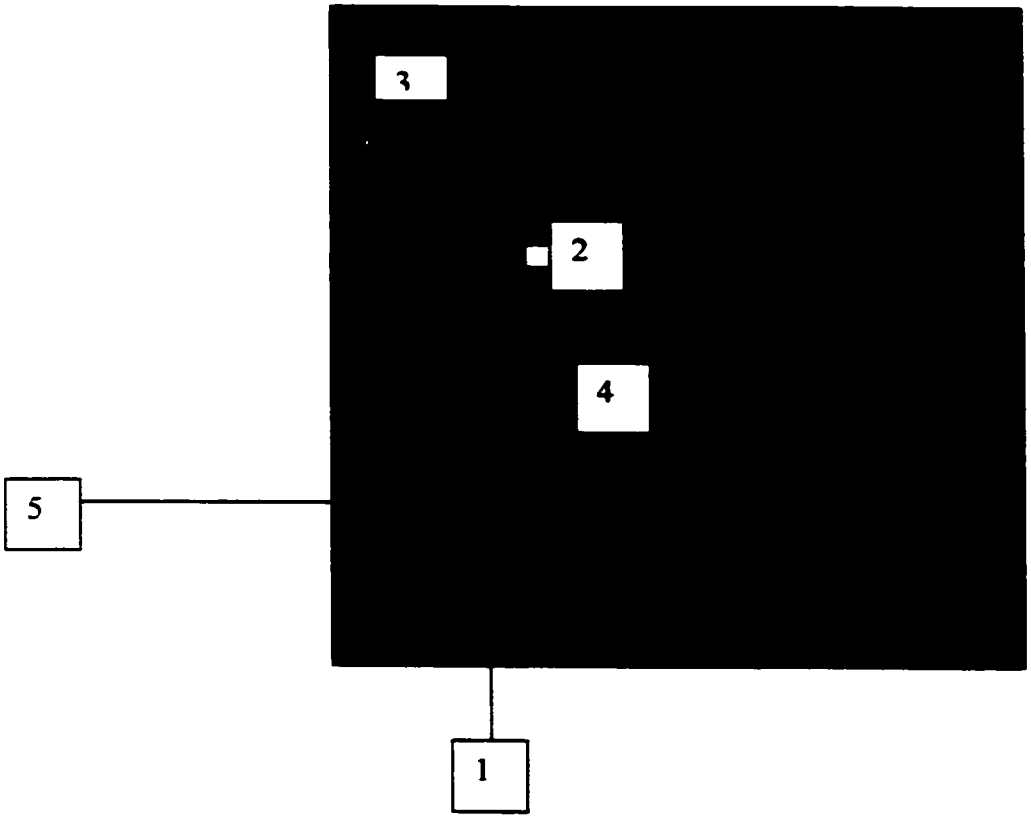

Figure 8.4 Photographic of the fracture surface showing the locations chosen for the micrographs in Figure 8.5

From the fracture surface of CWF sample 65, (Figure 8.4) five different areas were examined to observe the fiberglass orientation.

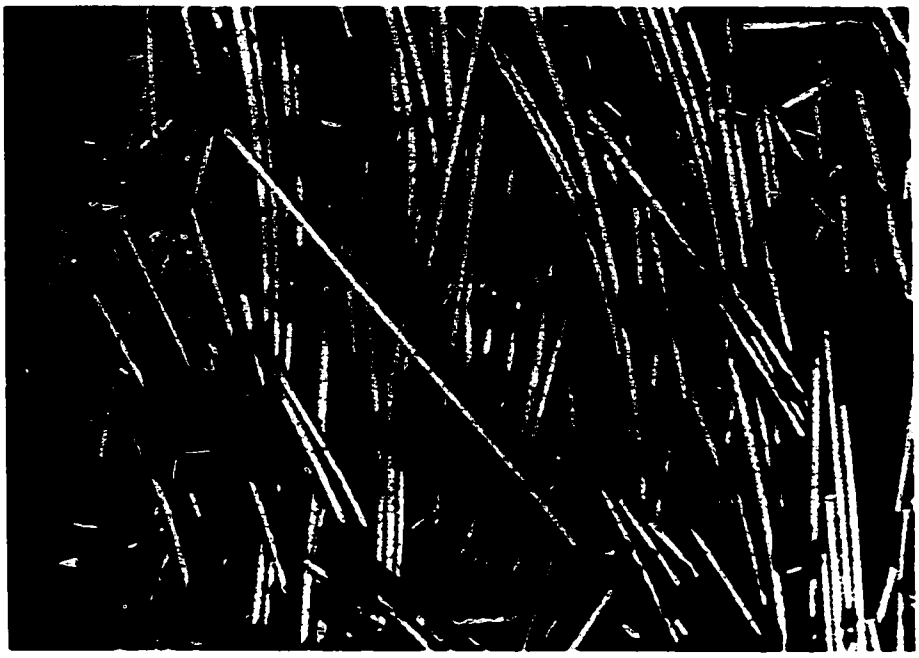

Figure 8.5a Long glass fibers at the area around point 1. The outer wall of the cap is on the left hand side of the picture.

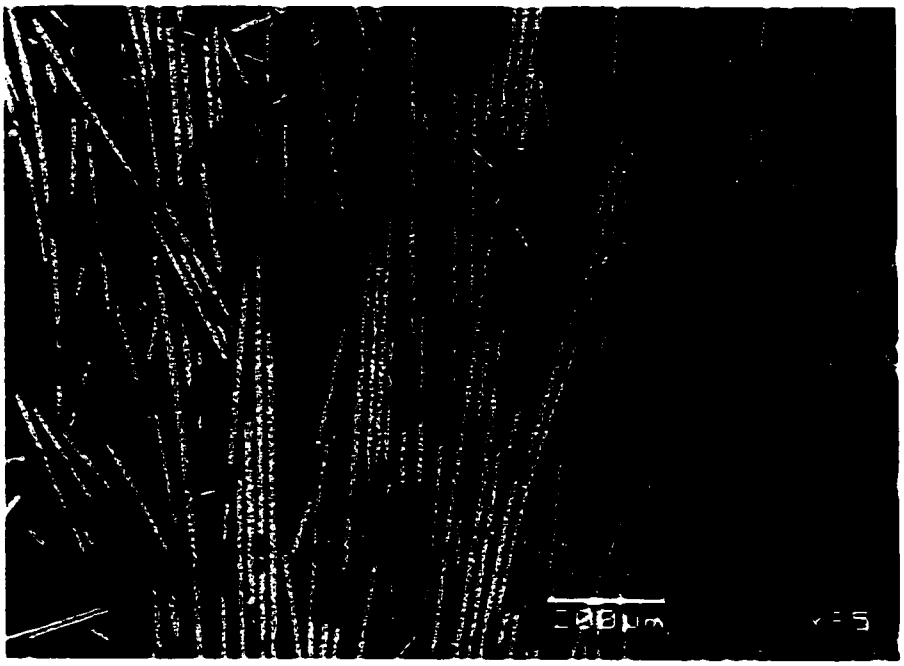

Figure 8.5b Fibers in the fracture surface around point 5;which is adjacent to Figure 8.5a

Figure 8.5C The area around point 4, adjacent to Figure 8.5b. The inner wall surface is on the right hand side of the figure.

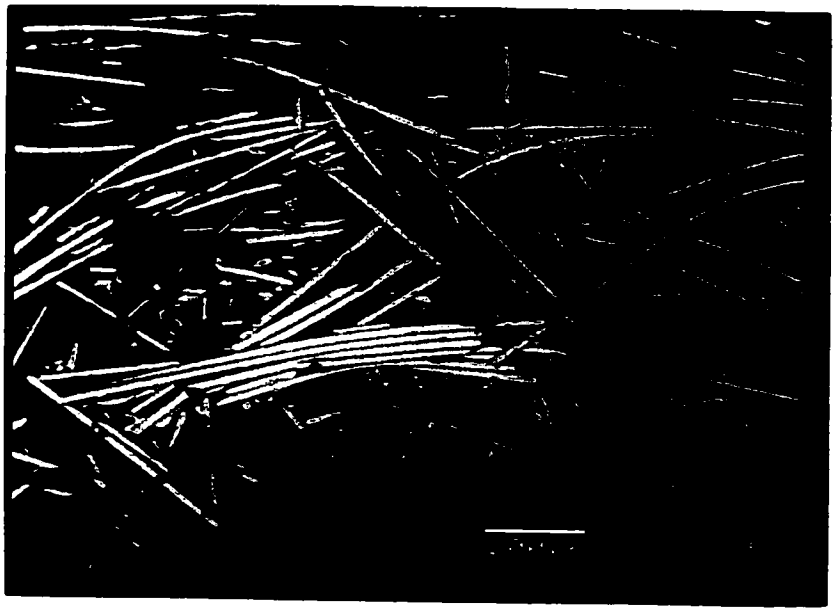

Figure 8.5d Fracture surface around point 2 near inner wall.

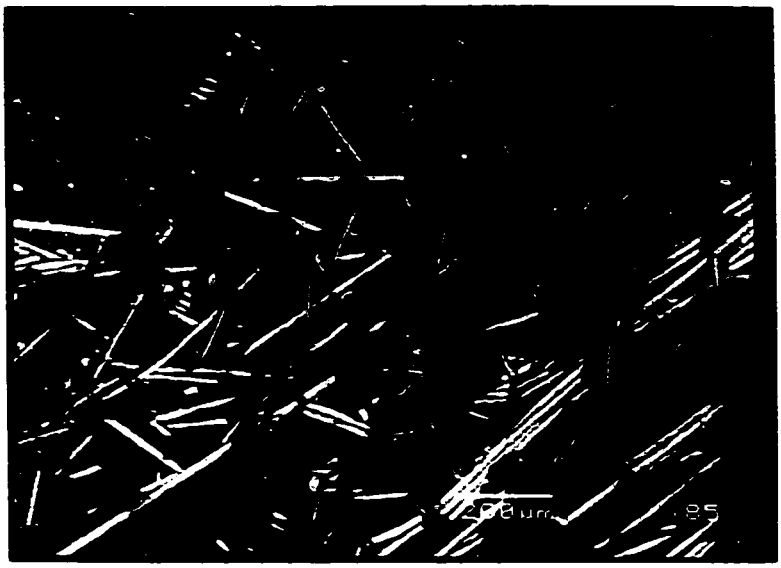

Figure 8.5e Fracture surface around point 3 near outer wall

Figures 8.5 have common characteristics in that the fiber orientation is still along the injection molding flow path. A weld line can be seen in Figure 8.5d. Figure 8.5a shows that the fiberglass orientation is along the edge of the curve. It also looks like there are no broken fibers at the fracture surface. So, in this case the orientation of fiberglass is not changed along the weld direction.

CHAPTER 9
RESISTANCE WELDING RESEARCH

9.1 Overview

In resistance welding, also called resistance implant welding [25], an electric current is applied to a conductive heating element or implant placed at the joint interface of the parts being welded. The implant temperature increases through Joule (I^2R) heating, and the surrounding plastic melts and flows together, forming a weld puddle. The current is shut off and the plastic freezes. Thermoplastics can be welded by this method, and it was originally developed for high performance thermoplastics reinforced with continuous carbon fibers.

To begin the welding cycle, pressure is applied to the weld stack, and then an electric current is passed through the heating element, as in Figure 9.1. During the assembly stage, a weld stack consisting of a heating element sandwiched between two adherents is put together. To begin welding, electrical contacts are connected to a power supply, and pressure is applied to the insulator. Joule heating of the implant causes a rise in temperature. Heat is transferred from the heating element to the thermoplastic material in the weld stack; the adjoining thermoplastic material melts and flows or softens under pressure. Any surface irregularities are smoothed out, and molten plastic is squeezed out of the weld interface, removing any interlaminar voids.

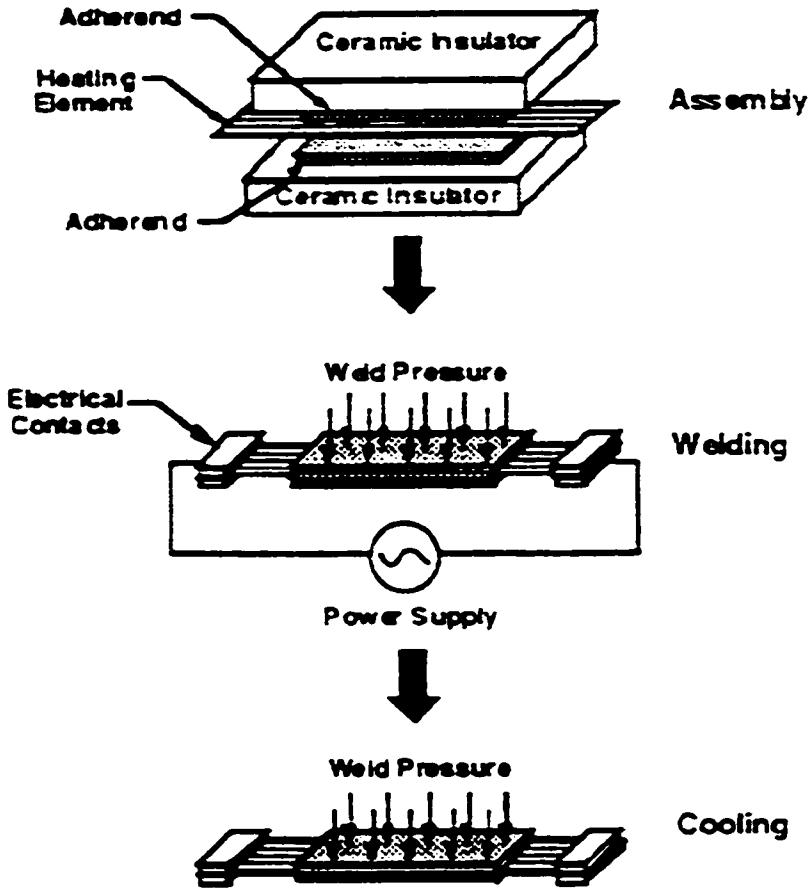

Figure 9.1 The resistance welding process

Intimate contact between the two thermoplastic parts combined with molecular diffusion on melting allows polymer chain entanglements and migration across the interface to occur. During the cooling stage, the power is turned off. Pressure is maintained after the current is shut off, allowing cooling and solidification of the weld under pressure.

Commercial resistance welding processes can be performed at either constant power or constant temperature. In constant power processing, a particular voltage and

current is set for the entire weld, and welding occurs for a specified time. This process is not isothermal, and peak temperatures are difficult to predict. In constant temperature resistance welding, sensors, such as thermocouples, are used to monitor the welding process in order to adjust current and voltage as necessary. The constant temperature process provides more thermal uniformity but is not commonly used.

A three stage welding cycle is used in resistance welding: a ramp up stage, a peak current stage, and a ramp down stage. Weld cycle times are about one minute. Process parameters include power or current applied to the heating element, weld pressure, peak temperature, and dwell time (time at the peak current).

Resistance welding is a useful method for joining dissimilar materials. It can be used to join materials that are difficult to weld, such as thermosets and metals with different melting points.

Maximum heat is generated at the joint interface, and the generated heat should be localized in the joint area. The process is simple to control, and process cycle times are short. It is not restricted to flat surfaces, as in vibration or hot plate welding. Because the heating element remains in the joint after welding, repair of poor quality joints is possible, and joints can be disassembled for recycling. A disadvantage of resistance welding is the possibility of some current leakage through the joint, which could present a safety issue. In addition, the heating element remaining in the joint and may affect joint quality.

The geometry of the implant has a big effect on the welding strength. Dr.Watt and another graduate student have done a lot of research work on induction welding, which has a lot in common with resistance welding. This work led to the development of an inductor geometry which is now proprietary. Using this geometry, the bonding area between the metal and plastic is increased much more than that of a flat conductor, and the joint is not weakened by an accumulation of fibers at the original interface.

9.2 Experimental Procedure

In resistance welding, current is applied to a conductive heating element placed at the joint interface of the parts being welded. The temperature increases through Joule (I^2R) heating, and the surrounding plastic melts and flows together, forming a weld.

The resistance welding discussed here was carried out using a screw driven Instron Tensile tester to apply the loads as shown in Figure 9.2, and discussed below. The current was supplied directly from a Variac adjustable transformer. Using the proprietary resister as an implant, the welding process is different from the normal resistance welding. Under pressure it was easily squeezed out or it collapsed. In the present research work, a one pound load was applied to the upper plaque before the current was turned on. During the period when the resister had been heated for five to ten seconds, the surface of the materials that were in contact with the implant melted, and then the final load was

applied. The current was then turned off, and the final load was maintained until the welding process was finished.

In this resistance welding process, a constant voltage input was used. A particular voltage is set for the entire weld process, and welding occurs for a specified time. The voltage was set at 10 volts.

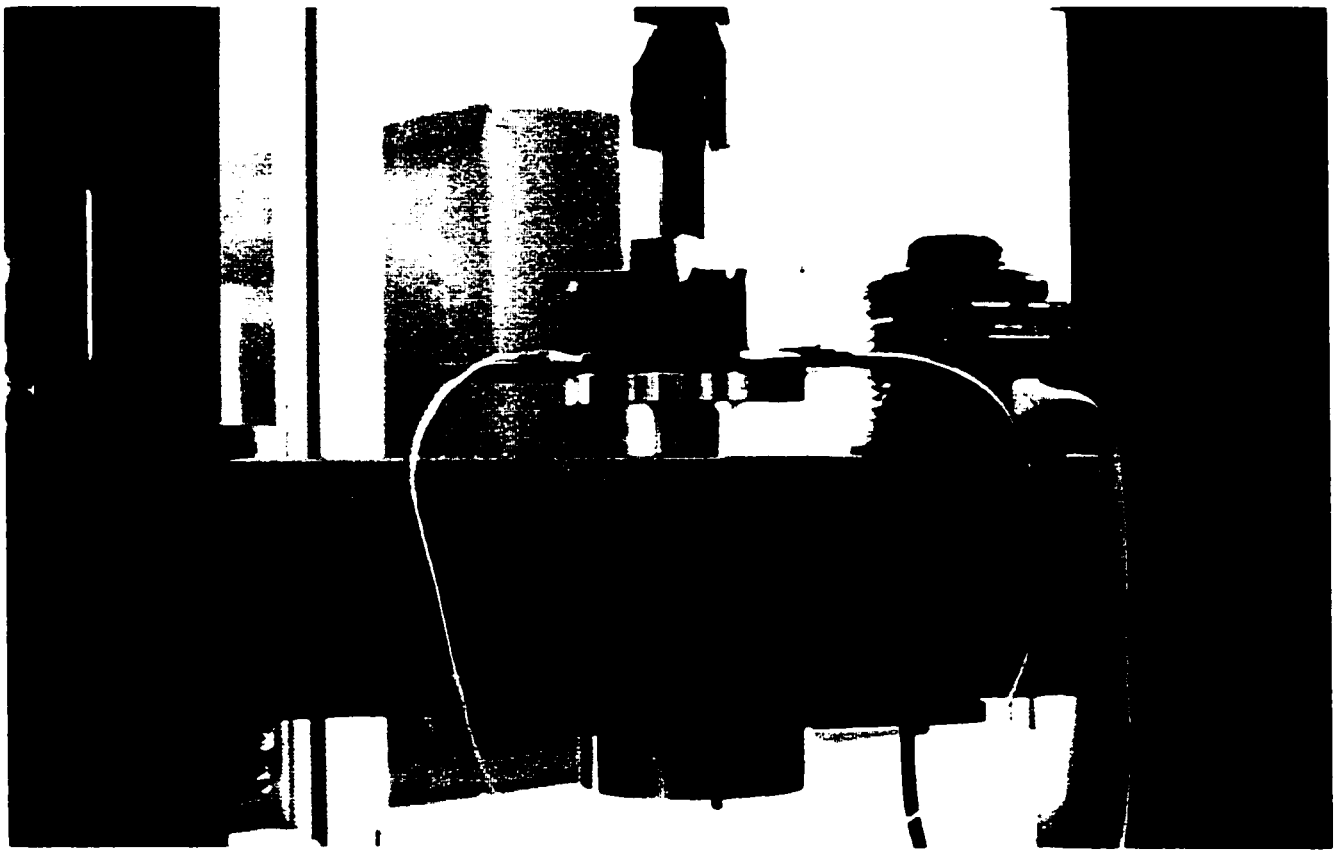

Figure 9.2 Sample being welded on the Instron machine.

In the present research work, only T-samples were made. This welding was performed on an Instron machine (Figure 9.2). The horizontal flange of the sample is in the lower position, and moves with the crosshead. The web of the sample is in the upper position and is held by a fixture. In order to keep uniform pressure on the 101mm long sample, a 150 mm long steel bar was inserted into the holding fixture on top of the web, because the fixture holding area is only 25 mm wide.

The conductor was placed along the middle of the T- joint flange surface and the two ends of the resistor were connected with the output of the transformer.

When doing the welding, the lower support beam was moved up until the two parts engage the resistor, and then a little further to put the initial load on the sandwich structure. The power was then turned on to heat the resistor and the plastic parts. A problem experienced at the beginning of this research work was that when the resistor was heated and with the pressure on the materials, the resistor was squeezed out. In order to solve this problem, the grooves were made on the joint surfaces of both the web and the flange (Figure 9.3).

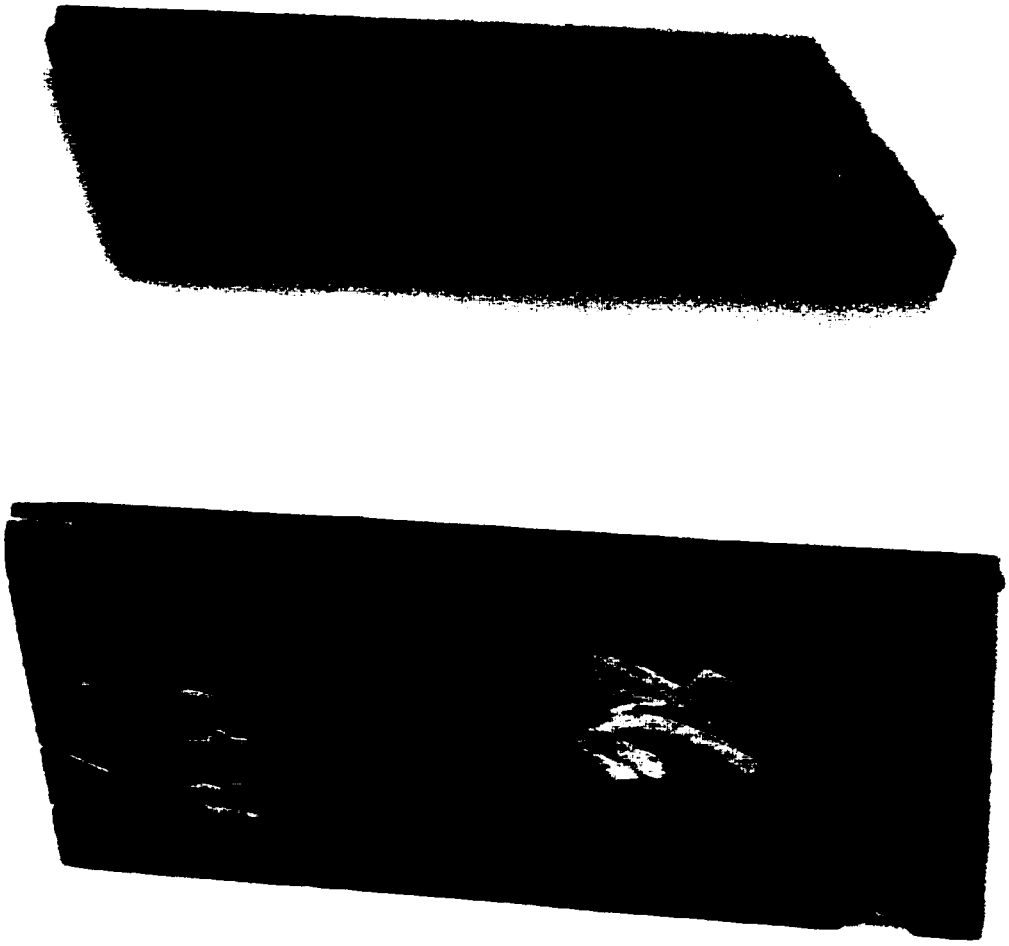

Figure 9.3 Before welding, grooves have been added to keep the resistor in place.

The depth of the grove is around 1.5 mm, in a web which was 6 mm in thickness. This dimension was chosen to match the resistor geometry. But the resistor stretched out when it was subjected to current. When welding dissimilar materials, pressure performed an important role. If the final pressure is applied before the high temperature material begins to melt, then the resistor is forced into the low temperature material, where it contributes almost nothing to the welding strength.

The materials used were nylon 66 70G33, nylon 6 73G30 and high temperature amide HTN52G35, which have melting temperatures of 262, 223, and 310^{0}C respectively. Experiments were carried out at different preloads, final loads and welding times. Welding time is defined as the time from power on to power off.

After welding, the two ends of sample were cut off, each about 10mm in length, from the 101mm long welded specimen. Figure 9.4 shows the welding sample 13C. The upper material is HTN and bottom material is 70G33. In this case the resistor crosses between two parts.

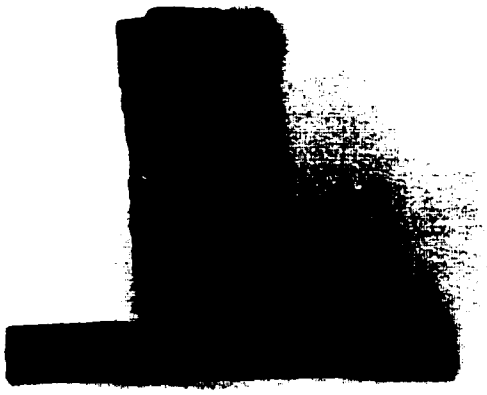

Figure 9.4 Sectioned resistance welded T sample

9.3 Resistance Welding Results and Analyses

The test results are shown below in Table 9.1.

Sample	Materials	Preload	Time 1	Final Load	Total Welding Time	Fracture Strength
ID	Leg / Arm	LB	Seconds		Seconds	MPa
2	70G33 / 70G33	5.4	3	20	40	17.29
3	70G33 / 70G33	4	3	15.5	40	11.78
4	70G33 / 70G33	4	3	10	40	11.19
5	70G33 / HTN52G35	1.5	10	8	50	9.44
6	70G33 / HTN52G35	2	10	10	50	9.00
7	HTN52G35 / 70G33	1.8	10	11	60	10.41
8	HTN52G35 / 70G33	1.8	10	10	90	14.97
9	70G33 / HTN52G35	0.1	10	9	90	13.2
10	73G30 / HTN52G35	0.1	10	10	90	13.04
11	70G33 / HTN52G35	0.1	10	6.8	90	14.28
12	70G33 / HTN52G35	0.1	10	6.8	90	18.22
13	70G33 / HTN52G35	0.1	10	5.4	90	11.08

Table 9.1 Resistance welding test results

From Table 9.1, it can be seen even for the same materials combination, the preload force and preload time are not the same. The reason is that the process is not sensor controlled, so the applied load is not repeatable. From Table 9.1, it can be seen

that the best weld is between the materials 70G33 and HTN52G35. The process parameters are: preload 0.1 lb, the preload time is 1 second, final load is 6.8 lb, and total welding time is 90seconds. The strength of similar and dissimilar materials welds do not have a big difference; 70G33/70G33 is 17.29 MPa, and 70G33/HTN is 18.22 MPa.. From the vibration T-weld test we know that the maximum strength is 31MPa on 3mm thick samples.

The welding strength of the resistance samples are very low compared with vibration welding results. Further inspection and analysis reveals some reasons that could affect the tensile strength.

On the fracture surface of the sample, the surface between the resistor and the base material has a lot of pores. The formerly molten material in the joint looks like a foam structure. This foam-like material is very brittle, and it is otherwise not like the base material. This is because there is not enough material to fill the cavity created by the resistor.

A second reason for the weakness is that there is a carbon phenomenon that is very serious. The decomposition of material is can be seen at the flash. The flash is hard and the surface is bright with oil. This also means at the joint surface a lot of carbon is involved in the joint surface.

A third reason is the geometry of the sample. Because the equipment limitations, when the two parts were welded together, the web was not perpendicular to the flange.

When the sample is pulled in the test fixture, there is a bending moment combined with a stress concentration on the welding area. This will lead to poor strength values.

CHAPTER 10

CONCLUSIONS AND DISCUSSION

In this research, two linear vibration weld geometries were studied in some detail. These were T-joint welds and butt welds. In agreement with other work reported in the literature, it was found that butt welds were stronger than T-joint welds.

The main body of the work was done on T-joint welds. Three separate Design of Experiments studies were conducted to determine the relationship between weld strength and welding process parameters. Because of previous work done locally, these studies were centered on the welding of dissimilar materials where the flange (upper arm) of the T-joint samples was a higher melting temperature amide, and the web (leg) was from the lower melting point material.

The first DOE set was nylon 66 welded to HTN52G35. The DOE comprised 18 orthogonal experiments, all at three levels for each parameter, plus one extra combination of welding parameters Each of these experiments provided 6 tensile samples. The obvious result was that the tensile strength, meltdown and flash weight all increased with weld pressure, vibration amplitude and weld time, but was not affected by hold time. The shortest hold time used was three seconds. The experiment conducted beyond the orthogonal set was just setting all four parameters to their high settings, a condition not included in the orthogonal set. The standard DOE analysis on the orthogonal set showed that both weld time and vibration amplitude were the most important parameters affecting

the weld strength. To further understand the influence of these parameters a somewhat unorthodox regression analysis was conducted making use of all 19 experiments. The first analysis consisted of using simple additive combinations of the welding parameters to find coefficients that would predict the UTS for the experimental range studied. This progressed, through the development of five other regression equations which attempted to incorporate the physics of the vibration welding process into these equations. All the results were similar in their predictive ability, and all came to the same conclusion. Their ability to predict an individual experiment (standard error of estimate) was lower than the average standard deviation of the six tensile strengths measured for a given experiment. The regression analyses all showed that the vibration amplitude was by far the most important parameter affecting the tensile strength.

The second DOE was 73G30 nylon 6 welded to A1133, again with the higher temperature A1133 in the flange position. The other main difference was that the product of the vibration amplitude and the weld time (A * Wt), which is proportional to the total sliding distance, was used as a single variable. The DOE comprised 9 orthogonal experiments, with the pressure, A*Wt, and hold time each set to three levels. An additional 4 experiments, outside of the orthogonal set were done to further examine the interaction of weld time and vibration amplitude. The results were in agreement with the first DOE, but the importance of vibration amplitude was made even more obvious by this set.

The third DOE was done between 70G33 nylon 66 and AS4137, and the strengths produced by this combination were very low compared with the main DOE sets discussed above.

It was found that the T joint samples flanges (arms) bent downwards at their tips. The arms actually remained straight and the bending was confined to the region over the intersection with the web (leg). This was a big clue towards understanding the reason why the T-joint samples made from dissimilar melting point amides, tested in a previous study, had a poorer strength when the lower temperature material was in the arm. This condition allowed the higher melting point material to penetrate into the arm, entrapping liquid which contracted after welding, bending the arms down and leaving a large hydrostatic tensile stress field.

A side result of this was that it was found that the strengths measured for T - joint samples were very dependent on the shape of the test fixture supporting the arm. If the fixture supported the arm through a large flat surface, then the strengths were low. This results from the arms being unbent, adding to the residual tensile stresses at the base of the arms. This leads to premature failure. If the arms are supported by single line supports close to the leg, then much higher tensile strengths are measured.

Butt welds were also made and tested, though very little attempt was made to optimize the welding conditions. Nevertheless the butt welds were much stronger than the

T joint welds, and it appears that butt welds in 6 mm thick material produces higher fracture strengths than those in 3 mm thick samples.

Resistance welding was also attempted, but the weld strengths were low due to overheating and difficulties with the special type of resistor employed.

REFERENCES

1. Val A. Kagan, "Joining of Nylon Based Plastic Components-vibration and Hot Plate Welding Technologies", *Society of Plastics Engineers ANTEC' 99*, p.1349-1359, published by SPE.

2. Chul S. Lee, "Optimization of Vibration Weld Joint Strength for Plastic Air Intake Manifold", *Society of Automotive Engineers, Technical Paper Series – plastic: Components, Process, and Technology (SP-1340)*, p.111-115 (1998).

3 David A. Grewell, "An Application Comparison of Orbital and Linear Vibration Welding of Thermoplastics", *SPE ANTEC' 99*, p.1365-1369.

4. Helmut Potente, "Process Data Acquisition in Vibration Welding of Thermoplastics", *Polymer Engineering and Science*, Mid-December 1989, Vol. 29, p.1661-1666.

5. Terry L. Richardson, "Industry Plastics", *Delmar Publishers Inc.* 1989.

7. Helmut Potente, "Friction Welding of Polyamides", *Polymer Engineering and Science*, Vol.37, 1997, p.726-737.

8. Vijay K. Stokes, "Joining Methods for Plastics and Plastic Components", *Polymer Engineering and Science*, Mid-October 1989, Vol. 29, p.1311-1319.

9 Vijay K. Stokes, "Joining Methods for Plastics and Plastic Composites", *SPE ANTEC' 89*, p. 442-445.

10 Susumu Yamaguchi, "Development of Plastic Intake Manifold by DRI Process", *SAE 2000 World Congress, Technical Paper Series-Plastic, Component, and Technology (SP-1534)*, 2000-01-0041.

11. Ian D. Froment, "Vibration Welding Nylon 6 and Nylon 66---A Comparative Study", *SPE ANTEC' 95*, p.1285-1289.

12. Sheila M Stevens, "Characterisation of Nylon 66 Vibration Welds", *SPE ANTEC' 97*, p.1228-1232.

13. Vijay K. Stokes, "Assessment of Geometries for Determining Strengths of Thermoplastic Vibration Welds", *SPE ANTEC' 98*, p.1045-1049.

14. Vijay K. Stokes, "Cross Thickness Vibration Welding of Polycarbonate, Polyetherimide, Poly (butylenes terphthalate), and Modified Polyphenylene Oxide", *Polymer Engineering and Science*, April 1997, Vol. 37, p.715-725.

15. H. Van Wijk, "Process Optimization of Ultrasonic Welding", *Polymer Engineering and Science*, Mid-May 1996, Vol. 36, p.1165-1176.

16. V. A. Kagan, "Optimizing the Vibration Welding of Glass-reinforced Nylon Joints", *Plastics Engineering*, September 1996, p.39-41.

17. Joel R. Fried, "Polymer Science and Technology", *Prentice Hall* PTR, New Jersey, 1995.

18. Valerie LeBlanc, Senior Undergraduate Thesis, "Vibration Welding of Dissimilar Nylons", *Mechanical, Automotive and Materials Engineering, University of Windsor*, 2000.

19. Valerie Leblanc, Bobbye Baylis, Li Ying Qi and D. F. Watt, "Vibration Welding of Dissimilar Nylons", *SPE ANTEC 2001*, p.1229-1289.

20 Joon Park, "Design of Experiment Procedures to Evaluate Ultrasonic Weldability of Materials", *SPE ANTEC 2000*, p.1222-1226.

21. Marc St. John, "Comparison of DOE Methods on Hot-plate Welding of Polypropylene", *SPE ANTEC 2000*, p.1126-1131.

22. Willian Mendenhall, Robert J. Beaver, Barbara M. Beaver, "Introduction to Probability & Statistics", *Brooks/Cole Publishing Company*, California, 1999.

23. Phillip J. Ross, "Taguchi Techniques for Quality Engineering", *McGraw-Hill*, New York, 1988.

24. V. Kagan, "The Optimized Performance of Linear Vibration Welded Nylon 6 and Nylon 66 Butt Joints", *SPE ANTEC' 96*, p.1266-1274.

25. Tom B. Jakobsen, "Two-dimensional Thermal Analysis of Resistance Welded Thermoplastic Composites", *Polymer Engineering and* Science, Mid-December 1989, Vol. 29, p.1722-1729.

26. Genichi Taguchi, System of Experimental Design, Volume 1, Pub. Kraus International, White Plains, CA.

Appendix I Process Parameters and Results for TC Group T-joint DOE

Sample ID	Am in	Wf lb	Wt Sec	Ht Sec	Meltdown mm	Flash weight (g) back	front	Sum	Fracture load lb	Width in	UTS psi	UTS MPa
TC 1B	0.04	75	8	6	0.70	0.018	0.028	0.046	151.6	1.018	1132.	7.81
TC 1C						0.011	0.031	0.042	137.8	1.024	1023.	7.06
TC 1D						0.007	0.025	0.032	129.1	1.019	963.	6.64
Mean Strength		7.17 MPa										
Mean Flash Weight		0.040 g										
TC 2B	0.04	75	12	6	2.15	0.077	0.122	0.199	238.7	1.026	1769.	12.20
TC 2C						0.079	0.123	0.202	197.9	1.0245	1468.	10.13
TC 2D						0.101	0.122	0.223	202.1	1.0205	1506	10.38
Mean Strength		10.90 MPa										
Mean Flash Weight		0.208 g										
TC 3B						0.108	0.124	0.232	195.4	1.016	1462.	10.08
TC 3C	0.05	75	12	6	2.35	0.117	0.119	0.236	202.7	1.0195	1511.	10.42
TC 3D						0.124	0.117	0.241	222.3	0.981	1723.	11.88
Mean Strength		10.79 MPa										
Mean Flash Weight		0.236 g										
TC 4B						0.124	0.124	0.248	235.2	1.0245	1745	12.04
TC 4C						0.113	0.132	0.245	228.2	1.027	1689.	11.65
TC 4D	0.05	75	10	6	2.40	0.111	0.133	0.244	220	1.027	1629.	11.23
Mean Strength		11.64 MPa										
Mean Flash Weight		0.246 g										
TC 5B						0.061	0.071	0.132	206	1.03	1520.	10.49
TC 5C						0.06	0.08	0.14	189.7	1.0275	1403.	9.68
TC 5D	0.05	75	8	6	1.71	0.08		0.08	181.7	1.0185	1356.	9.35
Mean Strength		9.84 MPa										
Mean Flash Weight		0.117 g										
TC 6B						0.08	0.06		161.5	1.0175	1207.	8.32
TC 6C						0.075	0.056		153.7	1.021	1144.	7.89
TC 6D	0.04	75	10	6	1.64	0.068	0.062	0.13	170.4	1.027	1261.	8.70
Mean Strength		9.30 MPa										
Mean Flash Weight		0.134 g										

Am is vibration amplitude
Wf is weld force
Wt is weld heating time
Ht is hold time

Appendix II Weld strengths and flash geometry

Weld flashes show a very large variation in shape, size, cross-sectionand angle of emergence. The flash of the linear vibration weld is a characteristic that may give further information about the weld. Logically, the flash shape should be related to the welding parameters Can examining the weld flash shape reveal other information about the welding process ?.

TB7 represents Experiment #2. The length of the flash is 2mm, and it varies along the length. This indicates that the pressure distribution is not the same over length of the welding direction. The pressure appears to be small at TB7A, and grows bigger out to the TB7E end. The fracture strength of the 3 T-joint samples were: TB7B = 15.04 MPa, TB7C = 14.67 MPa, and TB7D was 16.59 MPa.

From DOE experiment group 3, TB 11 was chosen. The shape the flash viewed from above is like the deck of a ship. The strength of each part was TB11B = 17.90 MPa, TB11C = 16.85MPa, and TB11D is 18.00 MPa.

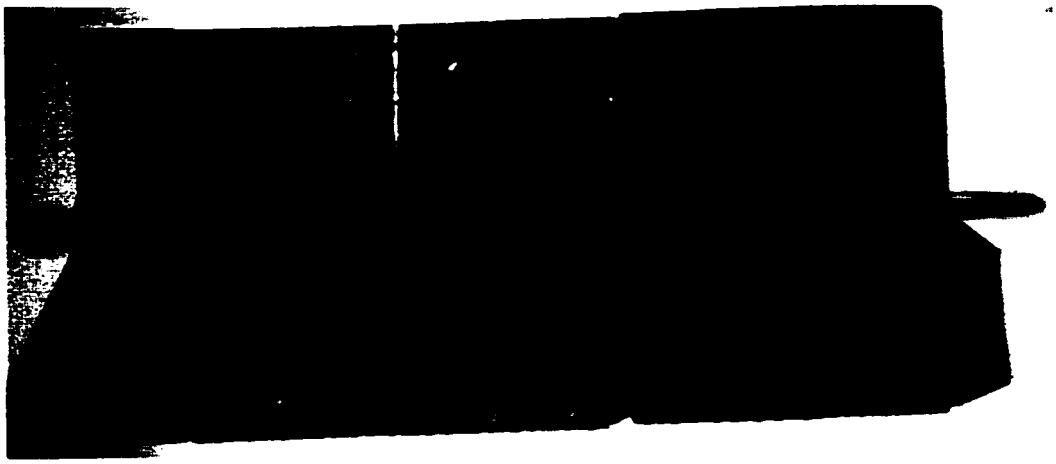

TB12 is from DOE experiment #4. The shape of the flash curled up in a roll like the barrel of a cannon. The strengths were TB12B = 10.89 MPa, TB12C = 9.35MPa, and TB12D = 7.59 MPa

In DOE experiment 6, the shape of the flash here is different from all others. The strengths of TB19B, TB19C, and TB19D were 9.02 MPa, 10.14 MPa, and 11.42 MPa respectively. The amount of flash was very large, but the samples were relatively weak.

In TB28 and TB33, there is no obvious relationship between the welding strength and flash shape.

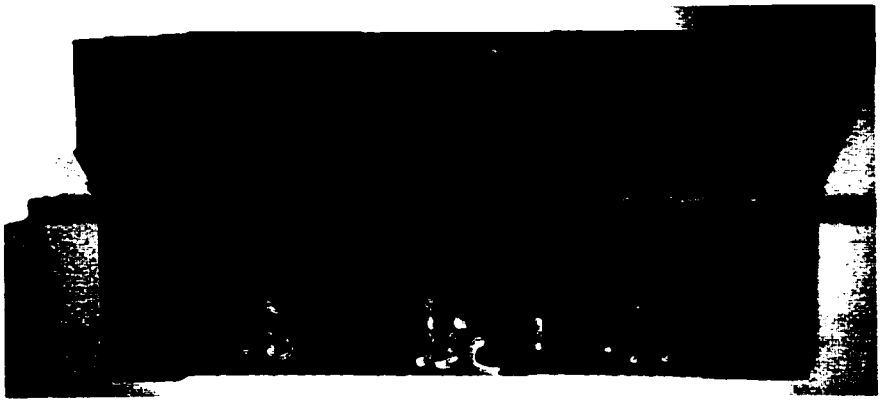

In summary, it is apparent that there is no simple relationship between the flash mass or shape and fracture strength. However TB11 had by far the most flash and also the highest strength of these three samples. As well, test sample TB7B was weaker than TB7D as the flash had indicated it should be, but TB7C was weaker than either 7B or 7D, which was not expect.

From the below three picture, we can see the TC3C has a big flash than that of TC2C. The only difference is that the amplitude. The amplitude of TC2C is 0.4in and TC3C is of 0.5in. The difference between the TC2C and TC6C is weld time, the weld time of TC2C is 12 seconds, and weld time of TC6C is10 seconds.

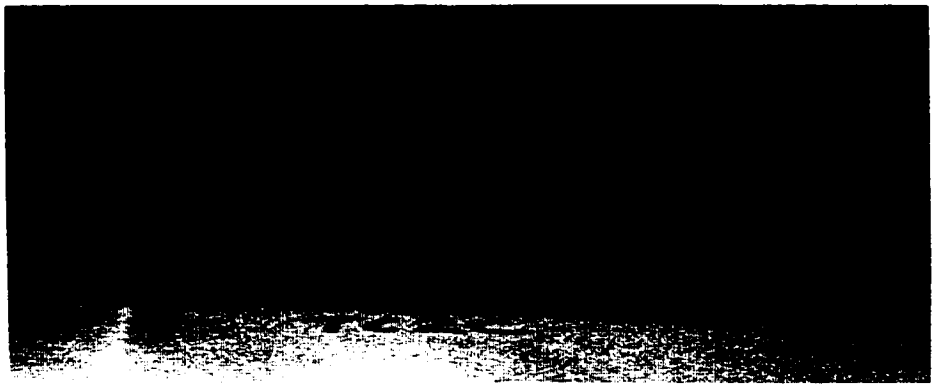

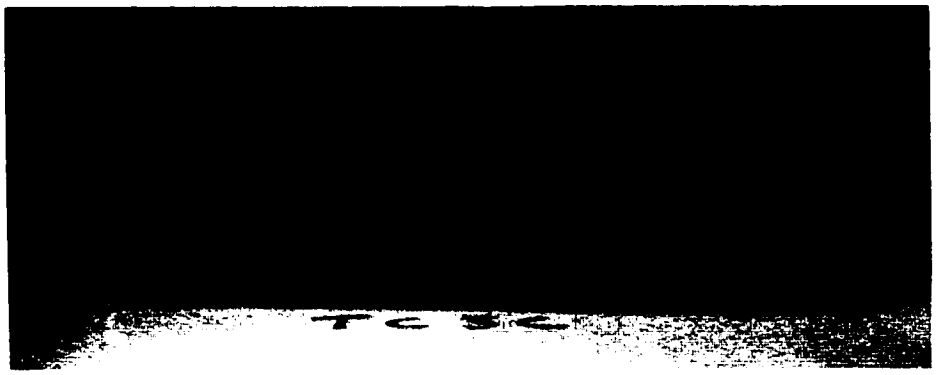

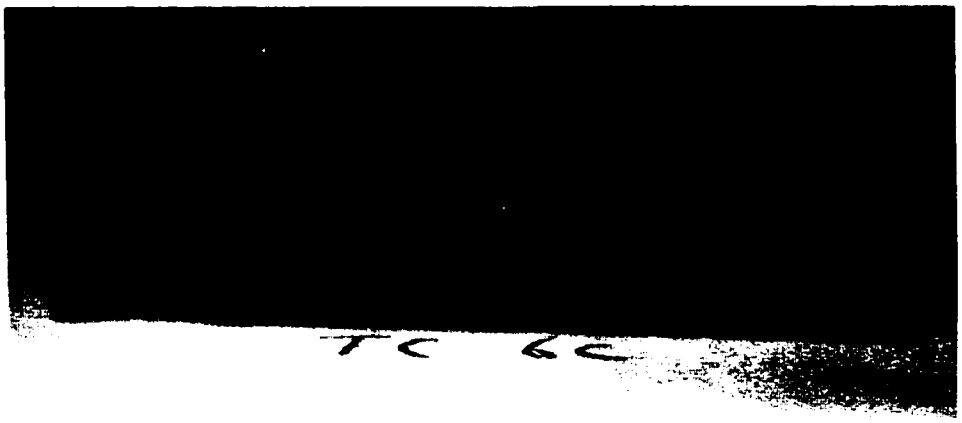

Appendix III Upper arm curvatures on TA Samples

#92 73G30/AS4133

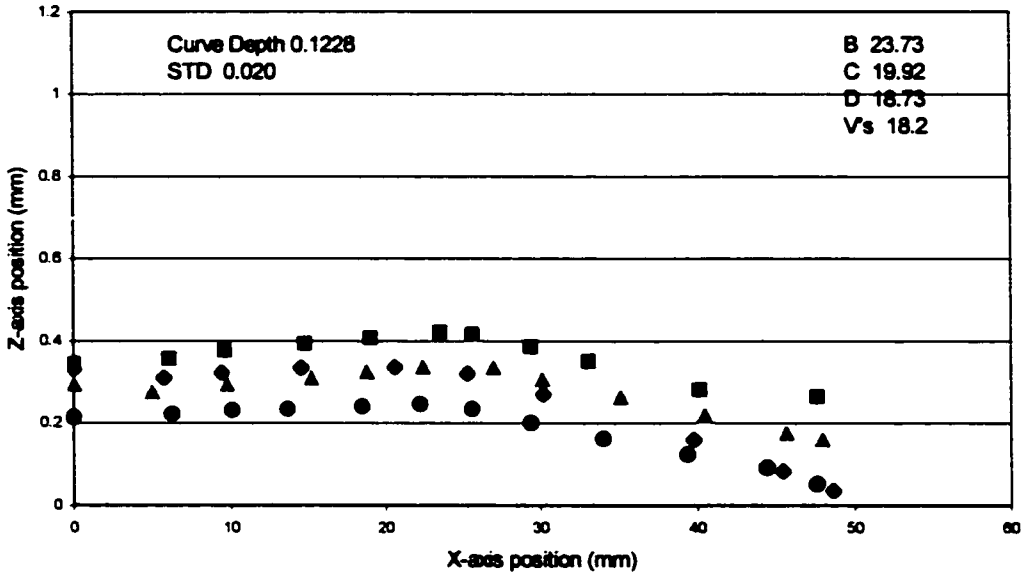

#42 A1133/70G33

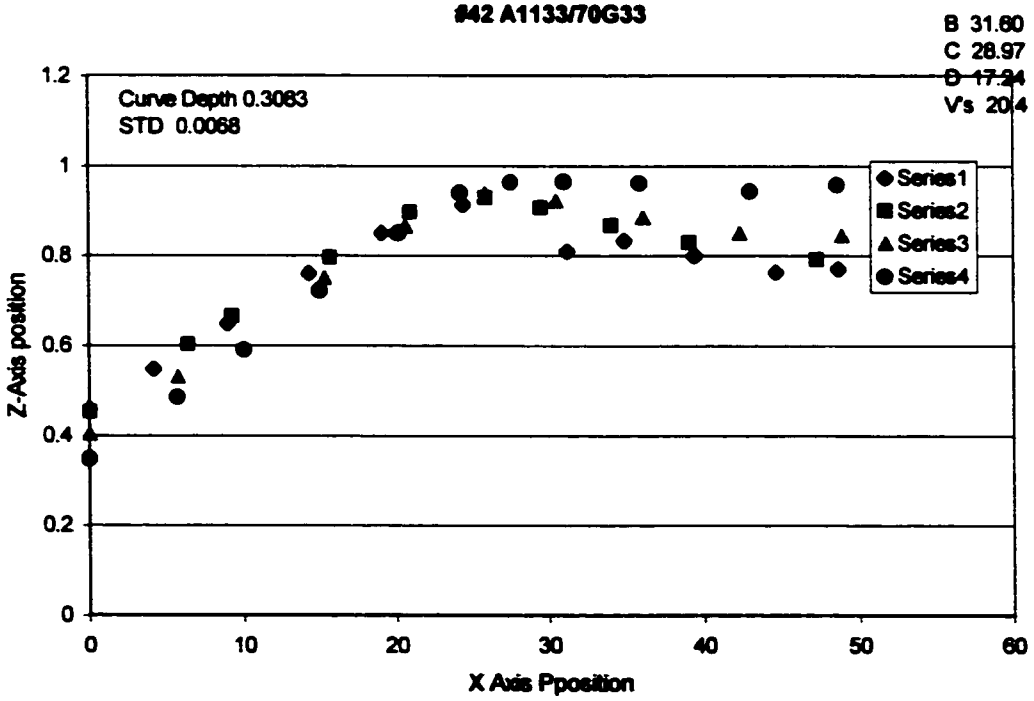

#34 73G30/70G33

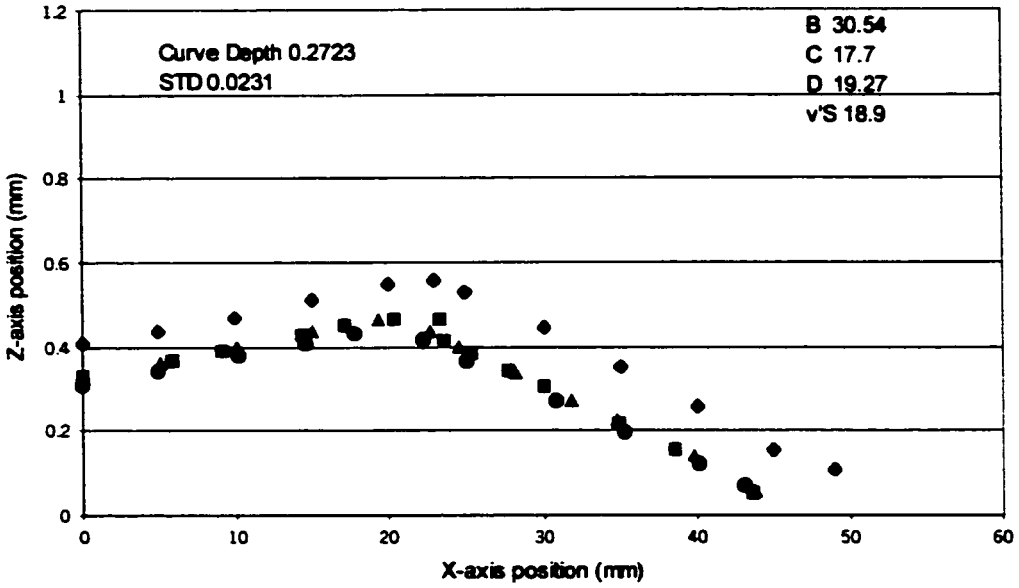

#8 A1133/A1133

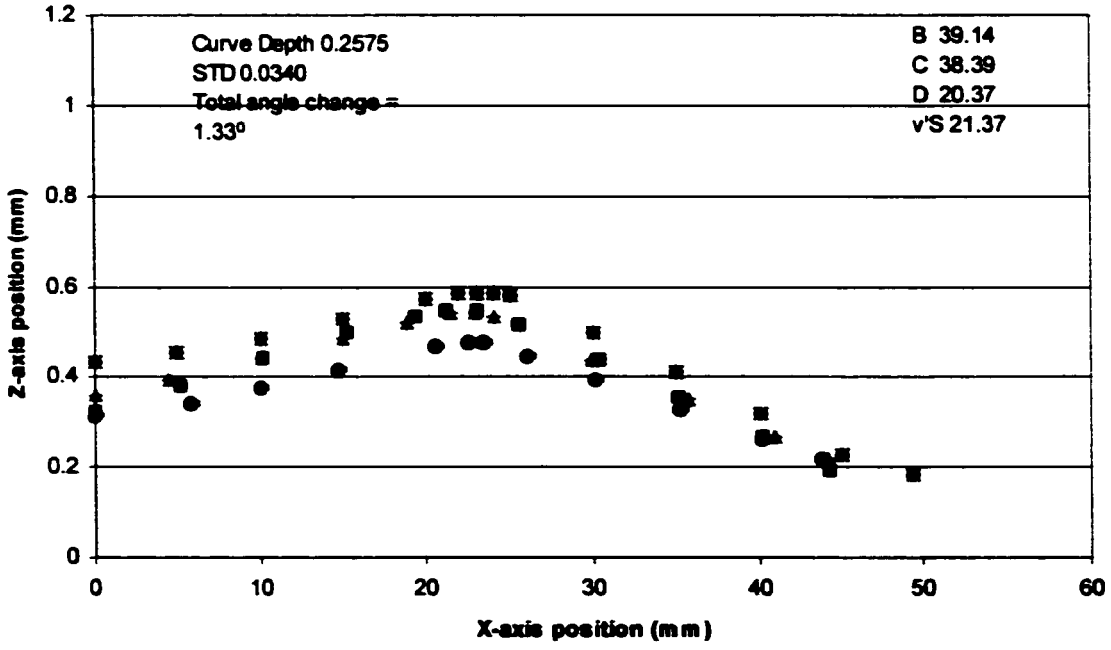

#66 A1340/70G33

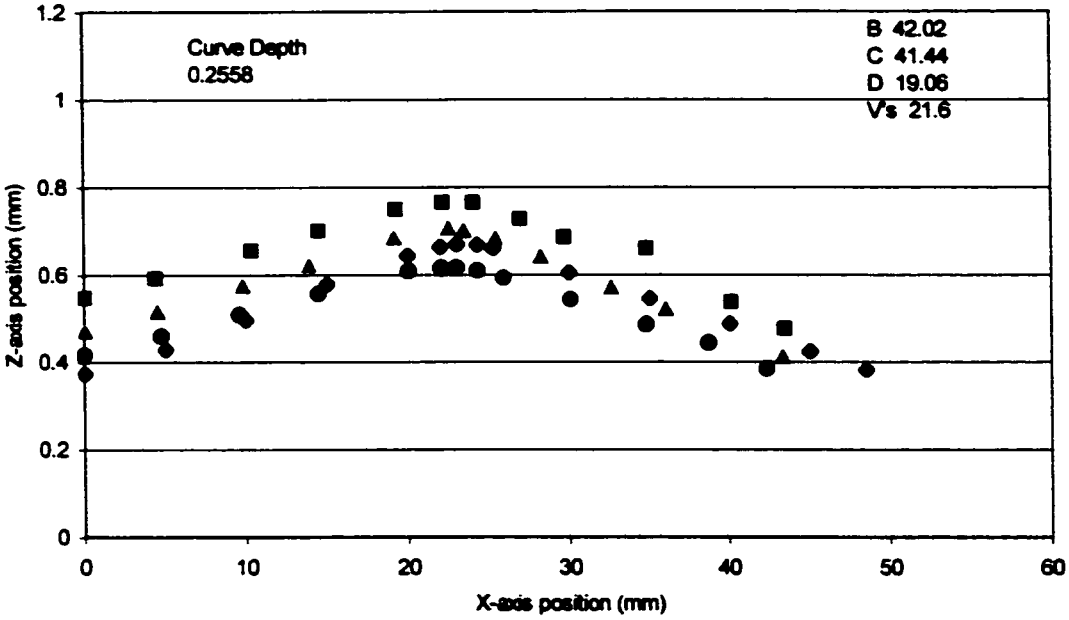

#49 73G30/A1133

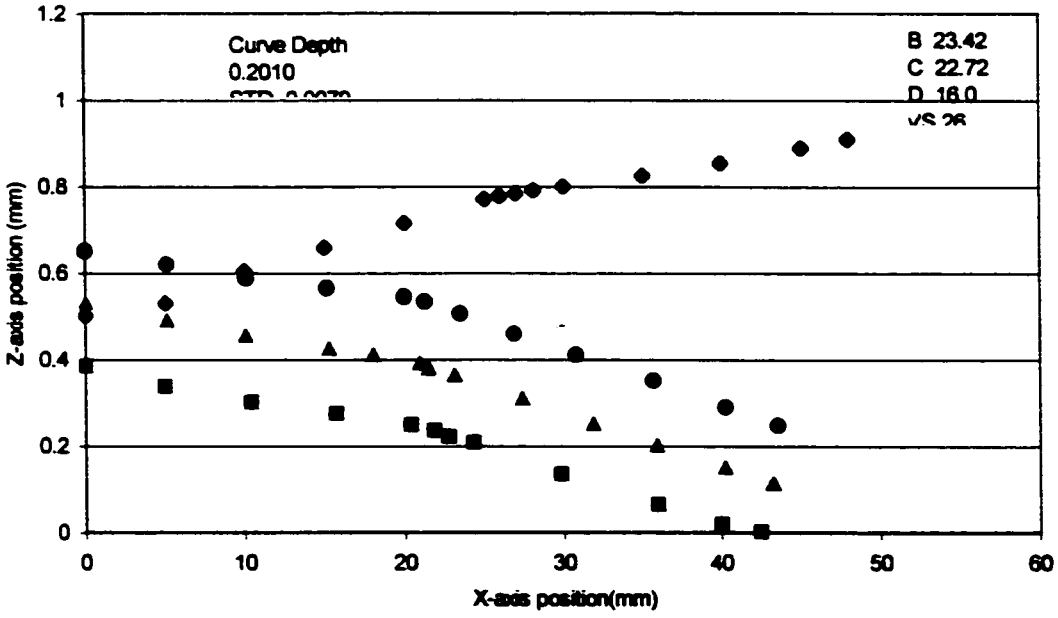

#10 A1133/A1133

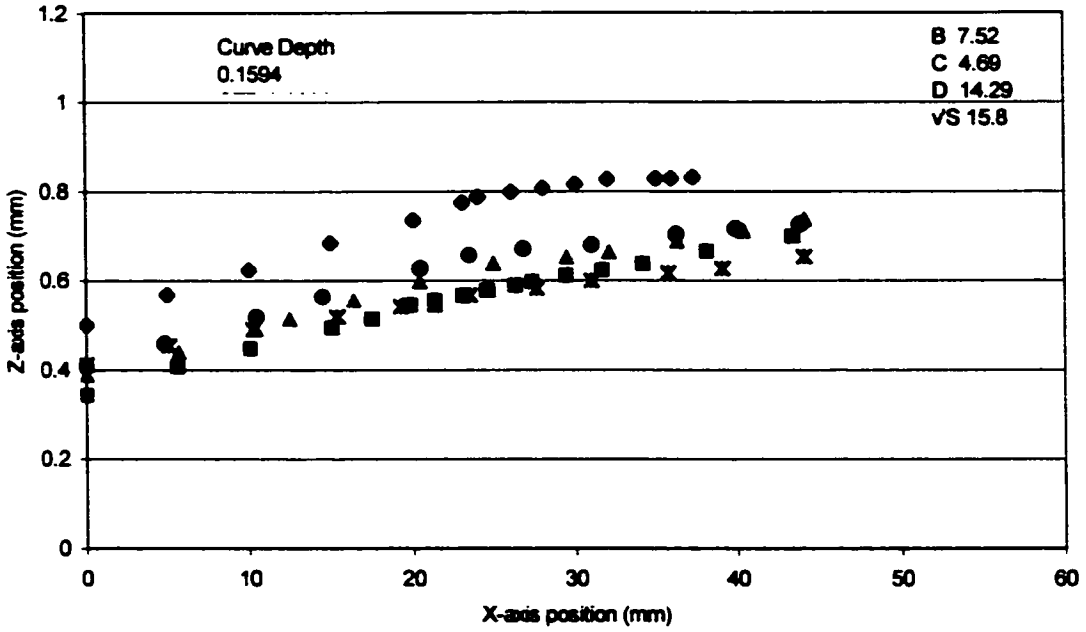

#17 AS4133/AS4133

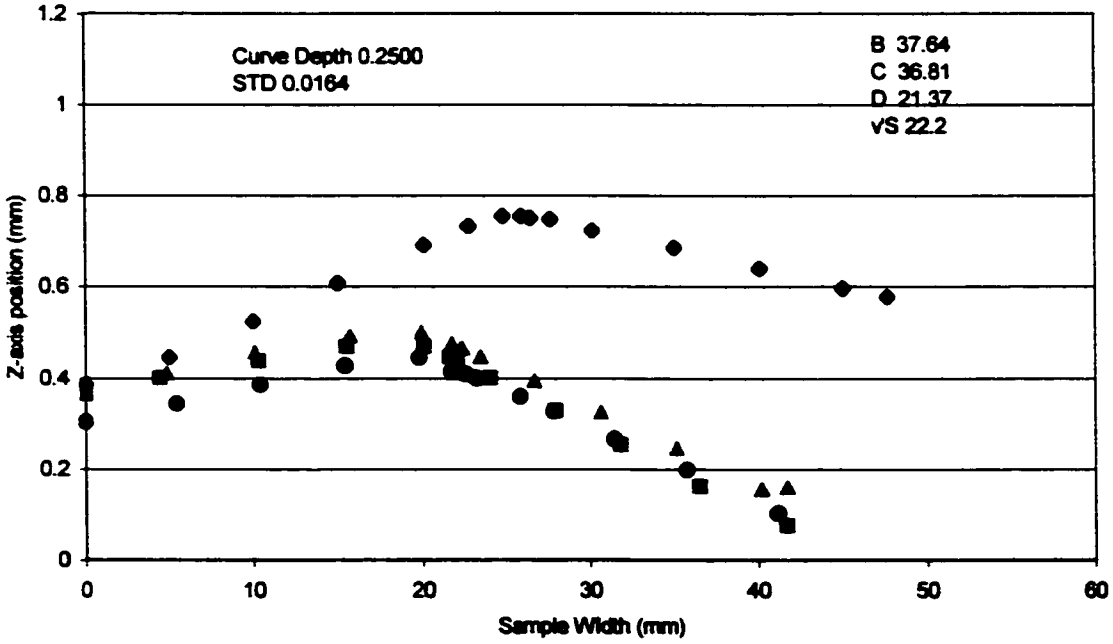

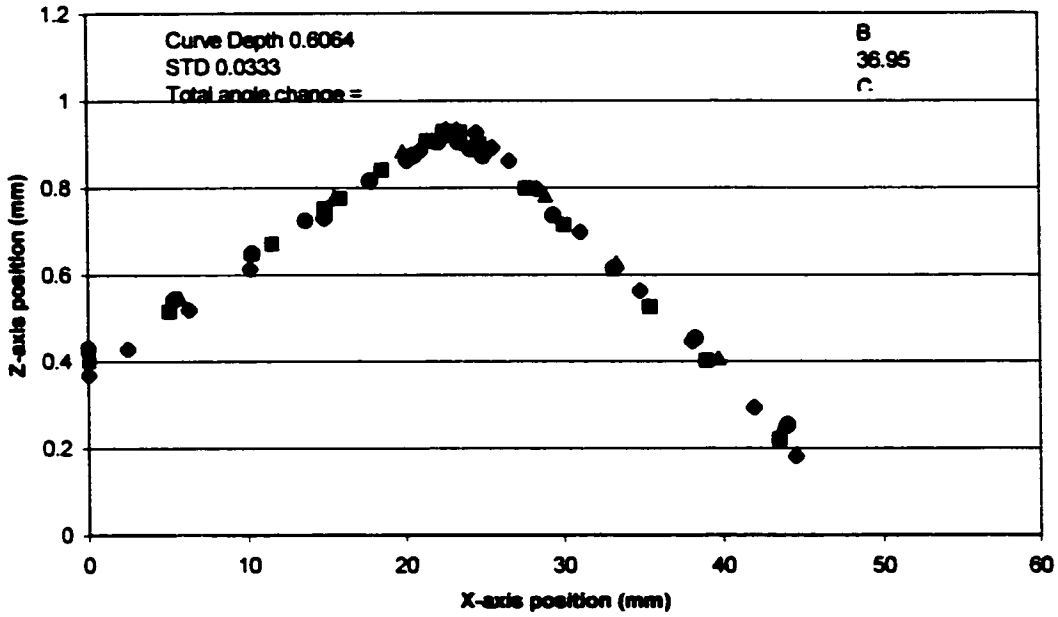
Curve Depth 0.6064
STD 0.0333
Total angle change =
B
36.95
C
Z-axis position (mm)
X-axis position (mm)
0
0.2
0.4
0.6
0.8
1
1.2
0
10
20
30
40
50
60

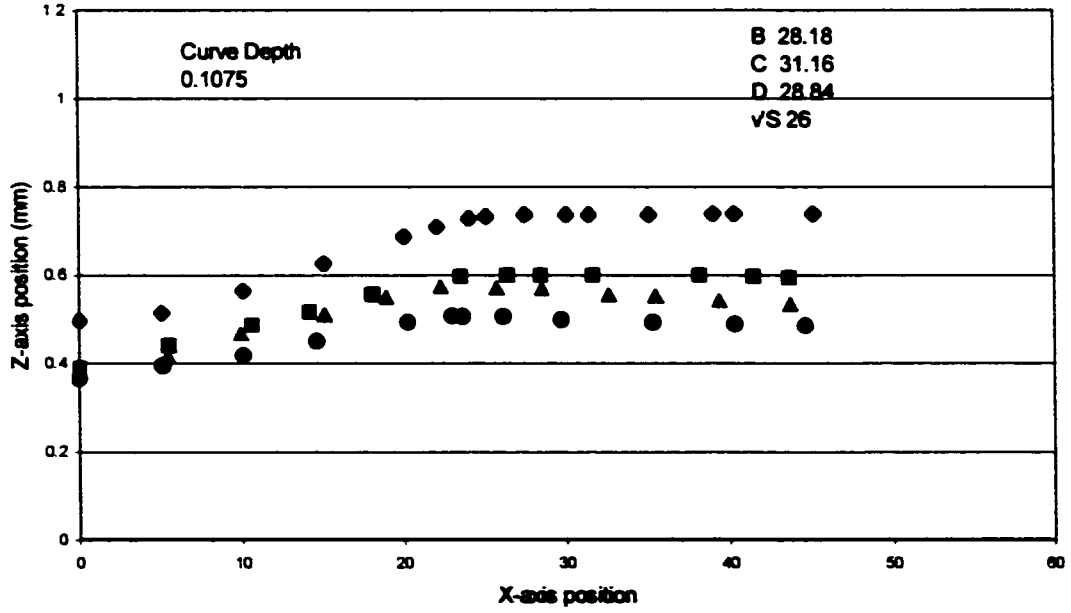
Curve Depth
0.1075
B 28.18
C 31.16
D 28.84
VS 26
Z-axis position (mm)
X-axis position
0
0.2
0.4
0.6
0.8
1
1.2
0
10
20
30
40
50
60

#60 73G30/A1133

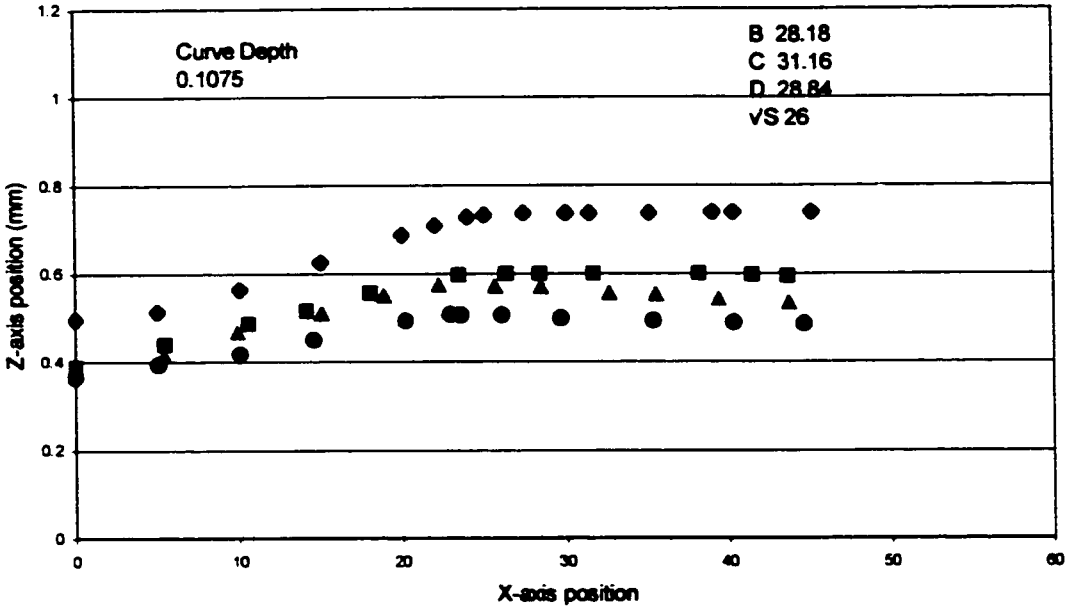

#94 AS4133/73G30

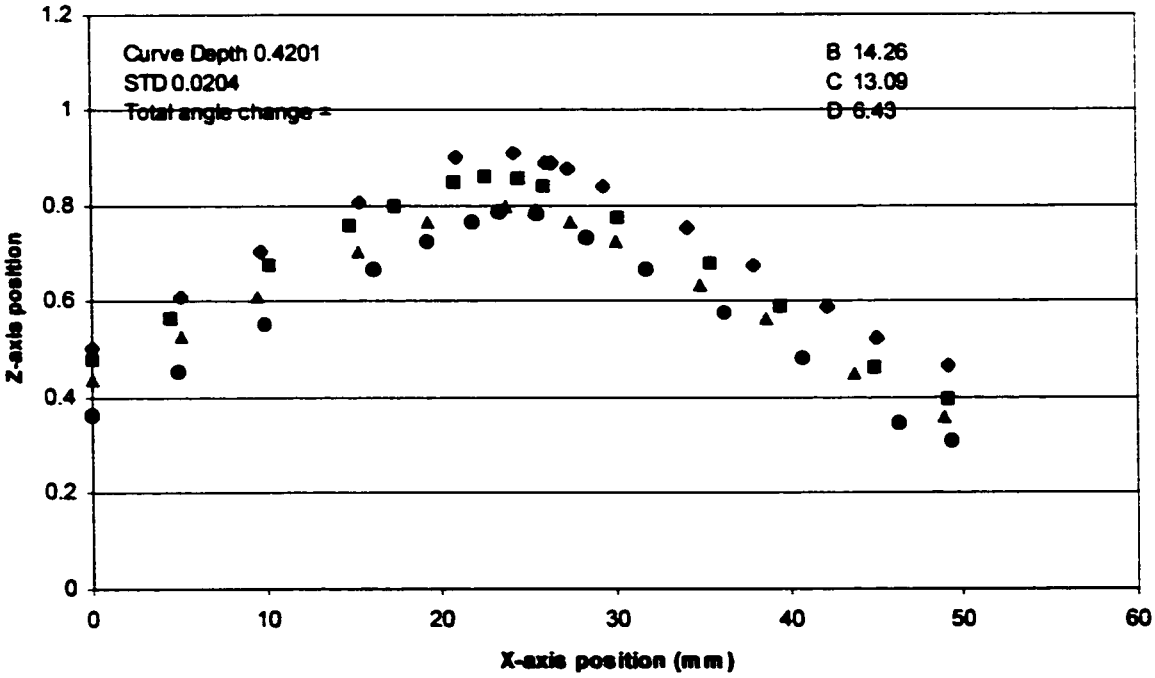

#56 AS4133/73G30

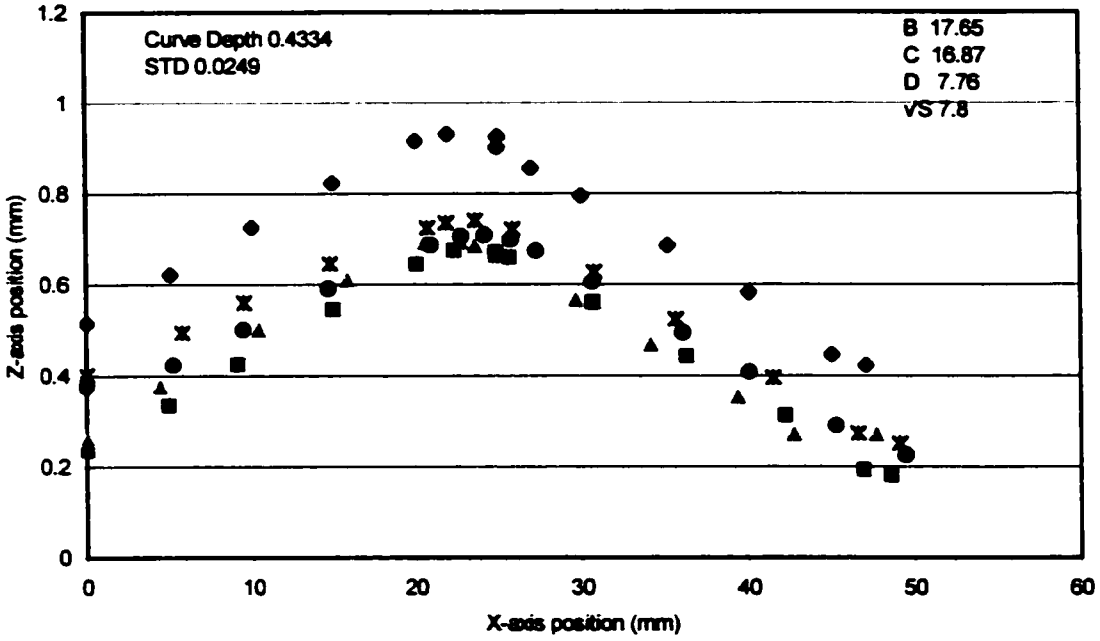

#56 A1133/73G30

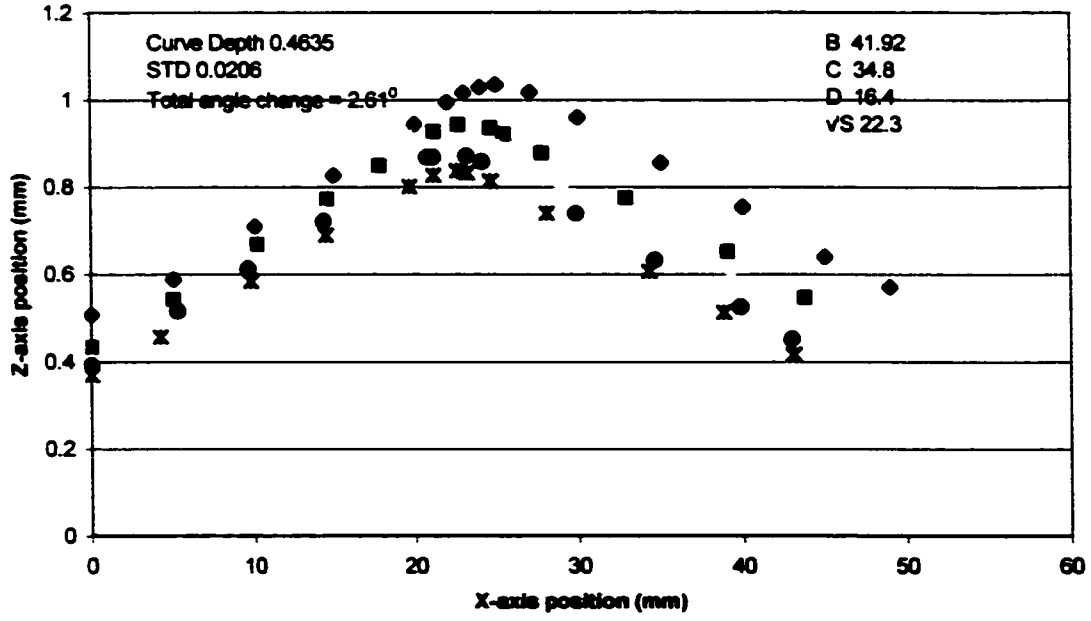

#46 70G33/A1133

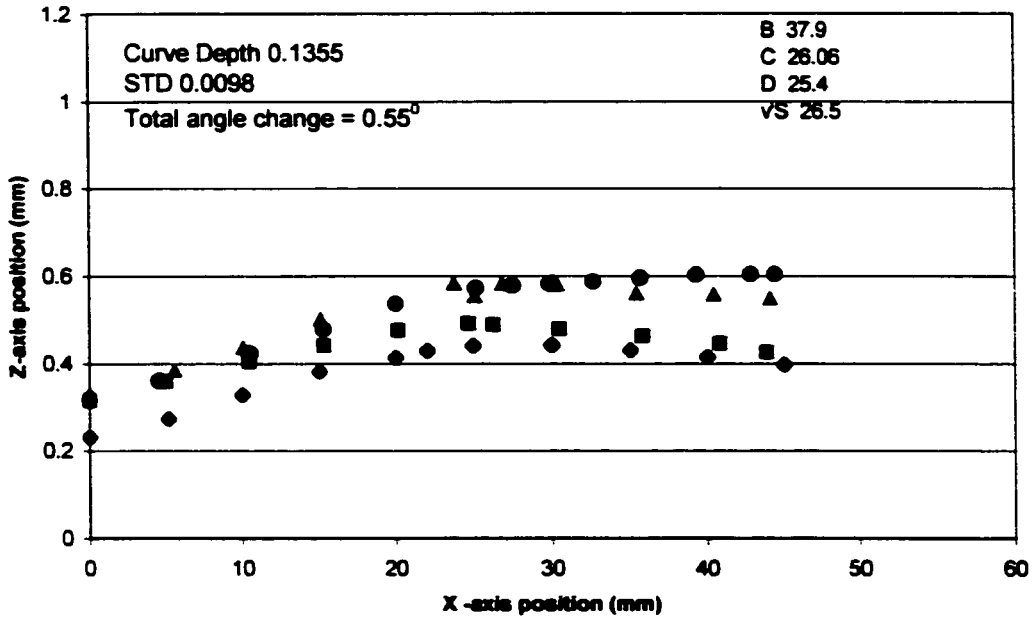

#5 A1340/A1340

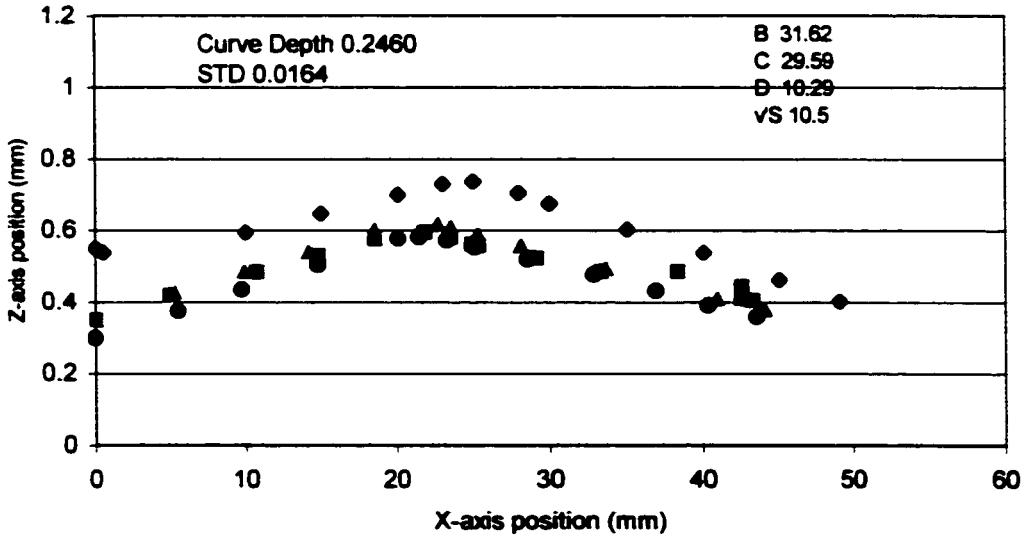

#35 73G30/70G33

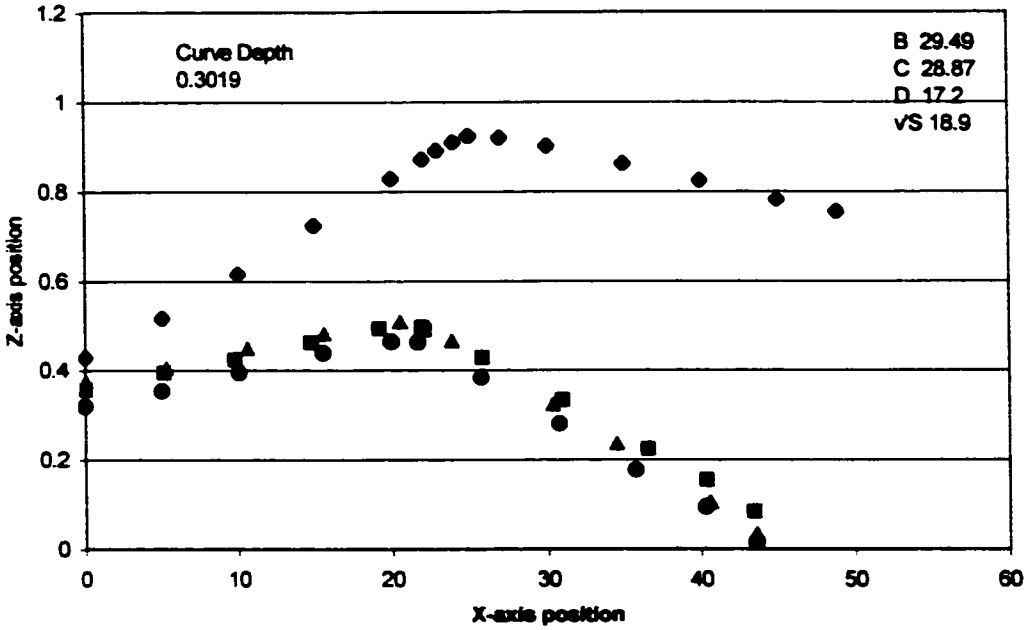

Appendix IV Butt Weld Results

6mm-6mm	Materials					
6mm-6mm	70G33/70G33	Ultimate Load	UTS	Average	Meltdown	Meltdown
Part NO.		LB	Mpa	Mpa (To)	mm	Ave mm
BA3 B		2234	62.89		0.6364	
BA3 C		2102	58.49			
BA3 D		2003	56.61			
BA4 B		1977	55.87		0.6694	
BA4 C		1992	56.34			
BA4 D		1043	29.71			
BA5 B		1742	49.38		0.718	
BA5 C		2010	56.94			
BA5 D		1904	53.23			
BA6 B		1743	49.74		0.7956	
BA6 C		1611	45.35			
BA6 D		1119	31.72	50.52		0.70485
BA7 B	HTN/70G33	910	25.75		0.734	
BA7 C		1006	28.47			
BA7 D		801	22.57			
BA8 B		1095	30.96		0.6706	
BA8 C		866	24.31			
BA8 D		1185	33.62			
BA9 B		1263	35.86		0.6113	
BA9 C		1116	31.45			
BA9 D		878	24.67			
BA10 B		817	23.29		0.6736	
BA10 C		959	27.07			
BA10 D		905	25.61	27.80		0.672375
BA11 B	HTN/HTN	590	16.84		0.2661	
BA11 C		606	17.07			
BA11 D		863	24.80			
BA12 B		734	20.69		0.326	
BA12 C		756	21.33			
BA12 D		751	21.56			
BA13 B		1103	31.70		0.4577	
BA13 C		1240	35.14			
BA13 D		901	25.25			
BA14 B		621	17.86		0.4669	
BA14 C		610	17.37			

BA14 D		LOOK AT SAMPLook sample				
BA15 B		878	24.63		0.3266	
BA15 C		937	26.50			
BA15 D		1043	29.63			
BA16 B		663	18.57		0.9602	
BA16 C		719	20.19			
BA16 D		724	20.78			0.4229
3MM-3MM						
BA17 B	G33/A1133 wh	826.6	45.50		1.615	
BA17 C		675.4	37.66			
BA17 D		784.7	43.21			
BA18 B		908.8	50.87		1.4355	
BA18 C		782.6	43.31			
BA18 D		837.4	46.78			
BA19 B		859.5	49.73		1.5299	
BA19 C		799.7	42.01			
BA19 D		842.9	48.83	46.93		1.5268
BA20 B						
BA20 C						
BA20 D						
BA21 B	G33/A1133 bla	802.1	44.11		1.4029	
BA21 C		982.3	55.16			
BA21 D		812.9	44.69			
BA22 B		968.2	54.89		1.1426	
BA22 C		908.7	51.07			
BA22 D		839.4	46.31			
BA23 B		890.9	49.34		1.1834	
BA23 C		908.2	51.53			
BA23 D		838.8	45.88			
BA24 B		871.1	48.27		1.1974	
BA24 C		925.6	51.29			
BA24 D		910.8	50.15	49.39		1.231575
BA25 B	70G33/A1340	886.6	48.72		0.9046	
BA25 C		930.1	51.29			
BA25 D		921.6	51.29			
BA26 B		727.6	40.55		1.4729	
BA26 C		679.4	37.24			

BA26 D		635	35.43			
BA27 B		626.7	35.31		1.2829	
BA27 C		729.6	40.47			
BA27 D		743.6	41.43			
BA28 B		803.9	44.25		1.0457	
BA28 C		814.1	44.93			
BA28 D		816.2	45.22	43.01		1.176525
BA29 B	70G33/AS146	500.4	27.53		0.846	
BA29 C		453.3	24.88			
BA29 D		375.8	20.51			
BA30 B		583.3	32.29		0.8176	
BA30 C		387.4	21.65			
BA30 D		640.7	35.46			
BA31 B		629.7	34.53		0.8992	
BA31 C		387.3	21.21			
BA31 D		515.3	28.33			
BA32 B		528.7	29.55		0.8751	
BA32 C		536.2	29.51			
BA32 D		654.5	35.88	28.44		0.859475
BA33 B	70G33/AS193	766.5	44.22		1.0776	
BA33 C		787	45.98			
BA33 D		818.5	46.00			
BA34 B		805	44.38		1.1649	
BA34 C		827	47.11			
BA34 D		858.5	47.36			
BA35 B		669.36	37.10		1.0054	
BA35 C		716.3	39.43			
BA35 D		820.2	46.47			
BA36 B		768.4	42.41		1.2197	
BA36 C		749.5	41.32			
BA36 D		846.3	46.97	44.06		1.1169
BA37 B	70G33/AS413	666	36.79		1.2078	
BA37 C		642.7	35.09			
BA37 D		598.2	32.91			
BA38 B		669.5	38.20		1.0299	
BA38 C		574.1	33.95			
BA38 D		620.3	34.68			
BA39 B		565.2	29.75		0.9855	

BA39 C		520.7	28.06			
BA39 D		567.6	30.14			
BA40 B		632.4	35.10		1.0116	
BA40 C		596.2	32.84			
BA40 D		291.2	16.05	31.96		1.0587
BA41 B	70G33/A1565	632.4	35.10		1.3829	
BA41 C		596.2	32.84			
BA41 D		291.2	16.05			
BA42 B		547.9	30.44		1.5061	
BA42 C		592.9	32.52			
BA42 D		608	33.53			
BA43 B		589.9	32.71		1.46	
BA43 C		573.2	31.65			
BA43 D		688	37.97			
BA44 B		514.5	29.07		1.264	
BA44 C		622.5	33.93			
BA44 D		526.3	29.18	31.25		1.40325
BA45 B	70G33/AS1133	652.2	36.45		1.3796	
BA45 C		823	45.67			
BA45 D		714.3	39.67			
BA46 B		608	33.60		1.1268	
BA46 C		513.5	28.18			
BA46 D		691.2	38.01			
BA47 B		799.7	44.02		1.4002	
BA47 C		742.5	40.37			
BA47 D		810	44.69			
BA48 B		750.4	40.92		1.1216	
BA48 C		749.2	43.63			
BA48 D		754	42.19	39.78		1.25705
BA49 B	70G33/70G33	653.4	36.03		2.5314	
BA49 C		641.8	36.77			
BA49 D		632.4	34.89			
BA50 B		699.2	38.14		2.4593	
BA50 C		724.3	39.74			
BA50 D		649.5	35.78			
BA51 B		613.8	33.64		2.646	
BA51 C		750.1	40.95			
BA51 D		674.2	36.79			

BA52	**B**	649.3	35.18	2.6123	
BA52	**C**	662	36.69		
BA52	**D**	644.7	35.75	36.70	2.56225

VITA AUCTORIS

The author was born in Xi'an, People's Republic of China.

She has a B. Sc. degree (1982-1986) in Chemistry,

and an M. Sc. degree (1989-1992) in Polymer Engineering,

both from Xi'an Jiaotong University, China.

She had worked for 10 years as a chemical engineer in P. R. China.

She came to Canada in 1998 and
currently works in a local mold company as an engineer.